Annex III

SUPPLEMENTARY INFORMATION AND FORMULAS USEFUL FOR PROGRAMMING

The material of this annex is organized into the following sections:

1. Line-of-sight
2. Diffraction over a single isolated obstacle
3. Diffraction over a single isolated obstacle with ground reflections
4. Diffraction over irregular terrain
5. Forward scatter
6. Forward scatter with antennas elevated
7. Long-term variability
8. List of special symbols used in annex III

Section 1 lists geometric optics formulas for computing transmission loss over a smooth earth, for determining the magnitude and phase of the reflection coefficient, and for computing a first Fresnel zone along a great circle path. Graphs of the magnitude R and phase c of the reflection coefficient are included. Section 2 gives mathematical expressions that approximate the curves $A(v, 0)$, $A(0, \rho)$ and $U(v\rho)$ for convenience in using a digital computer. Section 3 lists geometric optics formulas used to compute diffraction attenuation when several components of the received field are affected by reflection from the earth's surface. Section 4 defines the parameters K and b for both horizontally and vertically polarized radio waves. Section 5 shows the function $F(\theta d)$ for N_s = 250, 301, 350, and 400, and for values of s from 0.01 to 1. Curve fits to the function $F(\theta d)$ and equations for computing $H_o(\eta_s = 0)$ are included. Section 6 suggests modifications of the prediction methods for use when antenna beams are elevated or directed out of the great circle plane. Section 7 shows diurnal and seasonal changes in long-term variability. Mathematical expressions used to compute predicted distributions are shown and a method of mixing distributions is described. Section 8 is a list of special symbols used in this annex.

Section I.3 of annex I explains an easily programmed method for obtaining reference values of attenuation relative to free space A_{cr} for a wide range of applications. These reference values may be converted to estimates of transmission loss exceeded for $100\,p = 100\,(1 - q)$ percent of the time by subtracting the quantities $V(0.5)$ and $Y(q)$ defined by (10.4) and (10.5) of volume 1 and discussed also in section 7 of this annex.

III. 1 Line-of-Sight

Simple formulas for line-of-sight propagation which suffice for most applications, are given in section 5 of the report. Formulas for geometry over a smooth earth and for determining the magnitude and phase of the reflection coefficient are given here. These formulas may be used when the great circle path terrain visible to both antennas will support a substantial amount of reflection, and it is reasonable to fit a smooth convex curve of radius a to this portion of the terrain.

Figure 5.1b illustrates the geometry appropriate for reflection of a single ray by a smooth earth of effective radius a. In the figure, ψ is the grazing angle at the geometrical reflection point located at a distance d_1 from an antenna of height h_1 and at a distance d_2 from an antenna of height h_2. The total path distance $d = d_1 + d_2$ is measured along an arc of radius a. The difference, Δr, between the reflected ray path length $r_1 + r_2$ and the length of the direct ray, r_o, is calculated to find the phase of a radio field which is the sum of ground-reflected and free space fields. If Δr is less than 0.06λ, these ray optics formulas are not applicable. For almost all cases of interest the angle ψ is small and the straight line distances r_1, r_2 and r_o are very nearly equal to the mean sea level arc distances d_1, d_2 and d. The geometric optics formulas given below usually require double-precision arithmetic,

$$\tan\psi = \cot(d_1/a) - (1 + h_1/a)^{-1} \csc(d_1/a) \cong \frac{h_1}{d_1} - \frac{d_1}{2a} \tag{III.1}$$

$$\tan\psi = \cot(d_2/a) - (1 + h_2/a)^{-1} \csc(d_2/a) \cong \frac{h_2}{d_2} - \frac{d_2}{2a} \tag{III.2}$$

$$r_o = a\left\{(h_1/a)^2 + (h_2/a)^2 - 2(h_1/a)(h_2/a) + 2[1 + h_1/a + h_2/a + (h_1/a)(h_2/a)][1 - \cos(d/a)]\right\}^{1/2} \tag{III.3}$$

$$\left[(a\sin\psi)^2 + h_1(2a + h_1)\right]^{1/2} - a\sin\psi \tag{III.4}$$

$$\left[(a\sin\psi)^2 + h_2(2a + h_2)\right]^{1/2} - a\sin\psi \tag{III.5}$$

$$\Delta r = r_1 + r_2 - r_o = 4 r_1 r_2 \sin^2\psi / (r_1 + r_2 + r_o) . \tag{III.6}$$

Equating (III.1) and (III.2) and substituting $d - d_1$ for d_2 in (III.2), the distance d_1 may be determined graphically or by trial and error, and $\tan\psi$ is then calculated using (III.1).

Using double precision arithmetic, (III. 1) through (III. 6) give an accurate estimate of the path difference Δr for reflection of a single ray from a smooth earth. This value is then used in (5.4) or (5.5) of section 5 to compute the attenuation relative to free space.

If either h_1 or h_2 greatly exceeds one kilometer, and if it is considered worthwhile to trace rays through the atmosphere in order to determine ψ more accurately, values of d_1 or d_2, tabulated by Bean and Thayer [1959], may be used. Given h_1, h_2, and the surface refractivity, N_s, select trial values for ψ, calculate d_1 and d_2, and continue until $d_1 + d_2 = d$. Then (III.1) and (III.2) must be solved for new values of h_1 and h_2 if (III.3), (III.4), and (III.5) are used to obtain the path difference, $\Delta r = r_1 + r_2 - r_o$.

The symbols R in (5.1) and c in (5.4) represent the magnitude and the phase angle relative to π, respectively, of the theoretical coefficient $R \exp[-i(\pi - c)]$ for reflection of a plane wave from a smooth plane surface of a given conductivity σ and relative dielectric constant ϵ. Values of R and c as a function of the grazing angle ψ are shown in figures III.1 to III.8 for vertical and horizontal polarization over good, average, and poor ground, and over sea water. The magnitude R of the smooth plane earth reflection coefficient is designated R_v or R_h for vertical or horizontal polarization respectively, and is read on the left-hand ordinate scale using the solid curves. The phase angle relative to π, is designated c_v or c_h for vertical or horizontal polarization respectively, and is read in radians on the right-hand scale using the dashed curves. As seen from these figures in most cases when the angle ψ is small, R is very nearly unity and c may be set equal to zero. A notable exception occurs in the case of propagation over sea water using vertical polarization.

In preparing figures III.1 to III.8, the following general expressions for the magnitudes R_v and R_h and lags $(\pi - c_v)$ and $(\pi - c_h)$ were used. In these equations, ϵ is the ratio of the surface dielectric constant to that of air, σ is the surface conductivity in mhos per meter, f is the radio frequency in megacycles per second, and ψ is the grazing angle in radians.

$$x = 1.80 \times 10^4 \sigma / f, \quad q = x/(2p) \tag{III. 7}$$

$$2p^2 = \left[(\epsilon - \cos^2\psi)^2 + x^2\right]^{1/2} + (\epsilon - \cos^2\psi) \tag{III. 8}$$

$$b_v = \frac{\epsilon^2 + x^2}{p^2 + q^2}, \quad b_h = \frac{1}{p^2 + q^2} \tag{III. 9}$$

$$m_v = \frac{2(p\epsilon + qx)}{p^2 + q^2}, \quad m_h = \frac{2p}{p^2 + q^2} \tag{III. 10}$$

$$R_v^2 = \left[1 + b_v \sin^2 \psi - m_v \sin \psi \right] \left[1 + b_v \sin^2 \psi + m_v \sin \psi \right]^{-1} \qquad \text{(III. 11)}$$

$$R_h^2 = \left[1 + b_h \sin^2 \psi - m_h \sin \psi \right] \left[1 + b_h \sin^2 \psi + m_h \sin \psi \right]^{-1} \qquad \text{(III. 12)}$$

$$\pi - c_v = \tan^{-1}\left(\frac{x \sin \psi - q}{\epsilon \sin \psi - p} \right) - \tan^{-1}\left(\frac{x \sin \psi + q}{\epsilon \sin \psi + p} \right) \qquad \text{(III. 13)}$$

$$\pi - c_h = \tan^{-1}\left(\frac{-q}{\sin \psi - p} \right) - \tan^{-1}\left(\frac{q}{\sin \psi + p} \right) \qquad \text{(III. 14)}$$

The angle c_v is always positive and less than π, and c_h is always negative with an absolute magnitude less than π. The pseudo Brewster angle, where c_v suddenly changes from near zero to $\pi/2$, and where R_v is a minimum, is $\sin^{-1}\sqrt{1/b_v}$.

For grazing angles less than 0.1 radian, for overland propagation, and for frequencies above 30 Mc/s, excellent approximations to (III.11) and (III.12) are provided by the following formulas:

$$R_v = \exp(-m_v \psi) \qquad \text{(III. 15)}$$

$$R_h = \exp(-m_h \psi) \; . \qquad \text{(III. 16)}$$

The assumption of a discrete reflection point with equal angles of incidence and reflection as shown in figure 5.1 is an oversimplification. Actually, reflection occurs from all points of the surface. For irregular terrain, this is taken into account by a terrain roughness factor σ_h, (subsection 5.1), which is the r.m.s. deviation of terrain relative to a smooth curve computed within the limits of a first Fresnel zone in a horizontal plane. The outline of such a Fresnel ellipse is determined by the condition that the length of a ray path, $r_{11} + r_{21}$, corresponding to scattering from a point on the edge of the ellipse is half a wave length longer than the geometrical ray path, $r_1 + r_2$, where the angles of incidence and reflection are equal.

The first Fresnel ellipse cuts the great circle plane at two points, x_a and x_b kilometers from the transmitter. The distances x_a and x_b are defined by the relation

$$\sqrt{r_1^2 \sin^2 \psi + x^2} + \sqrt{r_2^2 \sin^2 \psi + \left[(r_1 + r_2) \cos \psi - x \right]^2} = r_1 + r_2 + \lambda/2 \; . \qquad \text{(III. 17)}$$

The exact solution for x is

$$2x_{a,b}(1+\delta) = [(r_1+r_2)(1+\delta) + (r_1-r_2)]\cos\psi \pm (r_1+r_2+\lambda/2)\,\delta\sqrt{1+4r_1r_2/[(r_1+r_2)^2\delta]} \tag{III. 18}$$

where

$$r_1^2 = h_1'^2 + d_1^2 , \quad r_2^2 = h_2'^2 + d_2^2 , \quad (r_1+r_2)^2 = (h_1'+h_2')^2 + d^2$$

$$\cos\psi = d_1/r_1 = d_2/r_2 , \quad \sin\psi = h_1'/r_1 = h_2'/r_2$$

$$\delta = \left[\frac{\lambda^2}{4(r_1+r_2)^2} + \frac{\lambda}{r_1+r_2}\right]/\sin^2\psi$$

d_1, d_2 are defined by (5.7), and λ is the radio wavelength in kilometers.

As an alternative method, the points x_a and x_b may be computed in terms of path distance, the heights h_1' and h_2', and the radio frequency. In this method, the distance x_0 to the center of the first Fresnel zone is first computed, then the distance x_1 from the center to the margin of the zone is subtracted from x_0 to give x_a, and added to give x_b.

$$x_0 = d/2\left[1 + B\,f(h_1'^2 - h_2'^2)\right] \quad \text{km} \tag{III. 19}$$

where

$$B = \left[0.3d(1+2h_1'h_2'/d^2) + f(h_1'+h_2')^2\right]^{-1} \tag{III. 20}$$

$$x_1 = 0.548\,B\,d^2\left\{\left[f\,h_1'h_2'/d + 0.075(1+2h_1'h_2'/d^2)\right]\left[\frac{1+(h_1'+h_2')^2/d^2}{1+2h_1'h_2'/d^2}\right]\right\}^{1/2} \tag{III. 21}$$

$$x_a = x_0 - x_1 \quad \text{km} , \quad x_b = x_0 + x_1 \quad \text{km} .$$

The method given in (III.19) to (III.21) is applicable whenever $d >> \lambda$. If in addition, $h_1' h_2' << d^2$, the computation of B, and x_1 may be simplified as follows:

$$B = \left[0.3d + f(h_1' + h_2')^2 \right]^{-1} \qquad \text{(III. 22)}$$

$$x_1 = 0.548\, B\, d^2 \left\{ \left[f\, h_1' h_2'/d + 0.075 \right] \left[1 + (h_1' + h_2')^2/d^2 \right] \right\}^{1/2} \qquad \text{(III. 23)}$$

THE COMPLEX REFLECTION COEFFICIENT $Re^{i(\pi - c)}$

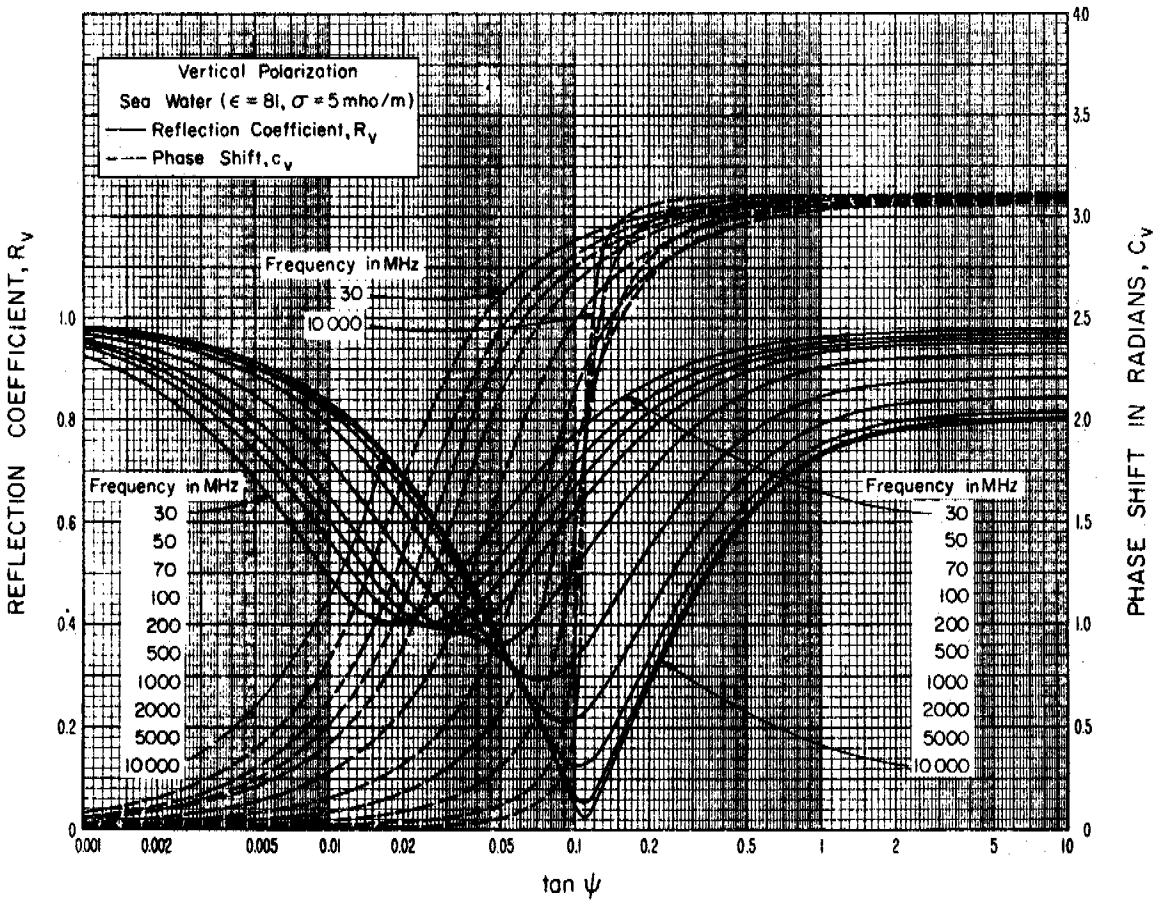

Figure III.1

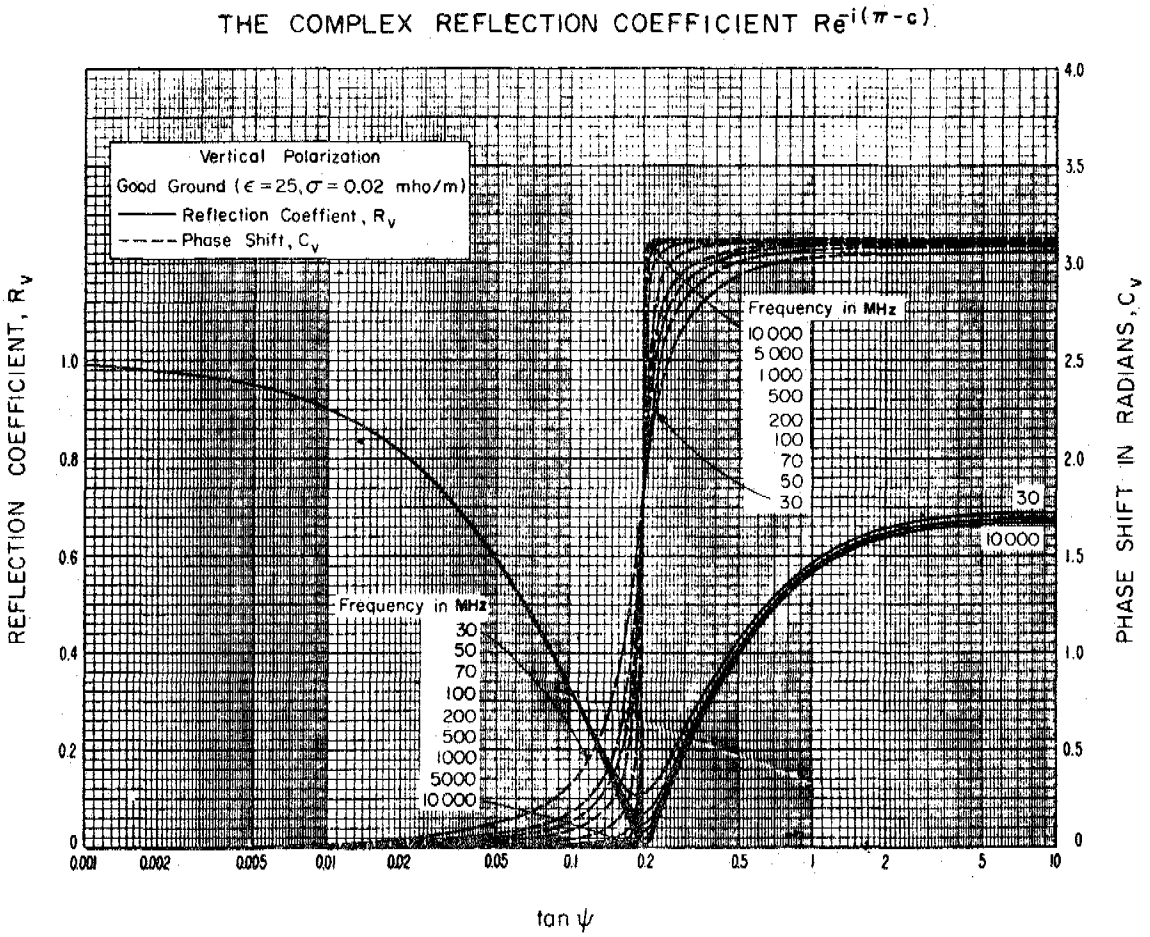
THE COMPLEX REFLECTION COEFFICIENT $Re^{i(\pi-c)}$
Vertical Polarization
Good Ground ($\epsilon = 25, \sigma = 0.02$ mho/m)
Reflection Coeffient, R_v
Phase Shift, C_v
Frequency in MHz
30
50
70
100
200
500
1000
5000
10 000
Frequency in MHz
10 000
5 000
1 000
500
200
100
70
50
30
30
10000
REFLECTION COEFFICIENT, R_v
PHASE SHIFT IN RADIANS, C_v
0
0.2
0.4
0.6
0.8
1.0
0
0.5
1.0
1.5
2.0
2.5
3.0
3.5
4.0
0.001
0.002
0.005
0.01
0.02
0.05
0.1
0.2
0.5
1
2
5
10
tan ψ

Figure III.2

THE COMPLEX REFLECTION COEFFICIENT $Re^{i(\pi-c)}$

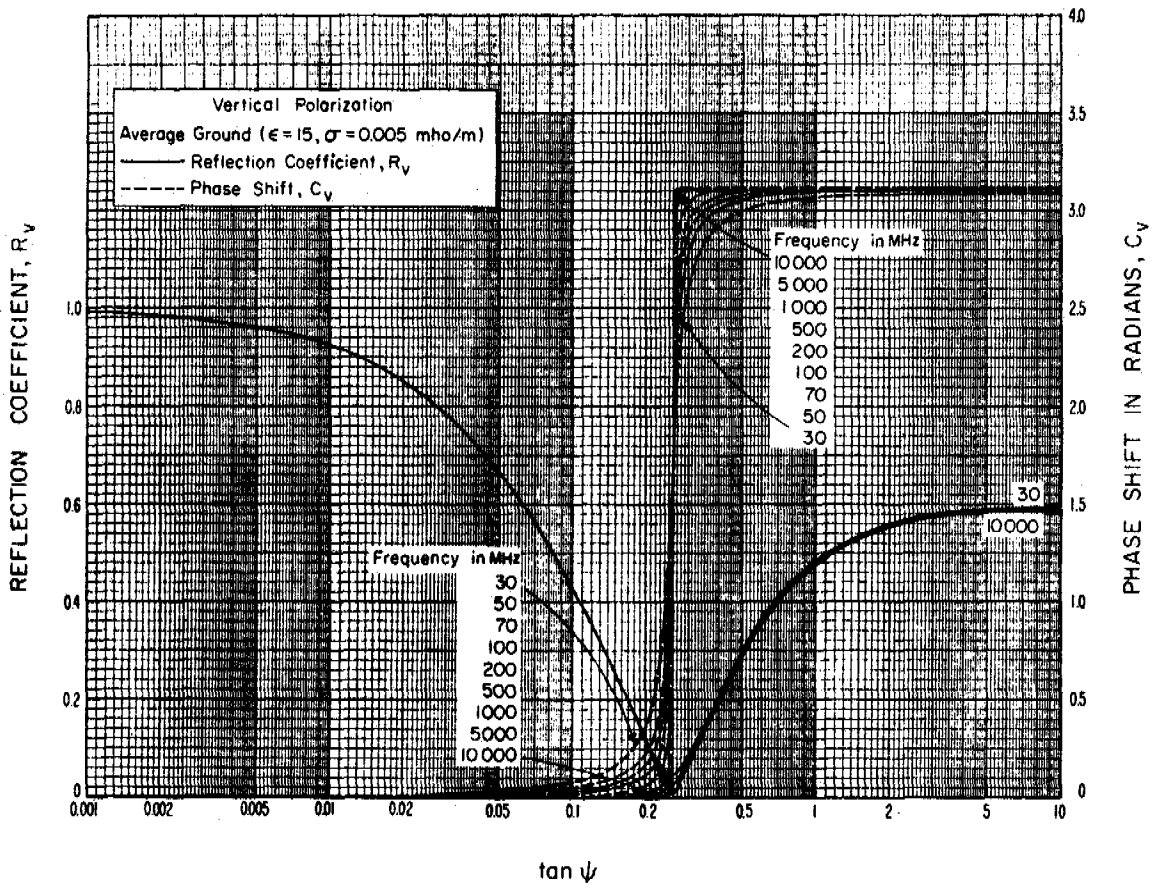

Figure III.3

THE COMPLEX REFLECTION COEFFICIENT $Re^{i(\pi - c)}$

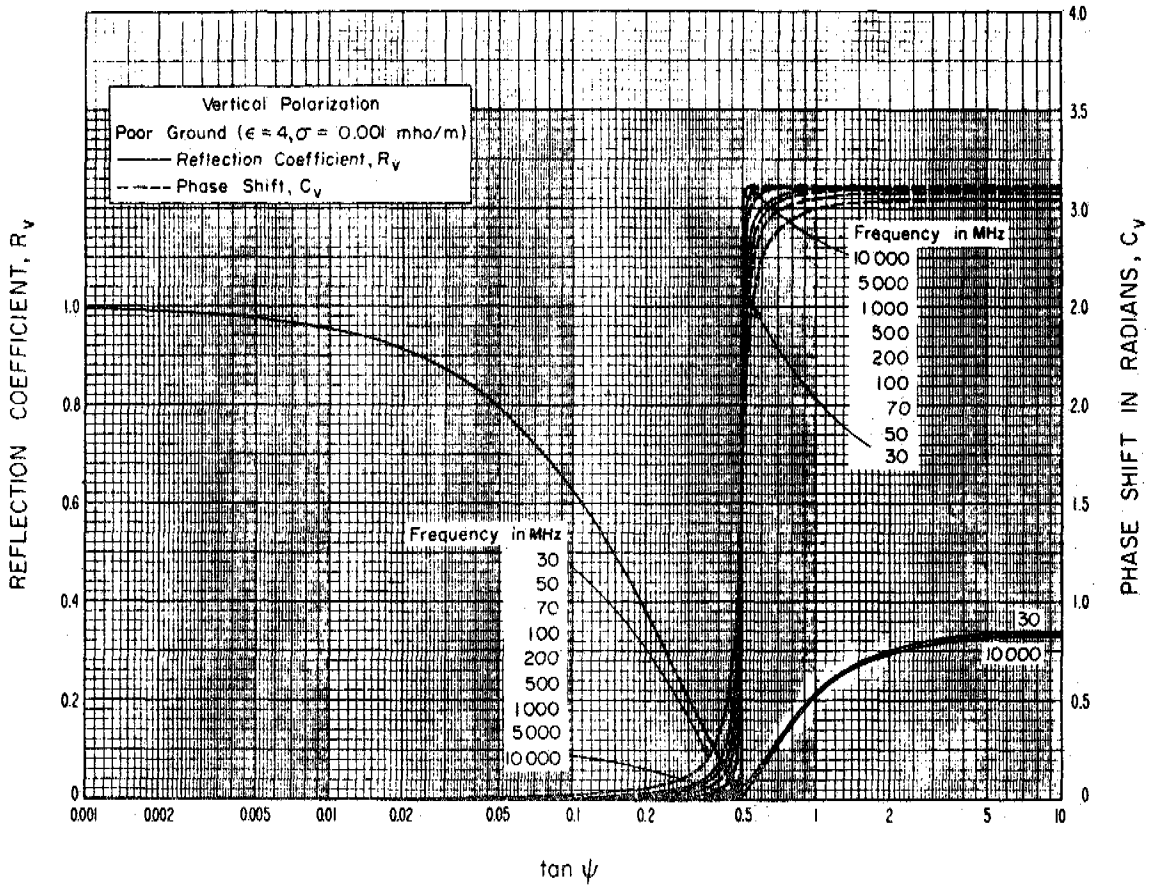

Figure III 4

THE COMPLEX REFLECTION COEFFICIENT $Re^{-i(\pi - c)}$

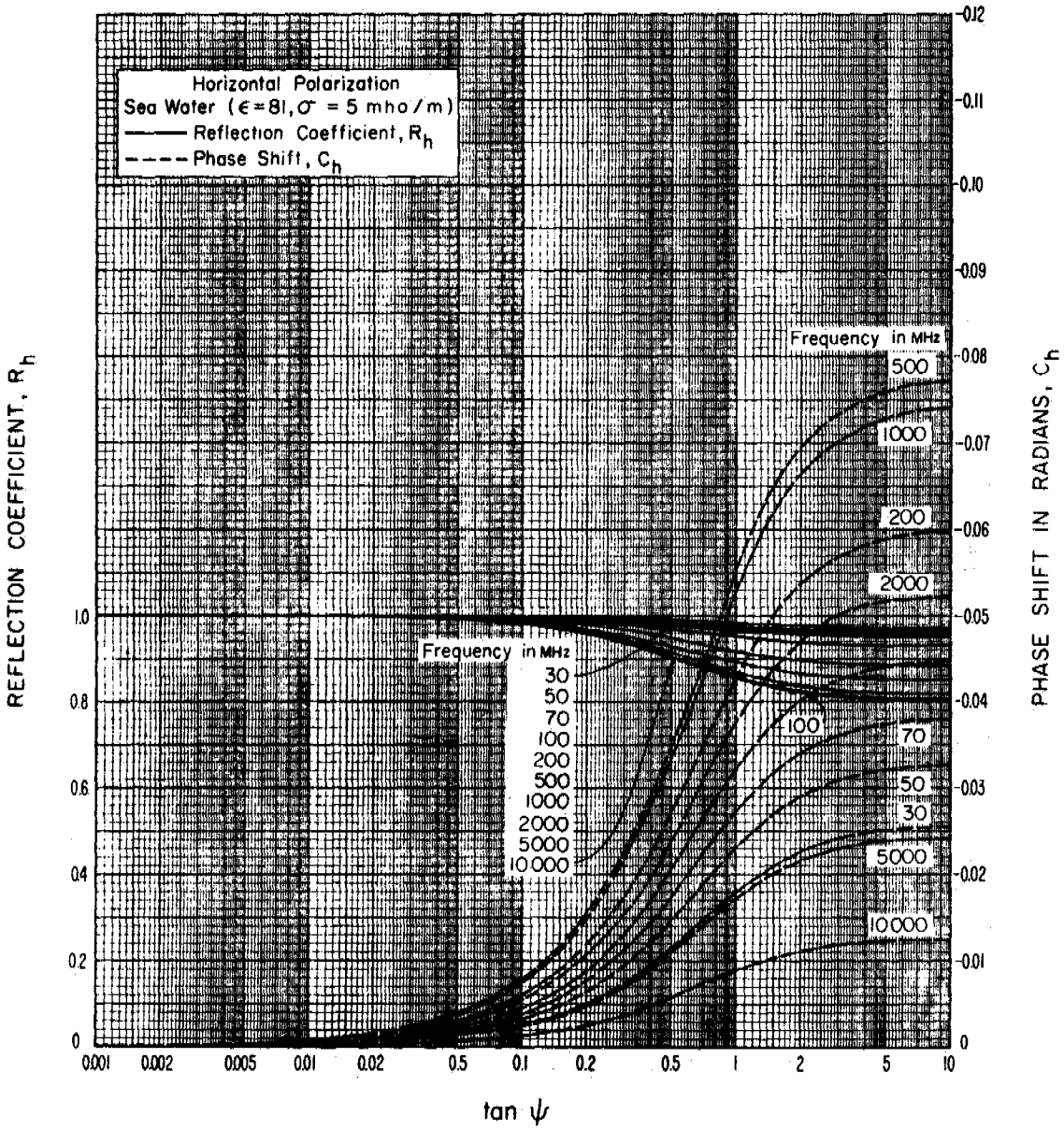

Figure III.5

THE COMPLEX REFLECTION COEFFICIENT $Re^{-i(\pi - c)}$

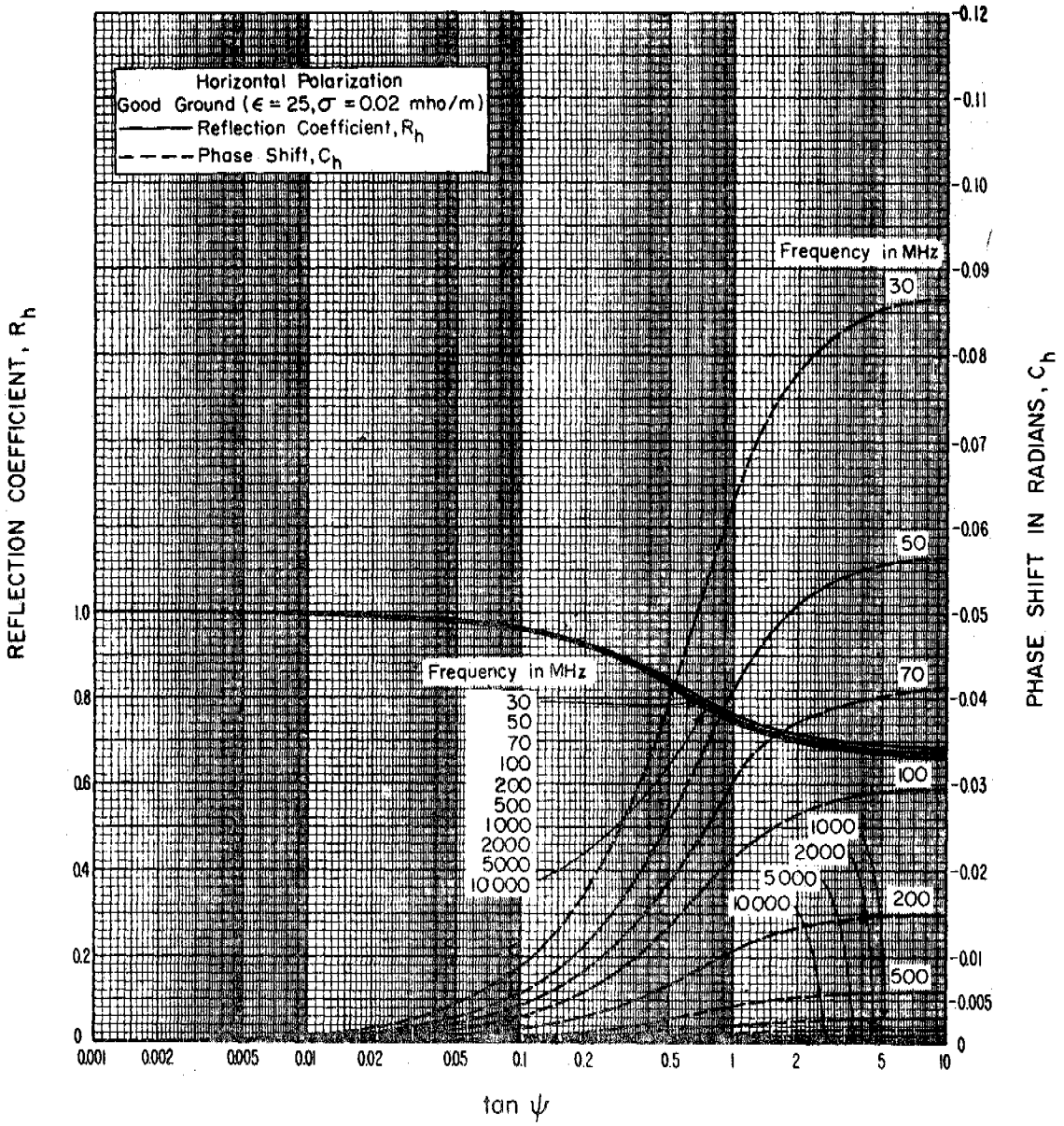

Figure III.6

THE COMPLEX REFLECTION COEFFICIENT $Re^{-i(\pi - c)}$

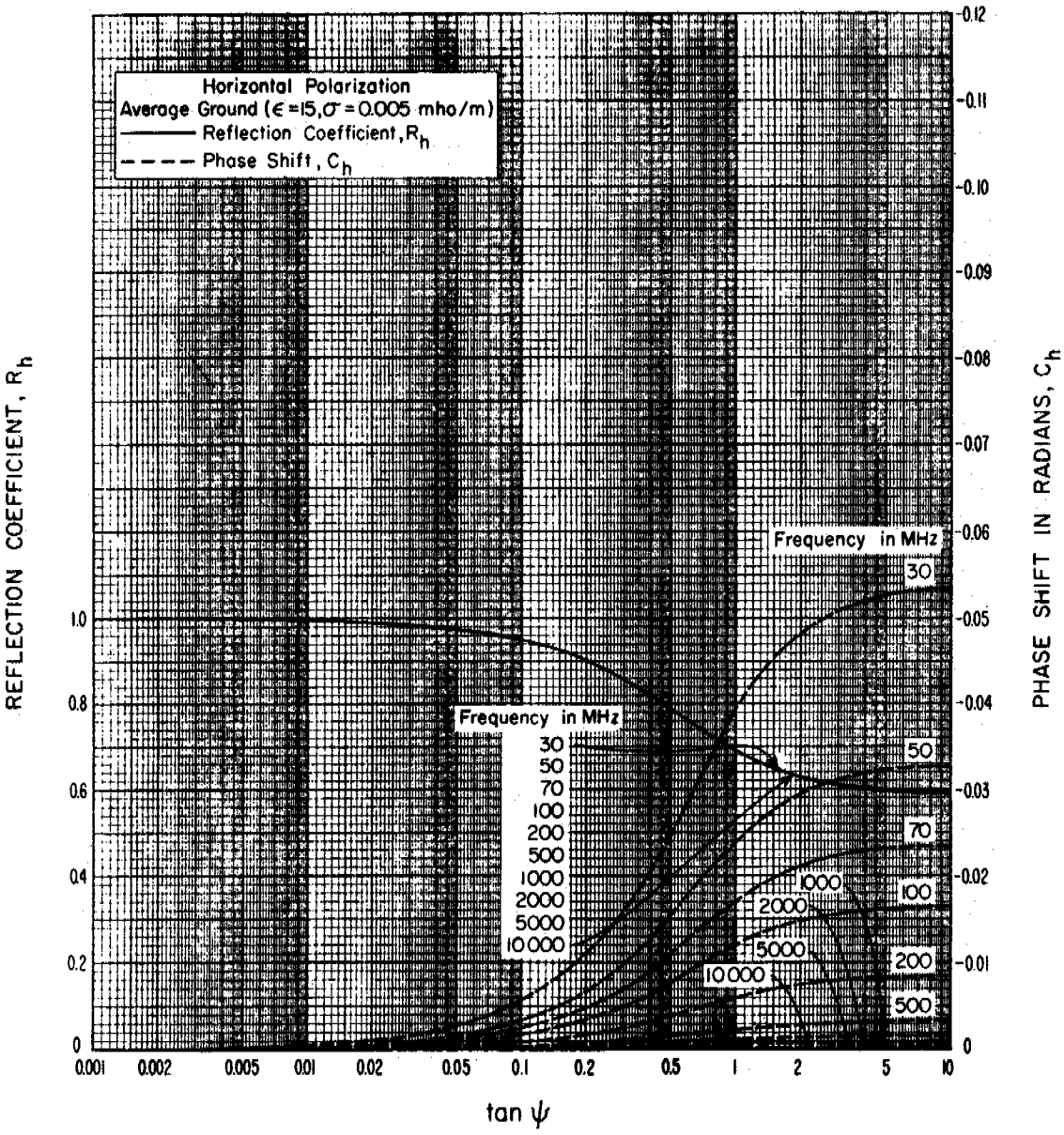

Figure III.7

THE COMPLEX REFLECTION COEFFICIENT $Re^{-i(\pi - c)}$

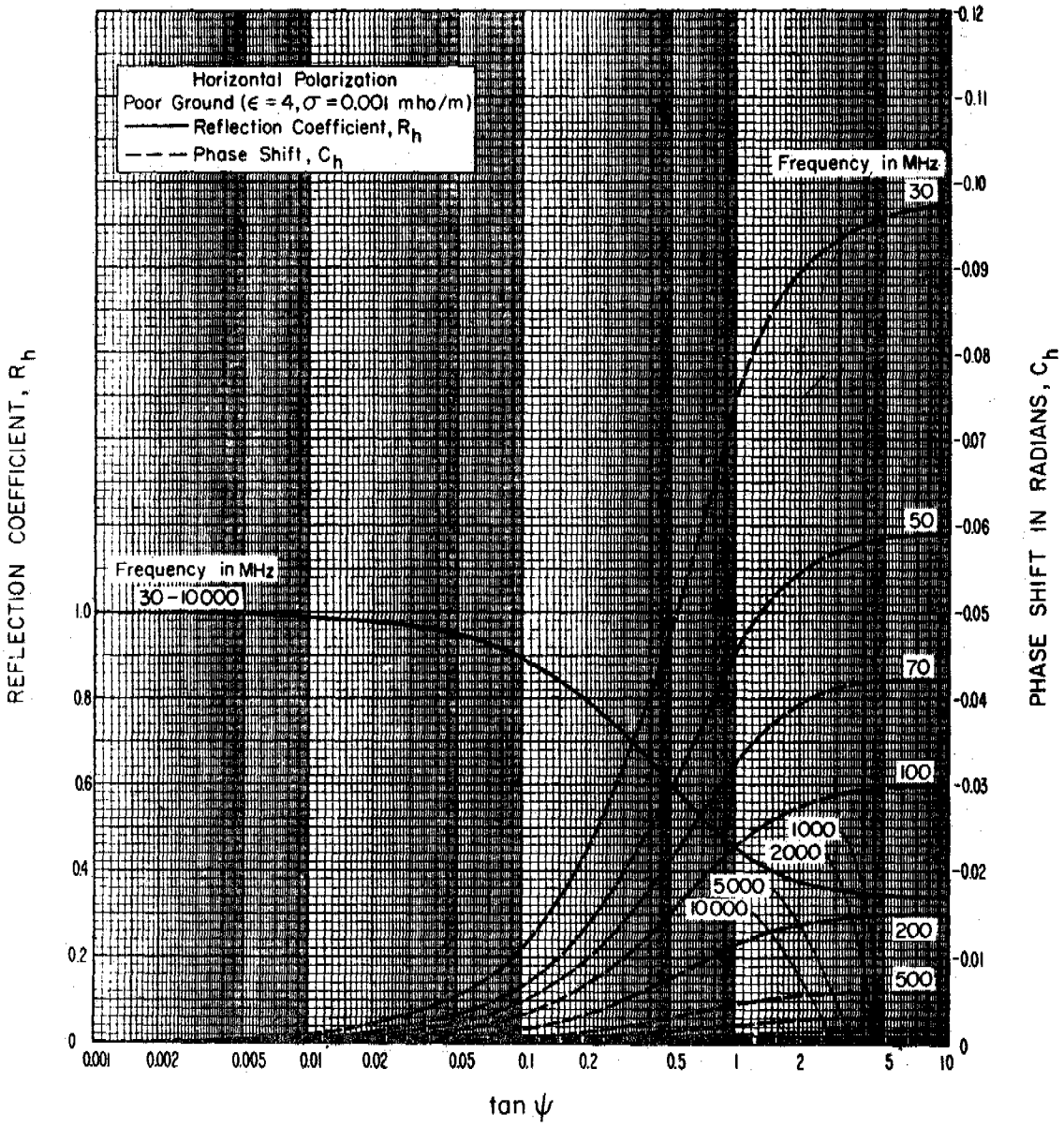

Figure III.8

III. 2 Diffraction over a Single Isolated Obstacle.

The theoretical diffraction loss curves on figures 7.1 to 7.4 have been fitted by arbitrary mathematical expressions for convenience in using a digital computer.

The diffraction loss for an isolated rounded obstacle and irregular terrain is given in section 7 as:

$$A(v, \rho) = A(v, 0) + A(0, \rho) + U(v\rho) \quad \text{db} \qquad (7.7)$$

where the parameter v is defined as

$$v = \pm 2\sqrt{\Delta r/\lambda} \cong \pm \sqrt{2d\,\alpha_o\beta_o/\lambda} \qquad (7.1a)$$

or

$$v = \pm 2.5830\sqrt{f\,d_1d_2/d} \qquad (7.1b)$$

and ρ an index of curvature of the rounded obstacles is defined as:

$$\rho = 0.676\, r^{1/3} f^{-1/6} [d/r_1r_2)]^{1/2} \qquad (7.8)$$

For an ideal knife edge, ($\rho = 0$), the diffraction loss is $A(v, 0)$ and is shown on figure 7.1. For values of v from -0.8 to large positive values, this curve may be approximated using the following mathematical expressions:

For $-0.8 \leq v \leq 0$,

$$A(v, 0) = 6.02 + 9.0\, v + 1.65\, v^2 \quad \text{db.} \qquad \text{(III. 24a)}$$

For $0 \leq v \leq 2.4$,

$$A(v, 0) = 6.02 + 9.11\, v - 1.27\, v^2 \qquad \text{(III. 24b)}$$

For $v > 2.4$,

$$A(v, 0) = 12.953 + 20 \log v \quad \text{db.} \qquad \text{(III. 24c)}$$

The theoretical curve for $A(0, \rho)$ is approximated by:

$$A(0, \rho) = 6.02 + 5.556\, \rho + 3.418\, \rho^2 + 0.256\, \rho^3 \quad \text{db,}$$

and the curve $U(v\rho)$ is approximated as follows:

For $v\rho \leq 3$: $U(v\rho) = 11.45\, v\rho + 2.19\,(v\rho)^2 - 0.206\,(v\rho)^3 - 6.02$ db. (III. 26a)

For $3 < v\rho \leq 5$: $U(v\rho) = 13.47\, v\rho + 1.058\,(v\rho)^2 - 0.048\,(v\rho)^3 - 6.02$ db. (III. 26b)

For $v\rho < 5$: $U(v\rho) = 20\, v\rho - 18.2$ db. (III. 26c)

An average allowance for terrain foreground effects may be made by adding a term $10 \exp(-2.3\,\rho)$ to $A(0, \rho)$. This term gives a correction which ranges from 10 db for $\rho = 0$ to 1 db for $\rho = 1$.

When reflections from terrain on either or both sides of the obstacle should be considered, the method given in the following section may be used. This method considers the diffraction loss and phase lag over the diffracting obstacle, and the path length differences and reflection coefficients of the reflected waves.

III. 3 Diffraction over a Single Isolated Obstacle with Ground Reflections

Diffraction over an isolated obstacle is discussed in section 7, where ways of approximating the effects of reflection and diffraction from foreground terrain are indicated. Where the effects of reflection are expected to be of great importance, such as in the case of propagation over a large body of water, the following geometric optics method may be used.

Figure III.9 illustrates four distinct ray paths over a knife edge; the first ray is not reflected from the ground, the second and third are each reflected once, and the fourth ray is reflected once on each side of the knife edge. Each ray is subject to a diffraction loss f_j and a phase lag Φ_j at the knife edge, where $j = 1, 2, 3, 4$. Both f_j and Φ_j depend on the knife-edge parameter v given in section III.2. When the isolated obstacle is rounded, rather than an ideal knife edge, the diffraction loss depends on v and ρ, where ρ is the index of curvature of the crest radius, defined in section III.2. The parameter v may be written:

$$v_j = \pm 2\sqrt{\Delta_j/\lambda} \cong \pm \sqrt{2d\,\alpha_{oj}\beta_{oj}/\lambda} \qquad \text{(III. 27)}$$

where Δ_j is

$$\Delta_1 = r_1 + r_2 - r_0, \quad \Delta_2 = r_{11} + r_{12} + r_2 - r_{02}$$

$$\Delta_3 = r_1 + r_{21} + r_{22} - r_{03}, \quad \Delta_4 = r_{11} + r_{12} + r_{21} + r_{22} - r_{04}. \qquad \text{(III. 28)}$$

Path differences Δ_j used to calculate v_j in (III. 27) are closely approximated by the following formulas:

$$\Delta_j = d_r\,\theta_j^2, \quad d_r = d_1 d_2/(2d), \quad \theta_j = \theta + \theta_{jr}$$

$$\theta_{1r} = 0, \quad \theta_{2r} = 2d_{11}\psi_1/d_1, \quad \theta_{3r} = 2d_{22}\psi_2/d_2, \quad \theta_{4r} = \theta_{2r} + \theta_{3r}. \qquad \text{(III. 29)}$$

The total phase change $\Phi(v, \rho)$ at an isolated rounded obstacle is

$$\Phi_j = \Phi_j(v, \rho) = 90\,v^2 + \phi(v, 0) + \phi(0, \rho) + \phi(v\rho) \qquad \text{(III. 30a)}$$

where the functions $\phi(v, 0)$, $\phi(0, \rho)$, and $\phi(v\rho)$ are plotted as dashed curves on figures 7.1, 7.4, and 7.5. For an ideal knife edge, where the radius of curvature of the crest is zero, $\rho = 0$, and (III. 30a) reduces to

for $v > 0$ $$\Phi_j(v, 0) = 90\,v^2 + \phi(v, 0) \qquad \text{(III. 30b)}$$

for $v \le 0$ $$\Phi_j(v, 0) = \phi(v, 0). \qquad \text{(III. 30c)}$$

The three components of the received field which are affected by reflection from the earth's surface depend also upon effective ground reflection coefficients $R_{e2} \exp[-i(\pi - c_2)]$ and $R_{e3} \exp[-i(\pi - c_3)]$, defined in section 5, and upon ray path differences Δ_{2r} and Δ_{3r}:

$$\Delta_{2r} = r_{11} + r_{12} - r_1 \cong 2\psi_1^2 d_{11} d_{12}/d_1$$

$$\Delta_{3r} = r_{21} + r_{22} - r_2 \cong 2\psi_2^2 d_{21} d_{22}/d_2. \qquad \text{(III. 31)}$$

Usually, it may be assumed that $c_2 = c_3 = 0$ so that the reflection coefficients are $-R_{e2}$ and $-R_{e3}$.

Introducing the propagation constant $k = 2\pi/\lambda$, the attenuation relative to free space is then

$$A = -20 \log \left\{ \left| f_1 \exp(-i\Phi_1) - R_{e2} f_2 \exp\left[-i(\Phi_2 + k\Delta_2)\right] \right.\right.$$

$$\left.\left. - R_{e3} f_3 \exp\left[-i(\Phi_3 + k\Delta_3)\right] + R_{e2} R_{e3} f_4 \exp\left[-i(\Phi_4 + k\Delta_2 + k\Delta_3)\right] \right| \right\} \text{ db} \qquad \text{(III. 32)}$$

where

$$f_j = +\tfrac{1}{2}\sqrt{(1 - C_j - S_j)^2 + (C_j - S_j)^2}, \quad \tan\Phi_j = \frac{C_j - S_j}{1 - C_j - S_j}$$

$$\int_o^{v_j} \cos\left(\frac{\pi t^2}{2}\right) dt, \quad S_j = \int_o^{v_j} \sin\left(\frac{\pi t^2}{2}\right) dt. \qquad \text{(III. 33)}$$

Pearcey [1956], and the NBS AMS 55 Handbook of Mathematical Functions [1964] give complete tables, series expansions, and asymptotic expressions for the Fresnel integrals C_j and S_j. The magnitude $f_j \equiv f(v_j)$ for $v = v_j$ may also be determined from figure 7.1 and the expression

$$\log f(v_j) = -A(v_j)/20 \qquad \text{(III. 34)}$$

and where v is larger than 3:

$$f_j = 0.22508/v_j, \quad \Phi_j = \frac{\pi}{4}\left(1 + 2v_j^2\right) \text{ radians} \qquad \text{(III. 35)}$$

Figure III.10 is a nomogram which may be used in the determination of $f(v_j)$ and $\Phi(v_j)$ for both positive and negative values of v. This nomogram is based on the representation

of Fresnel integrals by the Cornu spiral.

The general problem requires calculating θ, d, d_1, d_2, d_{11}, d_{12}, d_{21}, d_{22}, ψ_1, and ψ_2, as shown in figure III.9.

1. Calculate θ_j and Δ_j for $j = 1, 2, 3, 4$, using (III.29).
2. Calculate v_j, C_j, S_j, f_j, and Φ_j, using (III.27), (III.33), and figure 7.1.
3. Calculate Δ_{2r} and Δ_{3r} from (III.31).
4. Calculate R_{e2} and R_{e3} from (5.1), or assume that $R_{e2} = R_{e3} = 1$.
5. Substitute these values in (III.32).

To check the calculation of each v_j, the approximation given in (III.27) may be used, with the following formulas for $\alpha_{oj} = d_2\,\theta_j/d$ and $\beta_{oj} = d_1\,\theta_j/d$:

$$\alpha_{01} = d_2\,\theta/d \qquad \beta_{01} = d_1\,\theta/d$$

$$\alpha_{02} = \alpha_{01} + 2d_{11}\,\psi_1 d_2/(d_1 d) \qquad \beta_{02} = \beta_{01} + 2d_{11}\,\psi_1/d$$

$$\alpha_{03} = \alpha_{01} + 2d_{22}\,\psi_2/d \qquad \beta_{03} = \beta_{01} + 2d_{22}\,\psi_2 d_1/(d_2 d)$$

$$\alpha_{04} = \alpha_{02} + \alpha_{03} - \alpha_{01} \qquad \beta_{04} = \beta_{02} + \beta_{03} - \beta_{01}. \qquad \text{(III.36)}$$

Two special cases will be described for which (III.29) and (III.31) may be simplified. First, assume that each reflecting surface may be considered a plane. Let h_t and h_{tm} be the heights of the transmitting antenna and the knife edge above the first plane, and let h_{rm} and h_r be the heights of the knife edge and the receiving antenna above the second reflecting plane. Assume that Δr is very small for every Δ. In terms of the heights h_t, h_{tm}, h_{rm}, h_r, the parameters θ, d_1, and d_2 and the parameter $d_r \equiv d_1 d_2/(2d)$:

$$\Delta_{2r} = 2h_t h_{tm}/d_1, \quad \Delta_{3r} = 2h_r h_{rm}/d_2$$

$$\Delta_1 = d_r\,\theta^2, \quad \Delta_2 = d_r(\theta + h_{tm}\,\Delta_{2r})^2$$

$$\Delta_3 = d_r(\theta + h_{rm}\,\Delta_{3r})^2, \quad \Delta_4 = d_r(\theta + h_{tm}\,\Delta_{2r} + h_{rm}\,\Delta_{3r})^2. \qquad \text{(III.37)}$$

The second special case assumes a knife edge over an otherwise smooth earth of effective radius a, with antenna heights h_t and h_r small compared to the height of the knife edge. In this case, h_t and h_r are heights above the smooth curved earth. The angle of elevation of the knife edge relative to the horizontal at one antenna is θ_{ht} and relative to the horizontal at the other antenna is θ_{hr}. Referring to (5.12):

$$\Delta_{2r} = h_t\left[\sqrt{\theta_{ht}^2 + 4h_t/(3a)} + \theta_{ht}\right], \quad \Delta_{3r} = h_r\left[\sqrt{\theta_{hr}^2 + 4h_r/(3a)} + \theta_{hr}\right]. \quad \text{(III.38)}$$

For this special case, the formulas (III.29) for Δ_j may be simplified by writing

$$\theta_{2r} = \Delta_{2r}^2\, d_1/(2h_t), \quad \theta_{3r} = \Delta_{3r}^2\, d_2/(2h_r). \quad \text{(III.39)}$$

BEYOND-HORIZON KNIFE-EDGE DIFFRACTION WITH GROUND REFLECTIONS

(KNIFE-EDGE NORMAL TO RAY PATH)

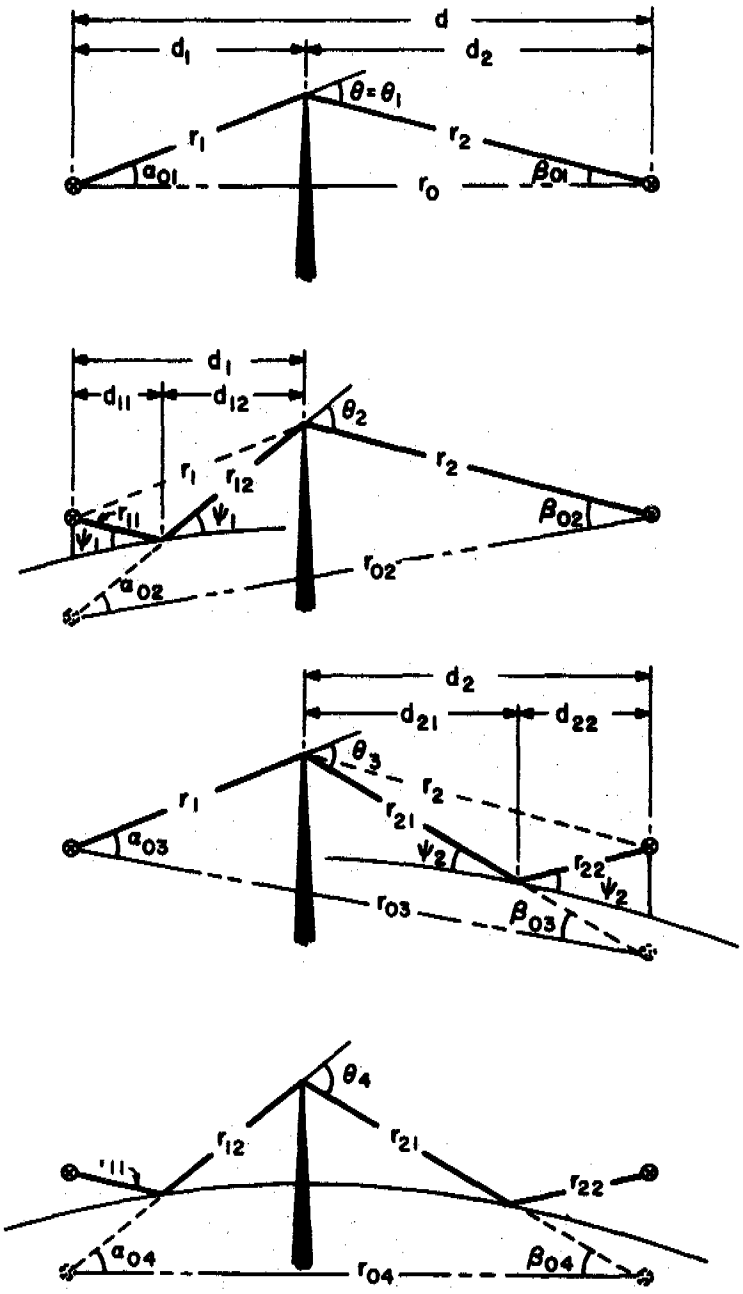

Figure III.9

CORNU'S SPIRAL

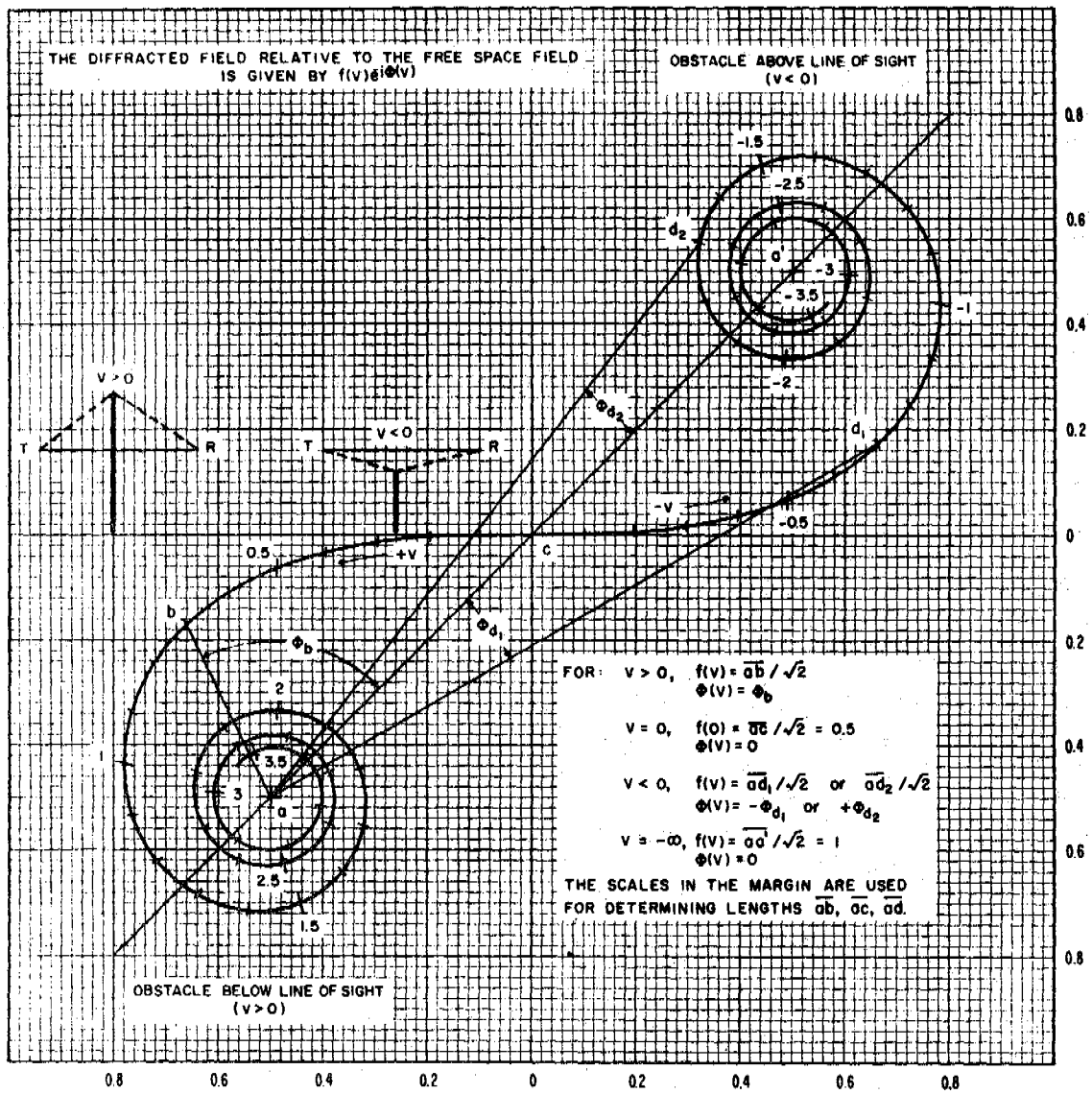

Figure III.10

III. 4 Parameters K and b° for Smooth Earth Diffraction

In section 8, the parameters K and b° are shown on figures 8.1 and 8.2 for horizontally and vertically polarized waves for poor, average, and good ground, and for sea water.

Assume a homogeneous ground in which the relative dielectric constant ϵ and conductivity σ of the ground are everywhere constant. K and b° are defined as follows:

For horizontal polarization,

$$K_h = 1.7778 \times 10^{-2} C_o f^{-\frac{1}{3}} [(\epsilon - 1)^2 + x^2]^{-1/4} \qquad \text{(III. 40a)}$$

$$b_h = 180^\circ - \tan^{-1}\left(\frac{\epsilon - 1}{x}\right) \quad \text{degrees} . \qquad \text{(III. 40b)}$$

For vertical polarization,

$$K_v = (\epsilon^2 + x^2)^{1/2} K_h \qquad \text{(III. 41a)}$$

$$b_v = 2 \tan^{-1}(\epsilon/x) - \tan^{-1}\left(\frac{\epsilon - 1}{x}\right) \quad \text{degrees} \qquad \text{(III. 41b)}$$

where x depends on the ground conductivity σ, in mhos per meter, and the radio frequency f, in megacycles per second, and has been defined by (III. 7) as

$$x = 1.8 \times 10^4 \sigma / f$$

C_o is defined in section 8 as

$$C_o = (8497/a)^{\frac{1}{3}}$$

where a is the effective earth's radius in kilometers.

When $\sigma/f >> (\epsilon/2) \times 10^{-4}$, the parameters K and b° may be written as

$$K_h \simeq 1.325 \times 10^{-4} C_o f^{1/6} \sigma^{-1/2} , \quad b_h \simeq 180^\circ \qquad \text{(III. 42)}$$

$$K_v \simeq 2.385 C_o \sigma^{1/2} f^{-5/6} , \quad b_v \simeq 0^\circ \qquad \text{(III. 43)}$$

and when $\sigma/f << (\epsilon/2) \times 10^{-4}$, the parameters K and b° may be written as

$$K_h \simeq 1.7778 \times 10^{-2} C_o f^{-\frac{1}{3}} (\epsilon - 1)^{-1/2} , \quad b_h \simeq 90^\circ \qquad \text{(III. 44)}$$

$$K_v \simeq \epsilon K_h , \quad b_v \simeq 90^\circ \qquad \text{(III. 45)}$$

III.5 Forward Scatter

The attenuation function $F(\theta d)$ for $N_s = 250$, 301, 350, and 400, shown in figure 9.1, may be used for most land-based scatter links. When a path is highly asymmetrical, the attenuation for a given value of θd is less than it would be for a symmetrical path. Figures III.11 to III.14 show the function $F(\theta d)$ for values of s from 0.01 to 1, and for $N_s = 250$, 301, 350 and 400. For values of $\theta d \leq 10$, the effect of asymmetry is negligible, but increases with increasing θd, particularly when $s < 0.5$.

For values of s between 0.7 and 1, the function $F(\theta d)$ for $N_s = 301$ may be computed as follows:

$$\text{for} \quad 0.01 \leq \theta d \leq 10, \qquad F(\theta d) = 135.82 + 0.33\,\theta d + 30 \log(\theta d) \tag{III.46}$$

$$\text{for} \quad 10 \leq \theta d \leq 70, \qquad F(\theta d) = 129.5 + 0.212\,\theta d + 37.5 \log(\theta d) \tag{III.47}$$

$$\text{for} \quad \theta d \geq 70, \qquad F(\theta d) = 119.2 + 0.157\,\theta d + 45 \log(\theta d). \tag{III.48}$$

The function $F(\theta d)$ may be obtained for any value of N_s, by modifying the value computed for $N_s = 301$:

$$F(\theta d, N_s) = F(\theta d, N_s = 301) - \left[0.1\,(N_s - 301)\, e^{-\theta d/40}\right].$$

The frequency gain function, H_o, for the special case $h_{te} = h_{re}$ frequently used in systems design, is shown as a function of r on figures III.15 to III.19 for $\eta_s = 1$, 2, 3, 4, 5, and for $s = 1$, 0.5, 0.25 and 0.1. In this case, no correction factor ΔH_o is required.

The function H_o for $\eta_s = 0$, shown on figure 9.5 corresponds to the assumption of a constant atmospheric refractive index. Except for the special case where $h_{te} = h_{re}$ this function may be computed as follows:

$$H_o(\eta_s = 0) = 10 \log \left\{ \frac{2(1 - h_{re}^2/h_{te}^2)}{r_2^2\,[h(r_1) - h(r_2)]} \right\} \tag{III.49}$$

where $r_1 = 4\pi\theta h_{te}/\lambda$; $r_2 = 4\pi\theta h_{re}/\lambda$,

$$h(r_1) = r_1 f(r_1) , \quad f(r_1) = Ci(r_1) \sin r_1 + [\pi/2 - Si(r_1)] \cos r_1 \qquad \text{(III. 50)}$$

and

$$h(r_2) = r_2 f(r_2) , \quad f(r_2) = Ci(r_2) \sin r_2 + [\pi/2 - Si(r_2)] \cos r_2$$

$$Ci(r) = \int_{\infty}^{r} \frac{\cos t}{t} \, dt , \quad Si(r) = \int_{0}^{r} \frac{\sin t}{t} \, dt . \qquad \text{(III. 51)}$$

Values of the sine integral Si(r) and the cosine integral Ci(r) for arguments from 10 to 100 are tabulated in volume 32 of the U. S. NBS Applied Math Series [1954]. See also [NBS AMS 1964]. The function h(r) is shown graphically in figures III.20 and III.21.

For the special case of equal effective antenna heights, $h_{te} = h_{re}$, equation (III.49) is not applicable. In this case $H_o(\eta_s = 0)$ is computed as:

$$H_o(\eta_s = 0) = 10 \log \left\{ \frac{4}{r^2 [h(r) - r\, g(r)]} \right\} \qquad \text{(III. 52)}$$

where

$$g(r) = Ci(r) \cos r - [\pi/2 - Si(r)] \sin r \qquad \text{(III. 53)}$$

When the effective height of one antenna is very much greater than that of the other, the computation may be simplified as follows:

$$\text{For } r_2 << r_1, \quad H_o(\eta_s = 0) = 10 \log \left\{ \frac{2}{r_2^2 [1 - h(r_2)]} \right\} \qquad \text{(III. 54a)}$$

$$\text{For } r_2 >> r_1, \quad H_o(\eta_s = 0) = 10 \log \left\{ \frac{2}{r_1^2 [1 - h(r_1)]} \right\} . \qquad \text{(III. 54b)}$$

THE FUNCTION $F(\theta d)$ FOR $N_s = 250$

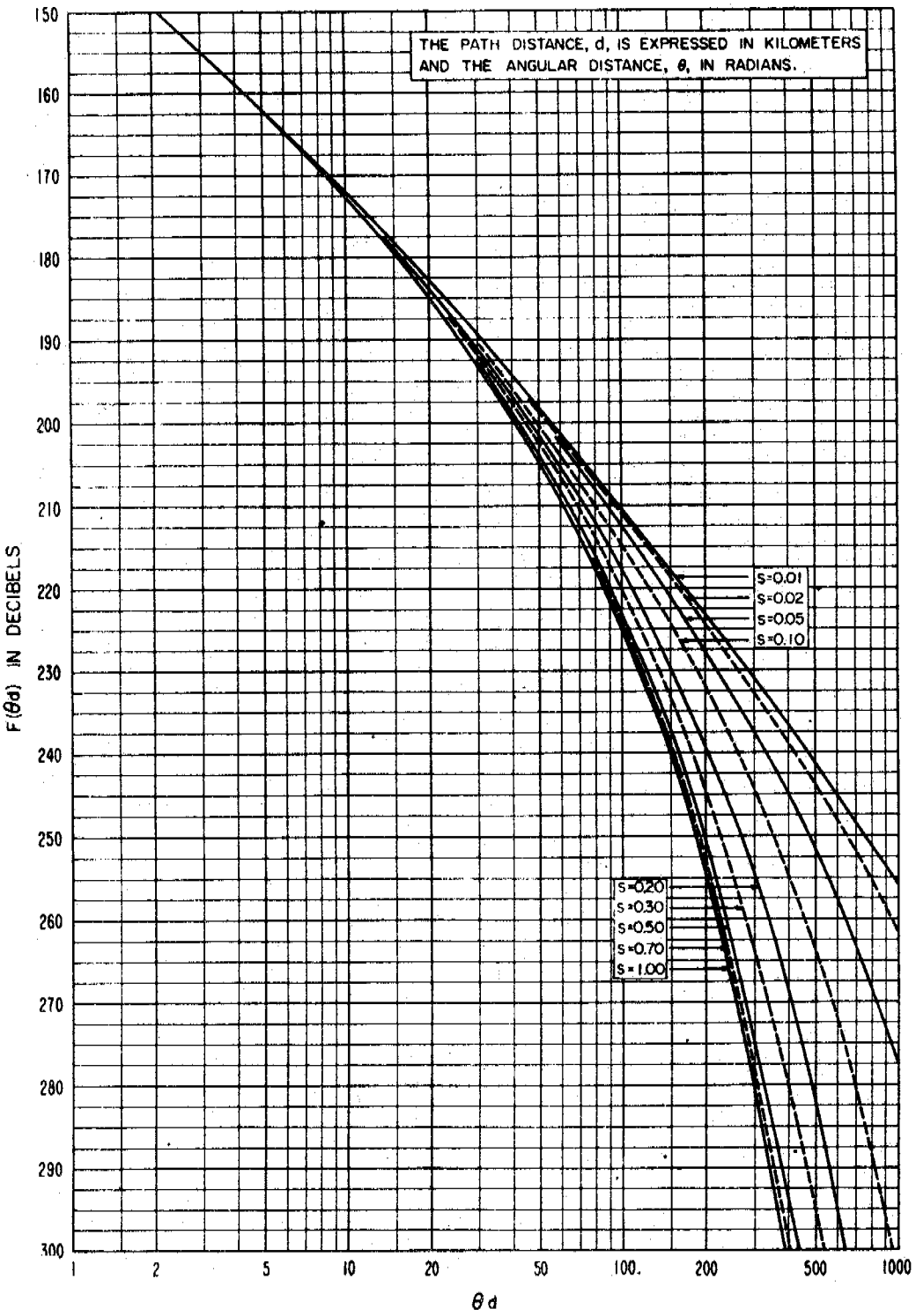

Figure III.11

THE FUNCTION $F(\theta d)$ FOR $N_S = 301$

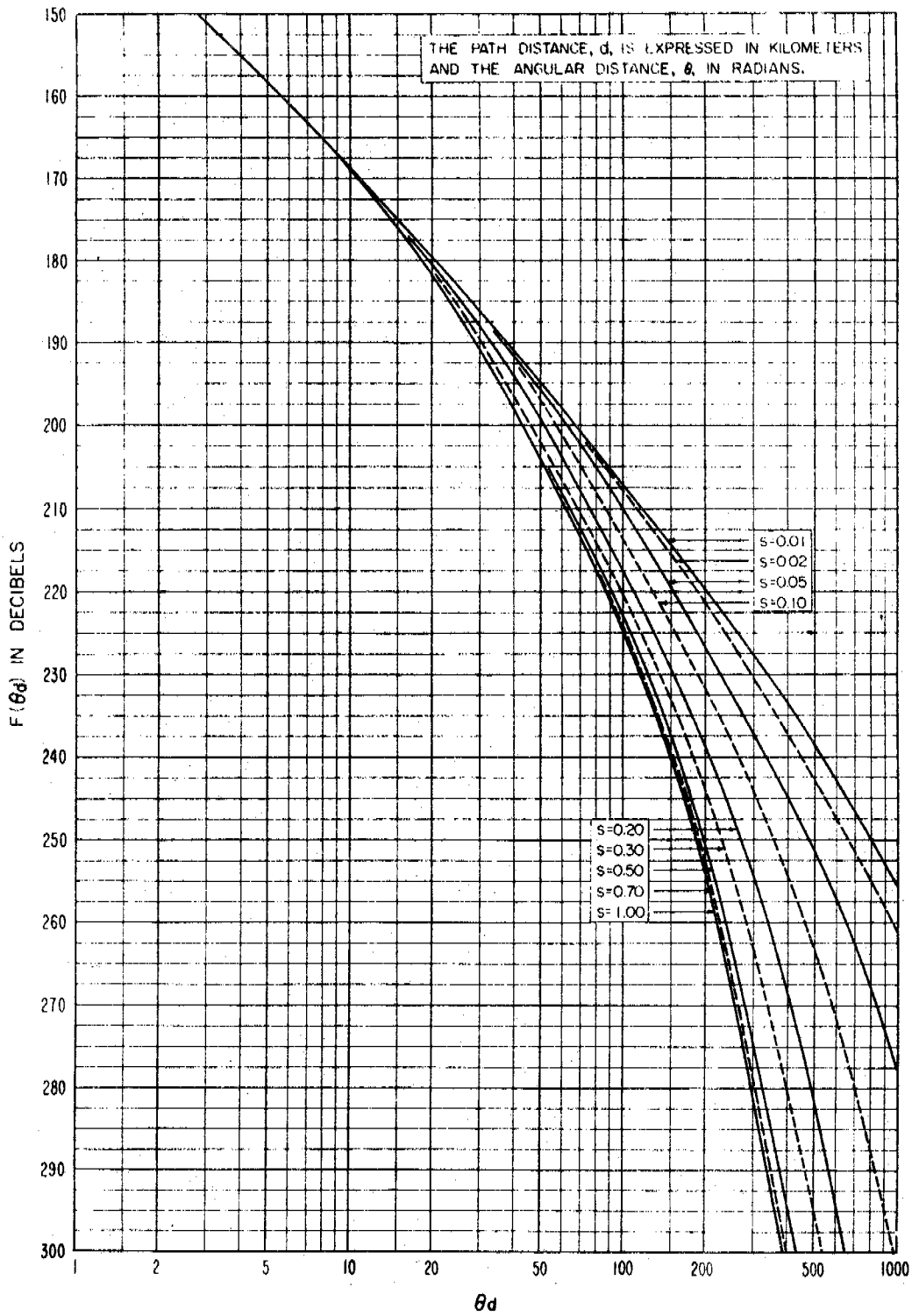

Figure III.12

THE FUNCTION $F(\theta d)$ FOR $N_S = 350$

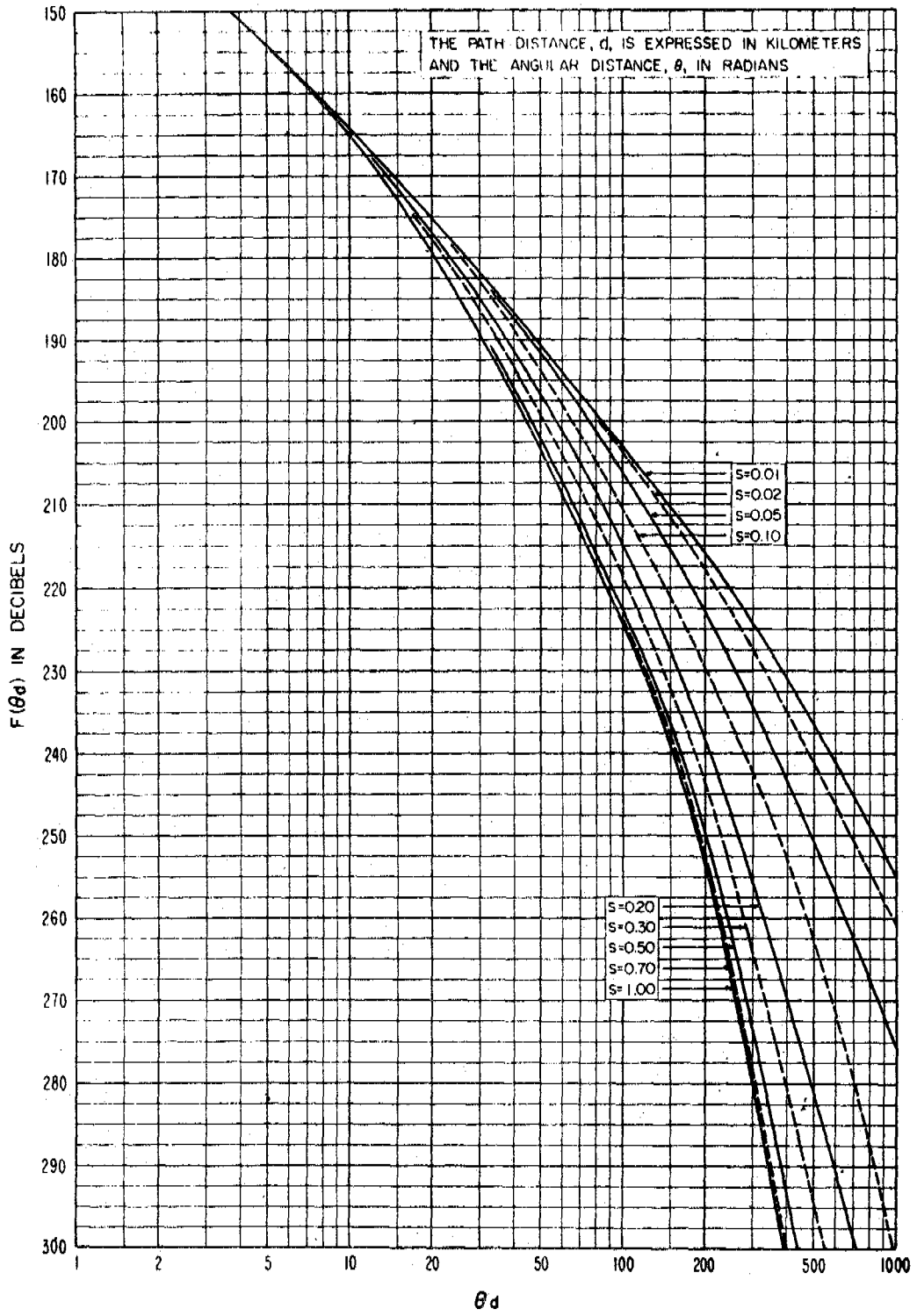

Figure III.13

THE FUNCTION $F(\theta d)$ FOR $N_s = 400$

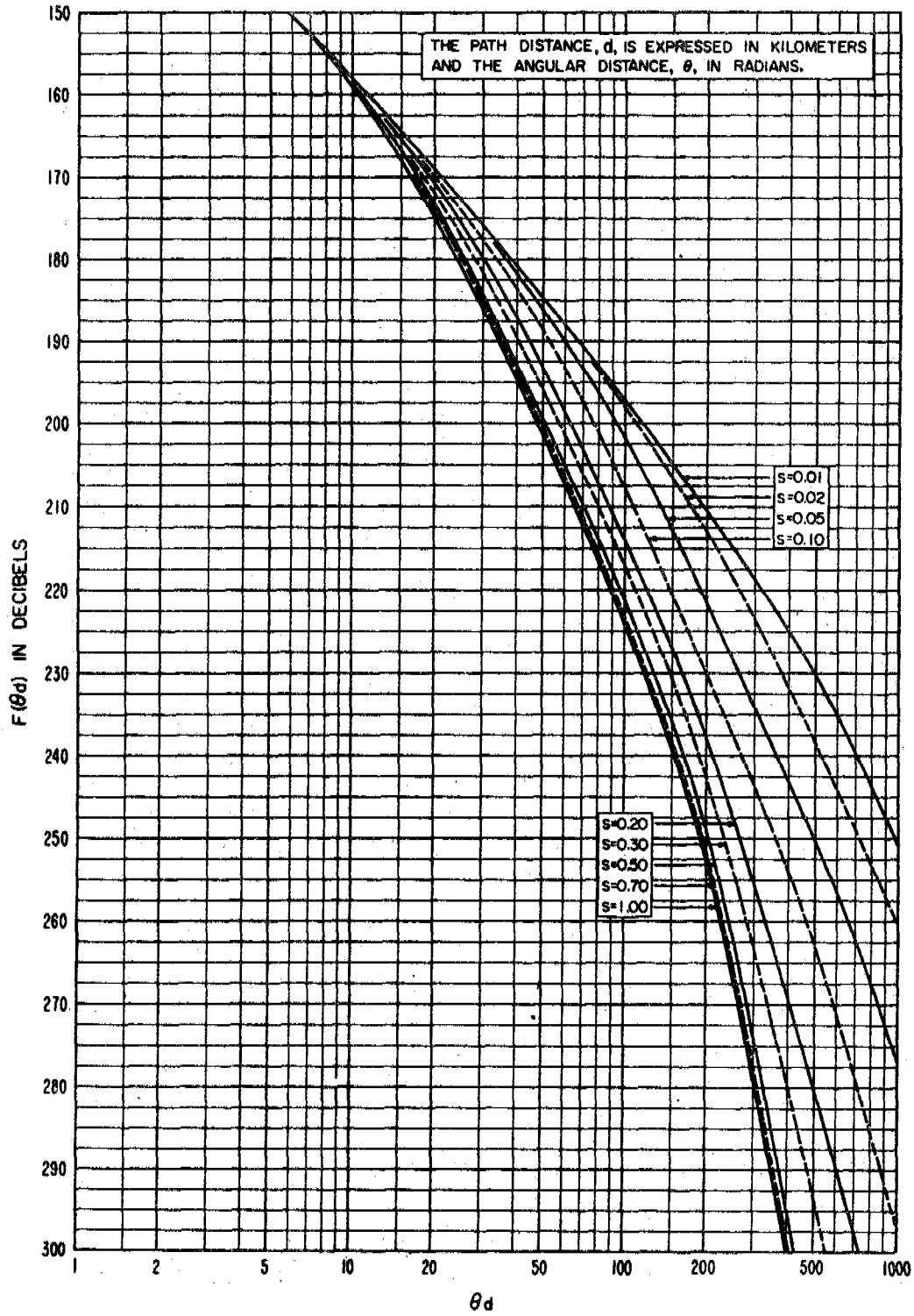

Figure III.14

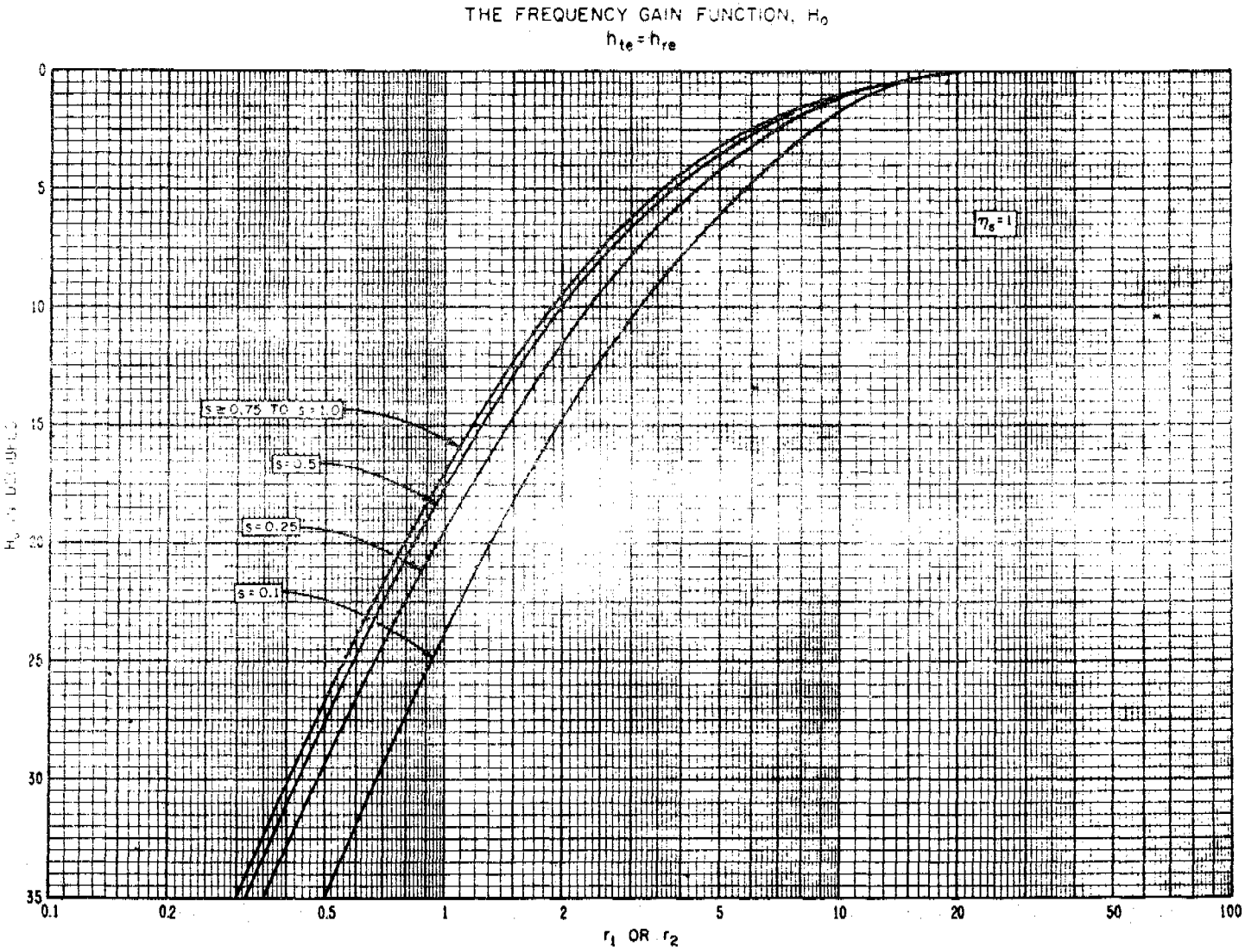

Figure III.15

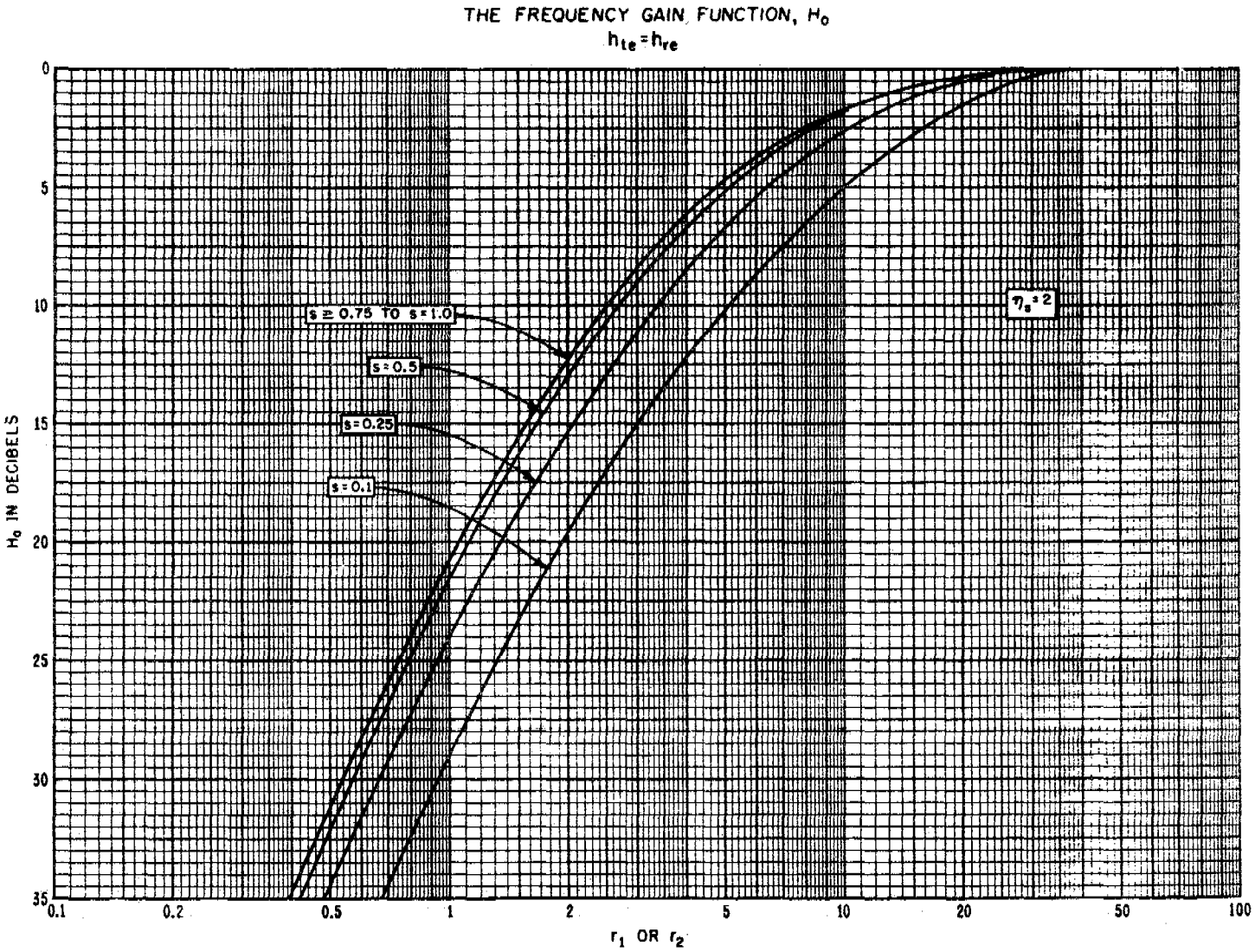

Figure III.16

THE FREQUENCY GAIN FUNCTION, H_o
$h_{te} = h_{re}$

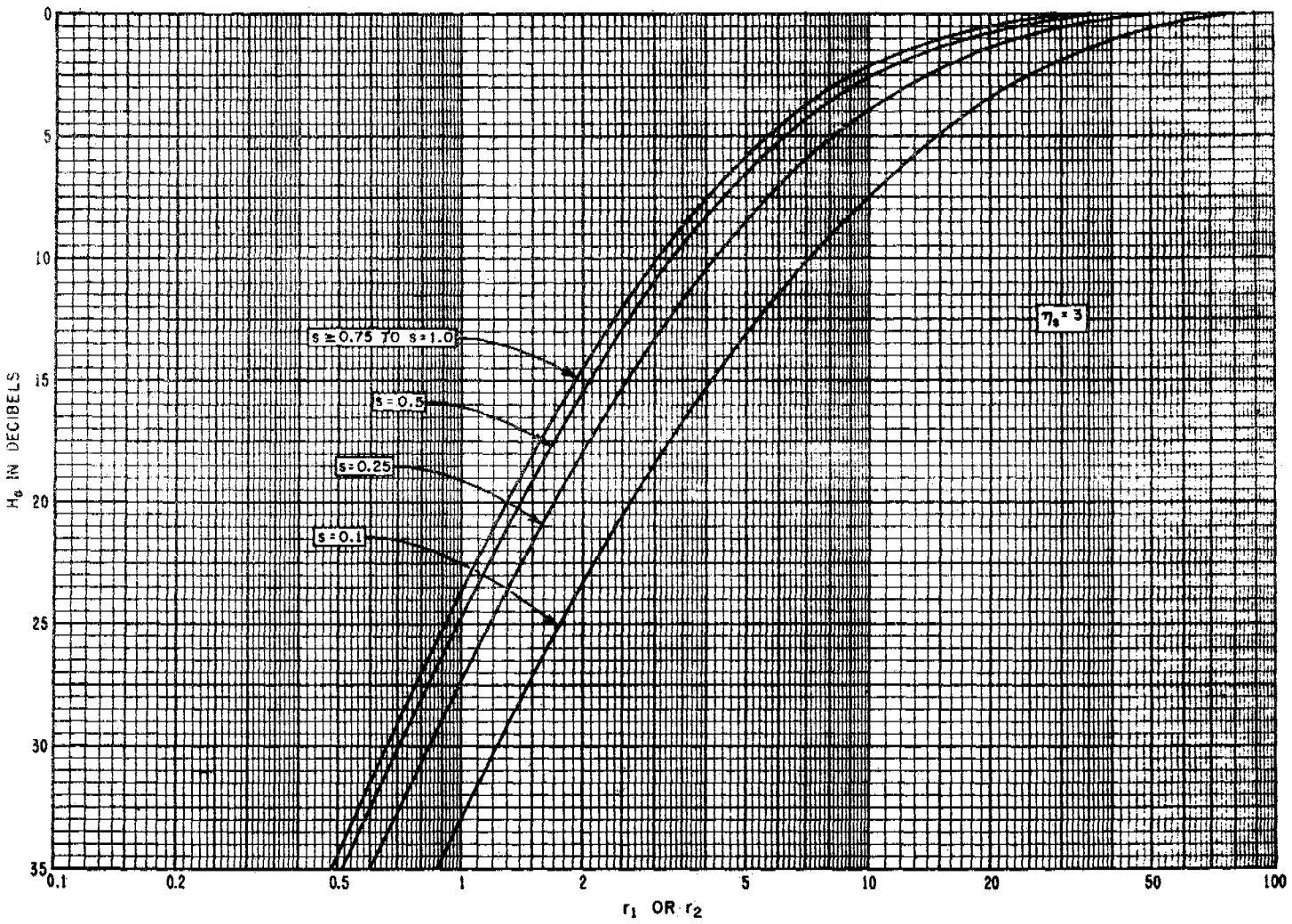

Figure III.17

THE FREQUENCY GAIN FUNCTION, H_o
$h_{te} = h_{re}$

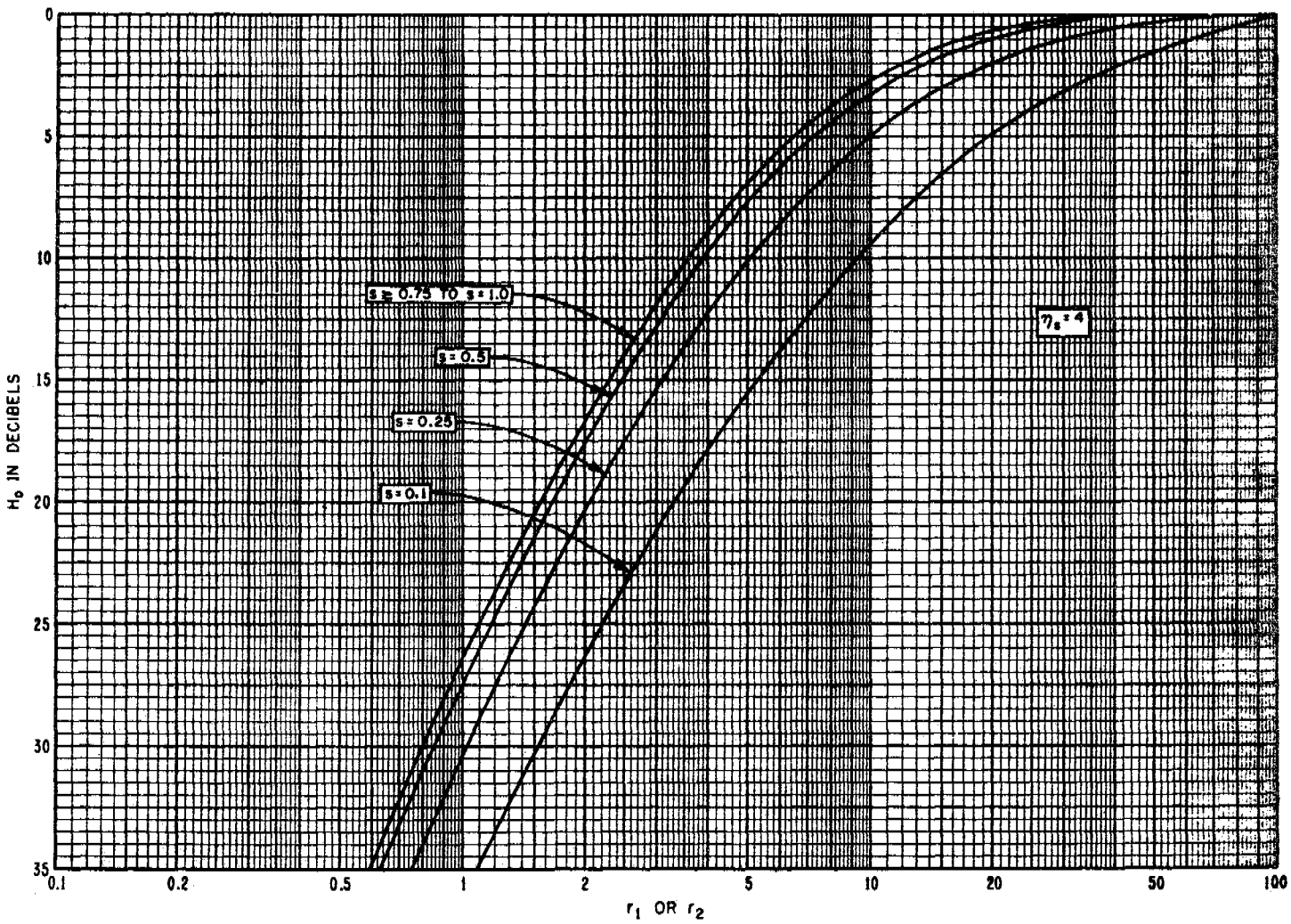

Figure III.18

THE FREQUENCY GAIN FUNCTION, H_o
$h_{te} = h_{re}$

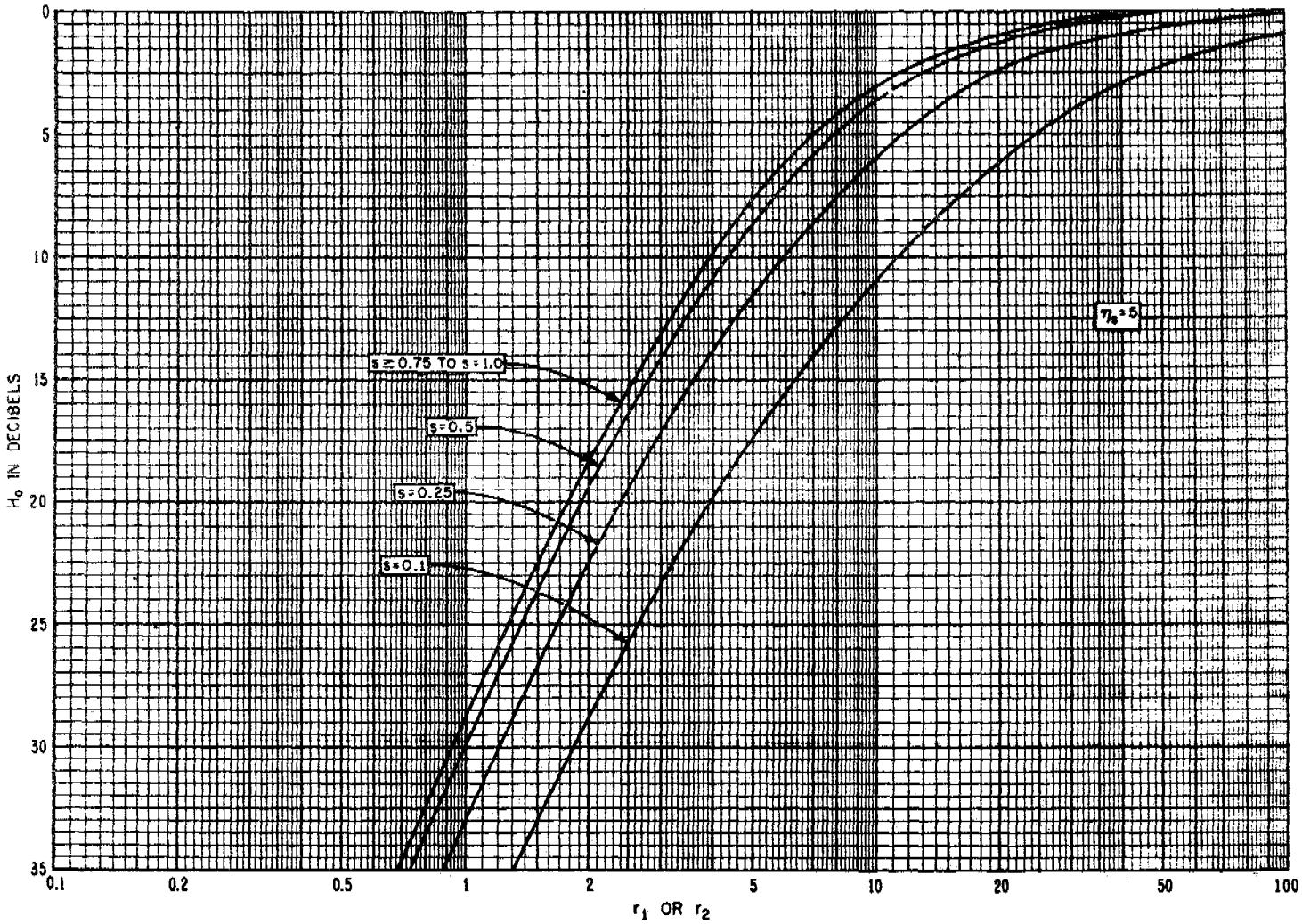

Figure III.19

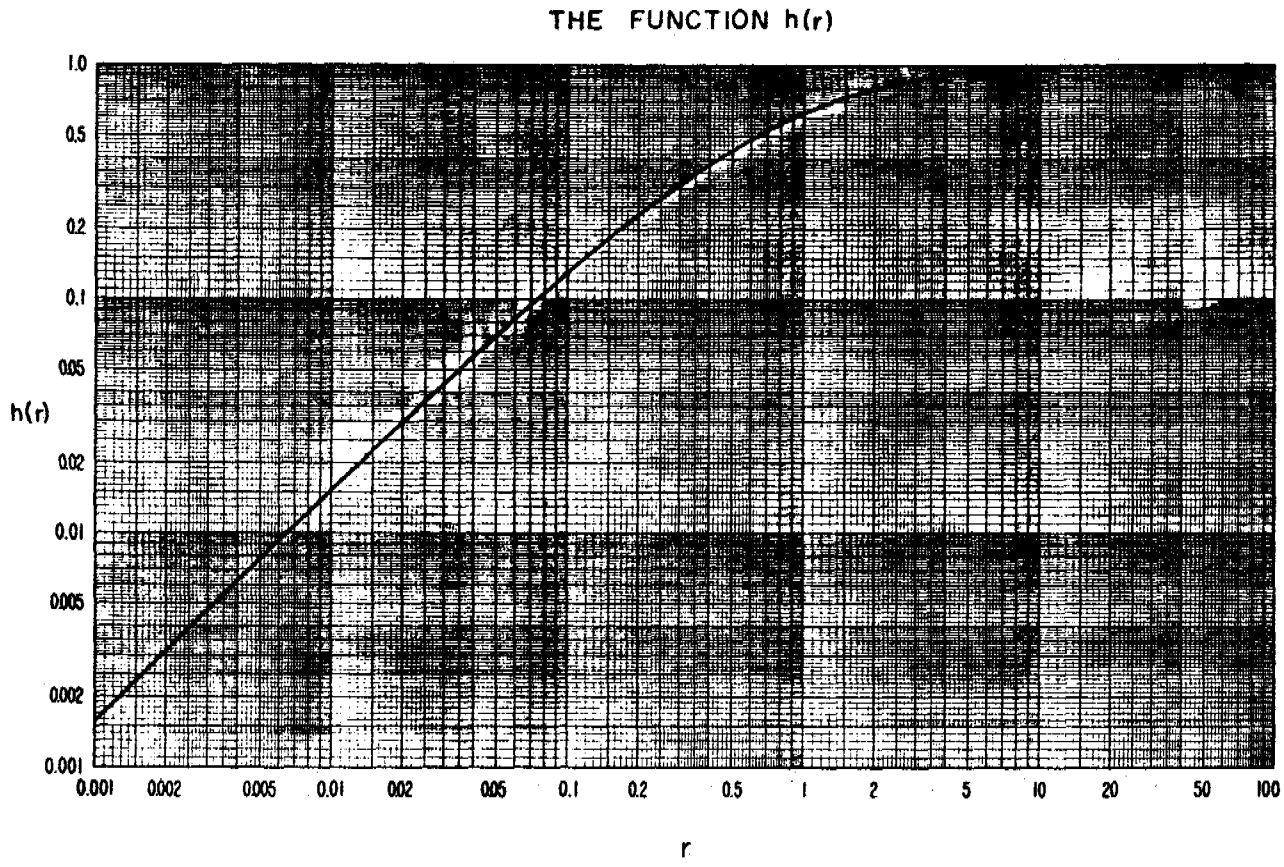

Figure III.20

THE FUNCTION h(r)

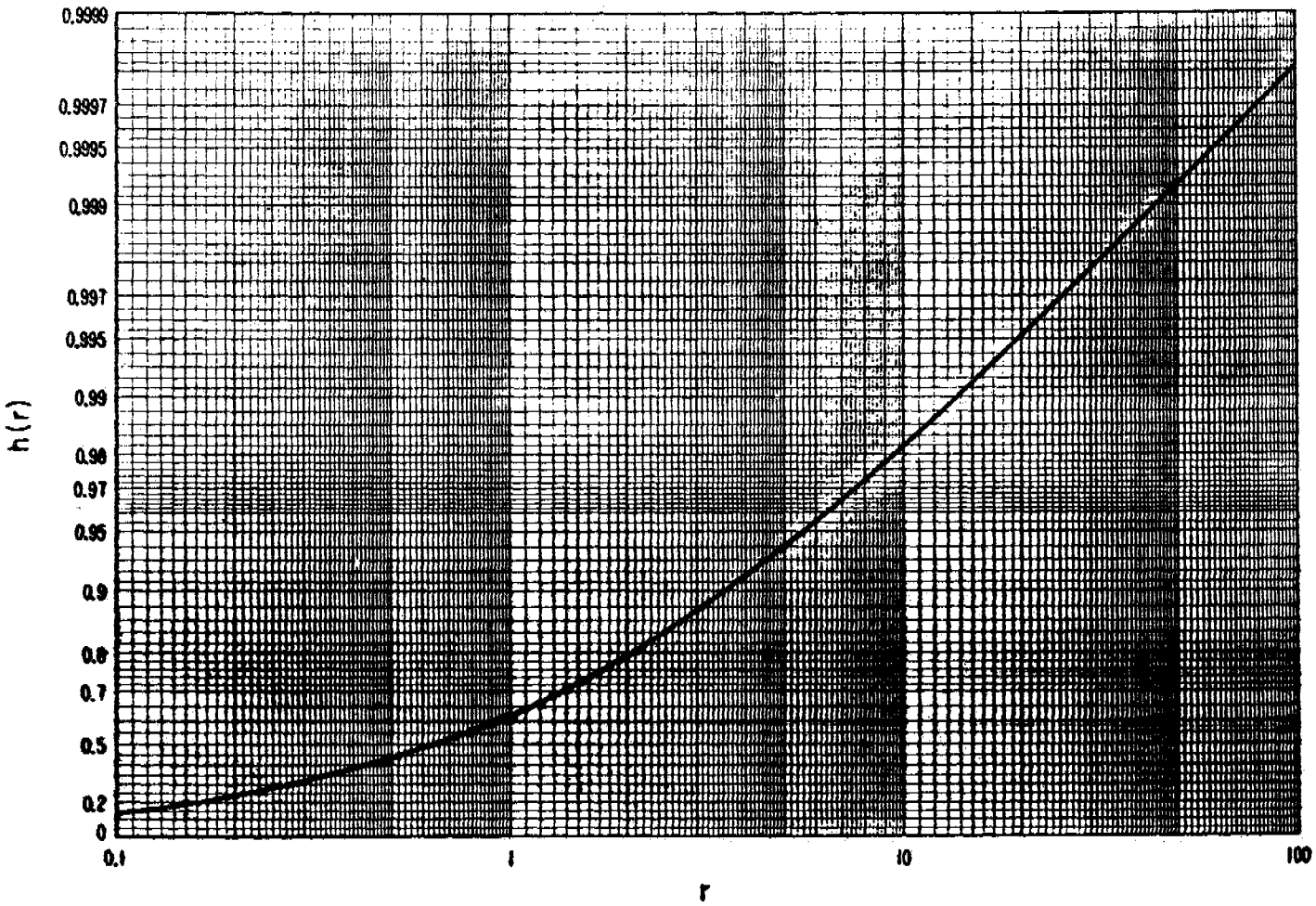

Figure III.21

III.6 Transmission Loss with Antenna Beams Elevated or Directed Out of the Great Circle Plane

The methods of section 9 may be modified to calculate a reference value of long-term median transmission loss when antenna beams are either elevated or directed away from the great circle path between antennas. For many applications, the average transmission loss between antennas with random relative orientation is about 10 db more than the basic transmission loss, which assumes zero db antenna gains.

Figure III.22 shows scattering subvolumes at intersections of antenna main beams and side lobes. A "scatter" theory assumes that the total power available at a receiver is the sum of the powers available from many scattering subvolumes. For high gain antennas, the intersection of main beams defines the only important scattering volume. In general, all power contributions that are within 10 db of the largest one should be added.

For a total radiated power w_t:

$$w_a/w_t = 10^{-0.1\,L_{sr}}, \quad w_{ai}/w_t = 10^{-0.1\,L_i} \tag{III.55}$$

where L_{sr} is the transmission loss and L_i is the loss associated with the ith power contribution, w_{ai}:

$$L_{sr} = -10 \log (w_a/w_t) = -10 \log \sum_i 10^{-0.1\,L_i} \tag{III.56}$$

$$L_i = 30 \log f - 20 \log (d^2/r_o) + F(\theta_{ei} d) - F_{oi} + H_{oi} + A_a - G_{ti} - G_{ri} + L_{gi} . \tag{III.57}$$

In (III.57) f, d, and A_a are defined as in (9.1) and the other terms are related to similar terms in (9.1). If the effective scattering angle θ_{ei} for the ith intersection is equal to the minimum scattering angle θ, then $F(\theta_{ei} d)$, F_{oi}, H_{oi} are equal to $F(\theta d)$, F_o, and H_o, and $G_{ti} + G_{ri} - L_{gi} = G_p$. Note that a term $20 \log(r_o/d)$ has been added in (III.57) to provide for situations where the straight line distance r_o between antennas is much greater than the sea-level arc distance d. Such differences occur in satellite communication.

Scattering planes, defined by the directions of incident and scattered energy, may or may not coincide with the plane of the great circle path. Each "scattering plane" is determined by the line between antenna locations and the axis of the stronger of the two intersecting beams, making an angle ζ with the great circle plane.

The free space directive gain patterns of the antennas are replaced by equivalent values for ease in computation. For an idealized pencil-beam antenna with a half-power beamwidth 2δ and a circular beam cross-section, the directive gain g is $4/\delta^2$, assuming that all of the power is radiated through the main beam and between the half-power points. An equivalent beam pattern with a square cross-section and a semi-beamwidth δ_o has a gain of π/δ_o^2, thus $\delta_o = \delta\sqrt{\pi/4}$, and the maximum free space gains are

$$G_t = 10 \log g_{to} = 4.97 - 10 \log \delta_{two}\, \delta_{tzo} \quad \text{db} \qquad \text{(III. 58a)}$$

$$G_r = 10 \log g_{ro} = 4.97 - 10 \log \delta_{rwo}\, \delta_{rzo} \quad \text{db} \qquad \text{(III. 58b)}$$

where the subscripts w and z refer to azimuthal and vertical angles. In most cases, δ_{wo} and δ_{zo} may be replaced by their geometric mean, $\delta_o = (\delta_{wo}\delta_{zo})^{1/2}$. The free space directive gain of a main beam may be measured or approximated as $g_o \simeq \pi/(2\,\delta_{wo}\delta_{zo})$. Gains for side lobes are determined from g_o and the ratios g_1/g_o, g_2/g_o, ..., which may be measured or calculated. The average gain g_b for other directions depends on the fraction of power radiated in those directions. For instance, if half the total power of a transmitter is radiated in these directions, and if the polarization coupling loss, L_{cp}, is 3 db, then

$$G_{bt} - L_{cp} = -6 \text{ db}$$

since the definition of the directive gain, G_{bt}, assumes for every direction the receiving antenna polarization appropriate for maximum power transfer.

Figure III.23 shows an antenna power pattern in several different ways, including a Mercator projection of the surface of a unit sphere.

The plane that determines the "bottom" of a beam is perpendicular to the great circle plane and forms an angle ψ_i with a horizon plane:

$$\psi_{ti} = \theta_{bti} - \theta_{et}\,, \qquad \psi_{ri} = \theta_{bri} - \theta_{er} \qquad \text{(III. 59)}$$

where θ_b is the angle of elevation of the lower half-power point of a beam above the horizontal, and θ_{et} is defined in section 6. If an antenna beam is elevated sufficiently so that ray bending may be neglected, the angles α_e and β_e are denoted α_{eo} and β_{eo}:

(III. 60)

where ζ is the angle away from the great circle plane. The angles α_{oo} and β_{oo} are defined as in section 6 using the actual radius, $a_o \simeq 6370$ km, instead of an effective radius a.

When ray bending must be considered, the equations for α_e and β_e are

$$\alpha_e = \alpha_{eo} + \tau\left(\theta_{bt}, \frac{d_{Lt}\sec\zeta}{2}, N_s\right) - \tau\left(\theta_{bt}, \frac{d\sec\zeta}{2}, N_s\right) \qquad \text{(III.61a)}$$

$$\beta_e = \beta_{eo} + \tau\left(\theta_{br}, \frac{d_{Lr}\sec\zeta}{2}, N_s\right) - \tau\left(\theta_{br}, \frac{d\sec\zeta}{2}, N_s\right) \qquad \text{(III.61b)}$$

where $\tau(\theta_b, d, N_s)$ is the bending of a radio ray which takes off at an angle θ_b above the horizontal and travels d kilometers through an atmosphere characterized by a surface refractivity N_s. The ray bending τ may be determined using methods and tables furnished by Bean and Thayer [1959]. For short distances, d, or large angles, θ_b, τ is negligible. If θ_b is less than 0.1 radians, the effective earth's radius approximation is adequate for determining τ,

$$\tau\left(\theta_b, \frac{d\sec\zeta}{2}, N_s\right) = \frac{d}{a_o}\left[1 - a_o/a(N_s)\right] . \qquad \text{(III.62)}$$

The reference value of long-term median transmission loss L_{sr} is computed using (III.56) where the losses associated with several scattering subvolumes are computed using (III.57). The attenuation function $F(d\theta_{ei})$ is read from figure 9.1 or figures III.11 - III.14 as a function of θ_{ei}.

The generalized scattering efficiency term F_{oi} is

$$F_{oi} = 1.086(\eta_{se}/h_e)(2h_o - h_1 - h_e - h_{Lt} - h_{Lr}) \quad \text{db} \qquad \text{(III.63)}$$

where

$$\theta_e = \alpha_e + \beta_e , \quad s_e = \alpha_e/\beta_e , \quad h_e = s_e\, d\,\theta_e/(1+s_e)^2 , \quad \eta_{se} = \eta_s(h_e, N_s) \qquad \text{(III.64)}$$

and the other terms are defined in section 9. In computing the frequency gain function H_{oi}, if $\alpha_e > \alpha_o$ use $r_1 = \infty$, if $\beta_e > \beta_o$ use $r_2 = \infty$; then $H_{oi} = H_o + 3$ db. If both antennas are elevated above the horizon rays, $H_{oi} = 6$ db. Atmospheric absorption A_a is discussed in section 3. The gains G_{ti} and G_{ri} are the free space directive gains defined by (III.58), and the loss in gain L_{gi} is computed as shown in section 9 replacing η_o, s, δ, and θ by η_{se}, s_e, δ_e, and θ_e.

In computing long-term variability of transmission loss for beams elevated above the horizon plane, the estimates of V and Y given in section 10 should be reduced by the factor $f(\theta_h)$ shown in figure III.24, with $\theta_h = \theta_b$:

$$V_e(0.5, d_e) = V(0.5, d_e)\, f(\theta_h) \qquad \text{(III.65a)}$$

$$Y_e(q, d_e) = Y(q, d_e)\, f(\theta_h) \quad . \qquad \text{(III.65b)}$$

The angle θ_h used in (III.65) should be the elevation above the horizontal of the scattering subvolume corresponding to the minimum value of L_i.

SCATTERING SUBVOLUMES IN A SCATTERING PLANE

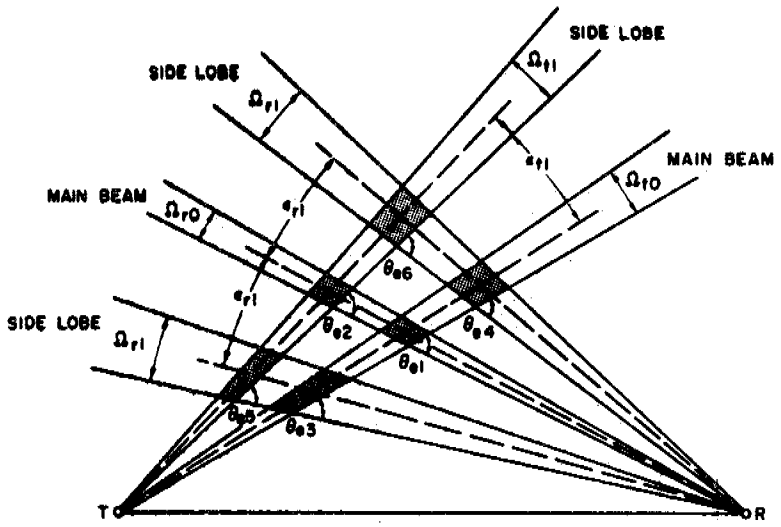

$\Omega = 2\delta$

ILLUSTRATION OF A SCATTERING PLANE CONTAINING THE MAIN BEAM OF THE RECEIVING ANTENNA

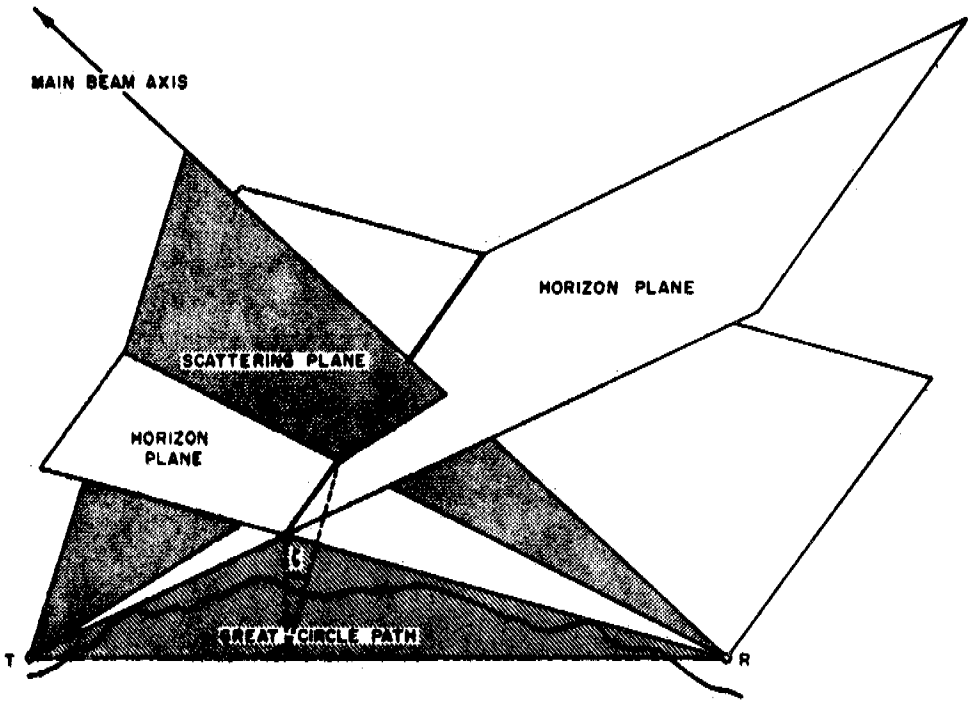

Figure III.22

FREE SPACE ANTENNA PATTERN

INTERSECTION OF AN EQUIVALENT ANTENNA POWER PATTERN WITH THE SURFACE OF A UNIT SPHERE

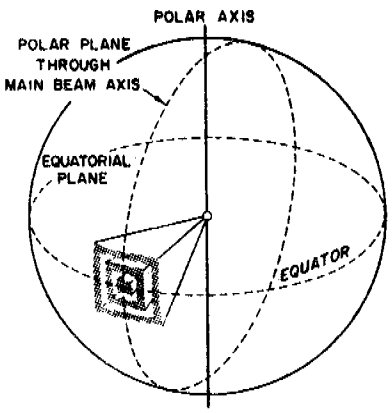

PATTERN PARAMETERS	
$\delta_{t0} = 0.04$	$\delta_{tw0} = 0.06$
$\delta_{tz1} = 0.02$	$\delta_{tw1} = 0.02$
$\delta_{tz2} = 0.02$	$\delta_{tw2} = 0.02$
$\epsilon_{tz1} = 0.12$	$\epsilon_{tw1} = 0.20$
$\epsilon_{tz2} = 0.22$	$\epsilon_{tw2} = 0.30$
$g_{t0} = 654.5$	$G_{t0} = 28.16$ db
$g_{t1} = 20.7$	$G_{t1} = 13.16$ db
$g_{t2} = 3.28$	$G_{t2} = 5.16$ db
$g_{bt} = 0.395$	$G_{bt} = -4.04$ db

ANTENNA VOLTAGE PATTERN. POLAR DIAGRAM IN THE EQUATORIAL PLANE

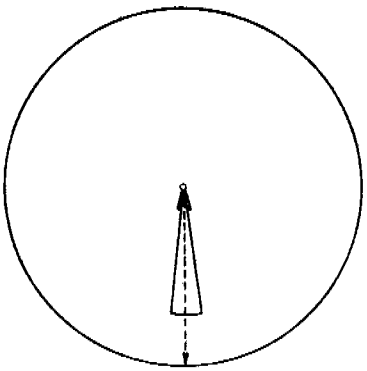

CARTESIAN DIAGRAM OF TRANSMITTING ANTENNA POWER PATTERN IN THE EQUATORIAL PLANE

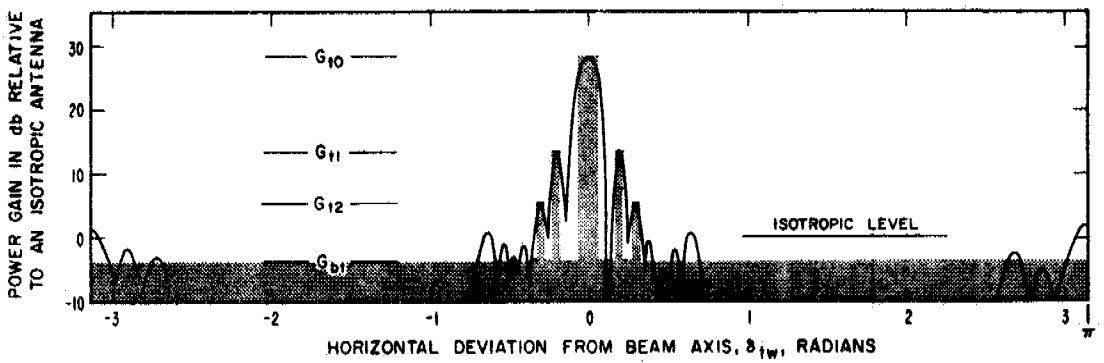

MERCATOR PROJECTION OF THE INTERSECTION OF THE EQUIVALENT TRANSMITTING ANTENNA POWER PATTERN WITH THE SURFACE OF A UNIT SPHERE

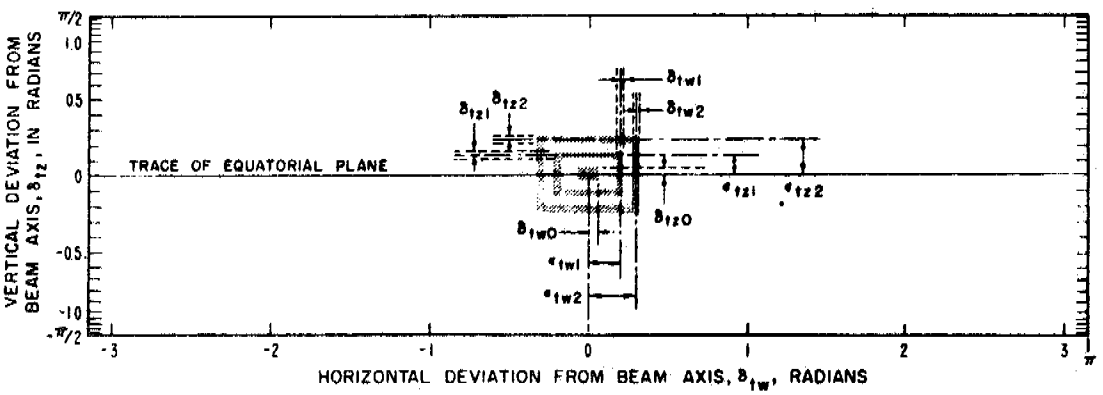

Figure III.23

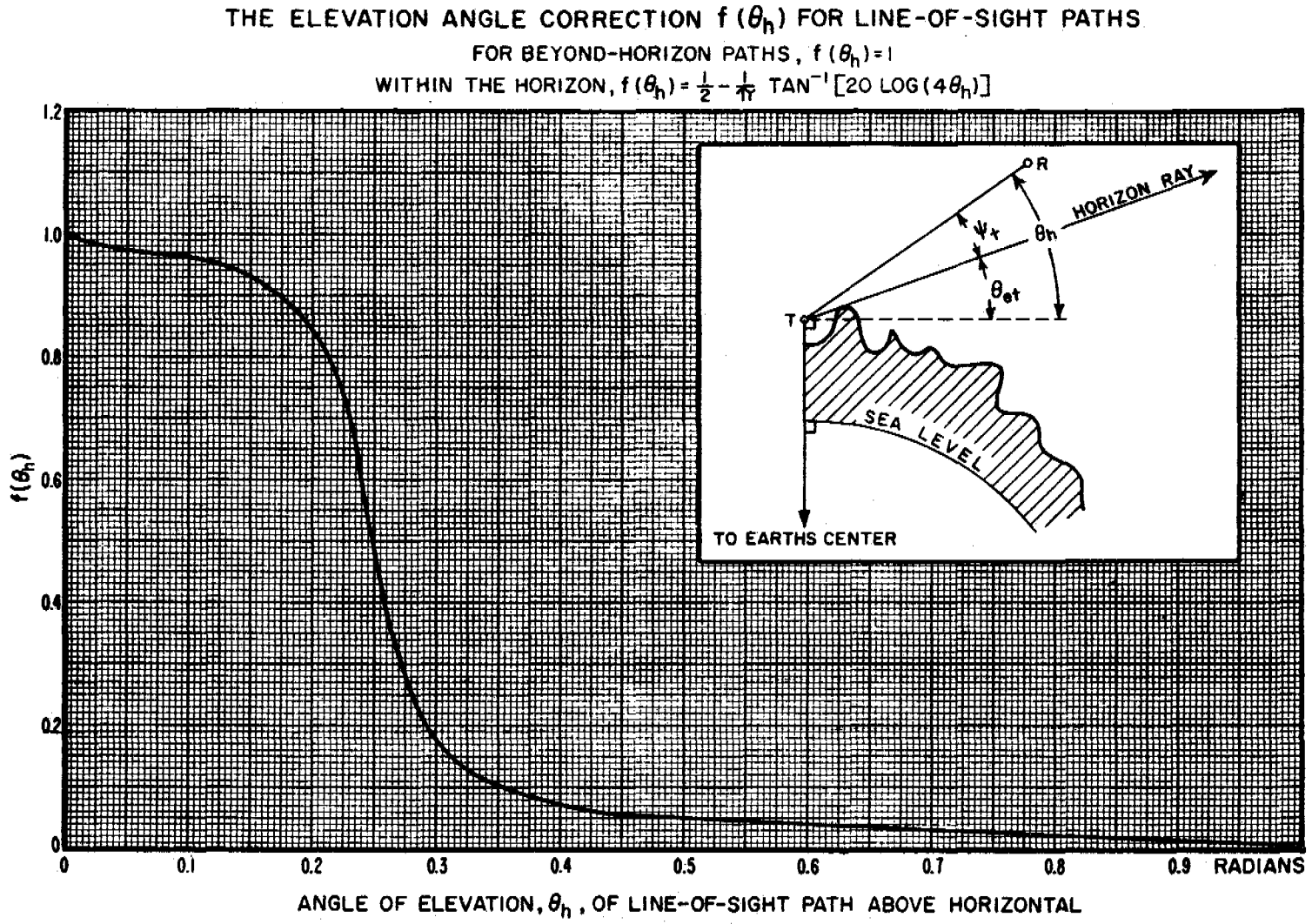

Figure III.24

III.7 Long-Term Power Fading

Long-term power fading is discussed in section 10. Figures 10.5 to 10.16 show empirical estimates of all-year variability for (1) continental temperate (2) maritime temperate overland and (3) maritime temperate oversea climates. The curves shown on these figures are based on a large amount of data. Estimates of variability in other climates are based on what is known about meteorological conditions and their effects on radio propagation, but have relatively few measurements to support them.

Figures III.25 to III.29 show curves of variability relative to the long-term median, prepared by the CCIR [1963 f] for the following climatic regions:

(4) Maritime Subtropical, Overland.

(5) Maritime Subtropical, Oversea.*

(6) Desert.

(7) Equatorial.

(8) Continental Subtropical.

In some cases, random path differences have undoubtedly been attributed to climatic differences. Available data were normalized to a frequency of 1000 MHz, and the curves correspond to this frequency. They show all-year variability $Y(q, d_e, 1000\ \text{MHz})$ about the long-term median as a function of the effective distance d_e defined by (10.3). Variability estimates for other frequencies are obtained by using the appropriate correction factor $g(f)$ shown in figure III.30:

$$Y(q) = Y(q, d_e, 1000\ \text{MHz})\ g(f). \qquad \text{(III.66)}$$

The empirical curves $g(f)$ are not intended as an estimate of the dependence of long-term variability on frequency, but represent an average of many effects that are frequency-sensitive, as discussed in section 10.

Variability about the long-term median transmission loss $L(0.5)$ is related to the long-term reference median L_{cr} by means of the function $V(0.5, d_e)$ shown on figure 10.1. The predicted long-term median transmission loss is then:

$$L(0.5) = L_{cr} - V(0.5, d_e) \qquad \text{(III.67)}$$

and the predicted value for any percentage of time is

$$L(q) = L(0.5) - Y(q). \qquad \text{(III.68)}$$

* Curves for climate 5 have been deleted. They were based on a very small amount of data. For hot, moist tropical areas use climate 4, and for coastal areas where prevailing winds are from the ocean, use climate 3.

III. 7. 1 Diurnal and Seasonal Variability in a Continental Temperate Climate

The curves shown in figures 10.5 to 10.16 and III.25 to III.29 represent variability about the long-term median for all hours of the day throughout the entire year. For certain applications, it is important to know something about the diurnal and seasonal changes that may be expected. Such changes have been studied in the continental United States, where a large amount of data is available. Measurement programs recorded VHF and UHF transmission loss over particular paths for at least a year to determine seasonal variations. Data were recorded over a number of paths for longer periods of time to study year-to-year variability.

As a general rule, transmission loss is less during the warm summer months than in winter, and diurnal trends are usually most pronounced in summer, with maximum transmission loss occurring in the afternoon. The diurnal range in signal level may be about 10 db for paths that extend just beyond the radio horizon, but is much less for very short or very long paths. Variation with season usually shows maximum losses in mid-winter, especially on winter afternoons, and high fields in summer, particularly during morning hours. Transmission loss is often much more variable over a particular path in summer than it is during the winter, especially when ducts and elevated layers are relatively common.

The data were divided into eight "time blocks" defined in table III. 1. The data were assumed to be statistically homogeneous within each of the time blocks. With more and shorter time blocks, diurnal and seasonal trends would be more precisely defined, except that no data would be available in some of the time blocks over many propag ation paths. Even with the division of the year into winter and summer and the day into four periods as in table III.1, it is difficult to find sufficient data to describe the statistical characteristics expected of transmission loss in Time Blocks 7 and 8.

Table III. 1

Time Blocks

No.	Months	Hours
1	Nov. - Apr.	0600 - 1300
2	Nov. - Apr.	1300 - 1800
3	Nov. - Apr.	1800 - 2400
4	May - Oct.	0600 - 1300
5	May - Oct.	1300 - 1800
6	May - Oct.	1800 - 2400
7	May - Oct.	0000 - 0600
8	Nov. - Apr.	0000 - 0600

In some applications, it is convenient to combine certain time blocks into groups, for instance, some characteristics of long-term variability are significantly different for the winter group (Time Blocks 1, 2, 3, 8) than for the summer group (Time Blocks 4, 5, 6, 7).

In other climatic regions, if the annual range of monthly average values of N_s is less than 20 N units (figure III.31), seasonal variations are expected to be negligible. One would also expect less diurnal change, for example, in a maritime temperate climate where changes in temperature during the day are less extreme. In climates where N_s changes considerably throughout the year, the consecutive 4-6 month period when N_s is lowest may be assumed to correspond to "winter", whatever months may be involved.

For the U.S. only, the parameter $V(0.5, d_e)$ for each of the eight time blocks and for "summer" and "winter" is shown in figure III.32. Curves of the variability $Y(q, d_e, 100\ \text{MHz})$ about the long-term median for each of these times of day and seasons are shown in figures III.33 to III.42. These curves are drawn for a frequency of 100 MHz. Figures III.33 and III.34 show the range 0.01 to 0.99 of $Y(q, d_e, 100\ \text{MHz})$ for the winter time blocks, 1, 2, 3, 8 and the summer time blocks 4, 5, 6, 7. Each group of data was analyzed separately. Some of the differences shown between time blocks 1, 2, 3, and 8 are probably not statistically significant. Marked differences from one time block to another are observed during the summer months.

Figures III.35 through III.42 show data coded in the following frequency groups, 88-108, 108-250 and 400 to 1050 MHz as well as curves for $Y(q)$ drawn for 100 MHz. In general these figures show more variability in the two higher frequency groups especially during "summer" (time blocks 4, 5, 6 and 7). Because of the relatively small amount of data no attempt was made to derive a frequency factor $g(q, f)$ for individual time blocks.

The curves for summer, winter, and all hours shown in figures 10.13 through 10.22 represent a much larger data sample, since time block information was not available for some paths for which summer or winter distributions were available.

The smooth curves of $V(0.5, d_e)$ and $Y(q, d_e, 100\ \text{MHz})$ versus d_e shown in figures 10.13, 10.14, III.25 to III.29 and III.32 to III.42 may be represented by an analytic function of the general form:

$$\left.\begin{matrix} V(0.5) \\ Y(0.1) \\ -Y(0.9) \end{matrix}\right\} = \left[c_1 d_e^{n_1} - f_2(d_e) \right] \exp\left(- c_3 d_e^{n_3}\right) + f_2(d_e) \qquad \text{(III.69)}$$

where

$$f_2(d_e) = f_\infty + (f_m - f_\infty) \exp\left(-c_2 d_e^{n_2}\right) \qquad \text{(III.70)}$$

The terms c_1, c_2, c_3, n_1, n_2, n_3, f_m, and f_∞ in (III.69) and (III.70) are constants for any given time block and value of q. The parameters f_m and f_∞ are maximum and asymptotic values, respectively. Tables III.2 to III.4 list values of the eight parameters required in (III.69) to obtain $V(0.5, d_e)$, $Y(0.1, d_e, 100\ \text{MHz})$ and $-Y(0.9, d_e, 100\ \text{MHz})$ for the eight time blocks in table III.1, and for summer, winter, and all hours. The constants given

in Tables III.2 to III.4 for summer, winter and all hours were determined using only radio paths for which time block information is available. They do not yield the curves shown in figures 10.13 and 10.14 of section 10, which represent a much larger data sample.

Tables III.5 to III.7 list values of the eight parameters in (III.69) required to compute $V(0.5)$, $Y(0.1, d_e, f_{MHz})$ and $Y(0.9, d_e, f_{MHz})$ for each of the climatic regions discussed in section 10, Volume 1, and section III.7 of this annex.

TABLE III.2

Constants for Calculating $V(0.5, d_e)$

Time Block	c_1	$\frac{d_e \text{ in km.}}{c_2}$	c_3	n_1	n_2	n_3	f_m	f_∞
4	1.35^{-6}	5.02^{-18}	1.32^{-7}	2.80	6.74	3.08	5.2	4.0
5	1.05^{-6}	5.02^{-18}	4.14^{-9}	2.70	6.74	3.70	2.4	1.8
6	2.04^{-4}	6.61^{-18}	2.82^{-9}	1.87	6.67	3.76	5.2	4.2
7	8.00^{-4}	3.91^{-16}	1.20^{-5}	1.68	5.94	2.25	7.1	5.6
S*	1.18^{-5}	6.72^{-17}	1.65^{-6}	2.40	6.32	2.61	5.1	4.0
1	2.11^{-4}	3.44^{-17}	1.73^{-4}	1.67	6.52	1.82	1.2	0.5
3	3.47^{-4}	3.76^{-14}	5.42^{-4}	1.60	5.30	1.58	1.3	0.6
8	3.63^{-4}	1.80^{-23}	1.55^{-5}	1.65	8.91	2.36	1.95	0.8
W*	1.40^{-3}	1.79^{-34}	1.05^{-5}	1.27	13.23	2.51	1.05	0.5
A*	1.63^{-4}	1.81^{-25}	8.12^{-6}	1.80	9.59	2.32	3.0	1.9

* Time Blocks "S", "W", and "A" are all hours summer, all hours winter, and all hours all year respectively. See Table III.1 for definitions of the other time blocks.
Small digits represent the exponent of the number, for example $2.33^{-2} = 2.33 \times 10^{-2}$.

TABLE III.3

Constants for Calculating $Y(0.1, d_e, 100\ MHz)$

Time Block	c_1	$\frac{d_e \text{ in km.}}{c_2}$	c_3	n_1	n_2	n_3	f_m	f_∞
4	1.22^{-2}	9.81^{-6}	1.09^{-8}	1.36	2.00	3.58	10.8	5.5
5	2.58^{-4}	3.41^{-6}	2.01^{-11}	2.05	2.25	4.78	8.0	4.0
6	3.84^{-3}	4.22^{-5}	7.76^{-9}	1.57	1.76	3.66	9.6	5.2
7	7.95^{-3}	3.76^{-5}	3.19^{-8}	1.47	1.76	3.40	11.2	5.5
S*	4.47^{-3}	1.66^{-5}	2.06^{-8}	1.55	1.90	3.48	9.98	5.1
1	1.09^{-4}	1.21^{-6}	8.29^{-8}	2.28	2.29	3.26	9.6	2.8
2	1.04^{-5}	4.28^{-8}	3.51^{-8}	2.71	2.91	3.41	9.15	2.8
3	2.02^{-4}	1.45^{-6}	4.27^{-8}	2.15	2.28	3.37	9.4	2.8
8	1.70^{-4}	7.93^{-7}	1.29^{-7}	2.19	2.37	3.18	9.5	3.0
W*	2.46^{-4}	1.74^{-7}	1.27^{-8}	2.11	2.64	3.62	9.37	2.8
A*	5.25^{-4}	1.57^{-6}	4.70^{-7}	1.97	2.31	2.90	10.0	5.4

* Time Blocks "S", "W", and "A" are all hours summer, all hours winter, and all hours all year, respectively. See Table III.1 for definitions of the other time blocks.
Small digits represent the exponent of the number, for example $2.33^{-2} = 2.33 \times 10^{-2}$.

TABLE III.4

Constants for Calculating - $Y(0.9, d_e, 100\ MHz)$

Time Block	c_1	d_e in km. c_2	c_3	n_1	n_2	n_3	f_m	f_∞
4	1.84^{-4}	2.22^{-6}	3.65^{-16}	2.09	2.29	6.82	8.0	4.0
5	3.80^{-4}	4.76^{-6}	8.39^{-17}	1.92	2.19	7.10	6.6	3.3
6	1.81^{-3}	5.82^{-6}	6.37^{-13}	1.67	2.15	5.38	8.4	4.1
7	3.19^{-3}	2.51^{-6}	5.03^{-9}	1.60	2.27	3.69	10.0	4.4
S *	7.42^{-4}	5.55^{-5}	4.37^{-8}	1.84	1.69	3.28	8.25	4.0
1	1.72^{-4}	6.39^{-8}	2.93^{-10}	2.10	2.79	4.24	8.2	2.4
2	1.05^{-5}	7.00^{-13}	7.64^{-9}	2.59	4.80	3.68	7.05	2.8
3	3.64^{-5}	3.74^{-9}	3.53^{-7}	2.40	3.28	2.94	7.8	2.2
8	1.64^{-6}	1.43^{-7}	3.14^{-7}	3.08	2.66	3.03	8.6	2.6
W *	3.45^{-6}	1.25^{-8}	7.50^{-7}	2.87	3.07	2.82	7.92	2.45
A *	2.93^{-4}	3.78^{-8}	1.02^{-7}	2.00	2.88	3.15	8.2	3.2

* Time Blocks "S", "W", and "A" are all hours summer, all hours winter, and all hours all year, respectively. See Table III.1 for definitions of other time blocks.
Small digits represent the exponent of the number, for example, $4.97^{-4} = 4.97 \times 10^{-4}$.

TABLE III. 5

Constants for Calculating $V(0.5, d_e)$ for Several Climatic Regions

Climate	c_1	c_2	c_3	n_1	n_2	n_3	f_m	f_∞
	d_e in km							
1. Continental Temperate	1.59^{-5}	1.56^{-11}	2.77^{-8}	2.32	4.08	3.25	3.9	0
2. Maritime Temperate Overland	1.12^{-4}	1.26^{-20}	1.17^{-11}	1.68	7.30	4.41	1.7	0
3. Maritime Temperate Oversea	1.18^{-4}	3.33^{-13}	3.82^{-9}	2.06	4.60	3.75	7.0	3.2
4. Maritime Subtropical Overland	1.09^{-4}	5.89^{-18}	2.21^{-7}	2.06	6.81	2.97	5.8	2.2
5. Maritime Subtropical Oversea	(deleted)							
6. Desert (Sahara) (Computes - V(0.5))	8.85^{-7}	2.76^{-14}	2.25^{-12}	2.80	4.82	4.78	8.4	8.2
7. Equatorial	3.45^{-7}	3.74^{-12}	6.97^{-8}	2.97	4.43	3.14	1.2	-8.4
8. Continental Subtropical	1.59^{-5}	1.56^{-11}	2.77^{-8}	2.32	4.08	3.25	3.9	0

Note - Corresponding curves of $V(0.5, d_e)$ are drawn on figure 10.13, section 10, Volume 1.

TABLE III.6

Constants for Calculating $Y(0.1, d_e, f_{MHz})$ for Several Climatic Regions

Climate	Figure	c_1	c_2	c_3	n_1	n_2	n_3	f_m	f_∞
1. Continental Temperate	10.14								
All hours and Summer		3.56^{-2}	9.85^{-8}	1.50^{-11}	1.13	2.80	4.85	10.5	5.4
Winter		3.56^{-2}	3.76^{-8}	2.05^{-11}	1.13	2.92	4.78	10.5	2.9
2. Maritime Temperate Overland									
Bands I & II (40-100 MHz)	10.23	6.96^{-3}	1.57^{-7}	1.15^{-11}	1.52	2.83	5.04	13.5	11.0
Band III (150-250 MHz)	10.25	3.60^{-2}	3.19^{-8}	6.91^{-18}	1.11	2.96	7.14	12.5	11.0
Bands IV & V (450-1000 MHz)	10.27	6.28^{-4}	3.19^{-8}	6.06^{-12}	1.92	2.96	5.05	13.0	12.5
3. Maritime Temperate Oversea									
Bands I & II (40-100 MHz)	10.24	1.37^{-2}	1.04^{-11}	1.42^{-5}	1.38	4.42	2.27	16.0	13.0
Band III (150-250 MHz)	10.26	2.67^{-3}	5.88^{-1}	8.25^{-8}	1.79	0	3.27	18.5	16.5
Bands IV & V (450-1000 MHz)	10.28	1.82^{-2}	2.40	6.92^{-15}	1.29	0	5.78	19.0	14.0
4. Maritime Subtropical Overland	III.25	4.33^{-2}	7.13^{-11}	1.19^{-12}	1.09	3.89	4.93	17.5	13.6
5. Maritime Subtropical Oversea	(deleted)								
6. Desert (Sahara)	III.27	6.09^{-2}	1.36^{-5}	3.18^{-11}	1.08	1.84	4.60	15.1	6.0
7. Equatorial	III.28	5.22^{-3}	1.57^{-4}	5.22^{-17}	1.39	1.46	6.78	8.5	3.2
8. Continental Subtropical	III.29	1.01^{-2}	2.26^{-7}	3.90^{-9}	1.46	2.67	3.78	16.0	9.1

Note - Corresponding curves of $Y(0.1, d_e)$ are drawn on the figures listed above.

TABLE III.7

Constants for Calculating $-Y(0.9, d_e, f_{MHz})$ for Several Climatic Regions

Climate	Figure	c_1	c_2	c_3	n_1	n_2	n_3	f_m	f_∞
1. Continental Temperate	10.14								
All Hours		9.48^{-3}	5.70^{-11}	5.56^{-6}	1.33	3.96	2.44	8.2	3.0
Summer		9.48^{-3}	1.81^{-11}	7.00^{-6}	1.33	4.23	2.40	8.2	4.3
Winter		9.48^{-3}	1.14^{-11}	7.36^{-6}	1.33	4.22	2.39	8.2	2.1
2. Maritime Temperate Overland									
Bands I & II (40-100 MHz)	10.23	1.45^{-3}	1.68^{-12}	8.07^{-6}	1.70	4.61	2.36	9.0	3.5
Band III (150-250 MHz)	10.25	9.32^{-4}	2.68^{-14}	1.02^{-16}	1.74	5.29	6.82	10.5	3.5
Bands IV & V (450-1000 MHz)	10.27	1.29^{-4}	1.93^{-15}	2.81^{-4}	2.14	5.80	1.65	10.0	4.5
3. Maritime Temperate Oversea									
Bands I & II (40-100 MHz)	10.24	4.52^{-2}	8.69^{-16}	1.28^{-3}	1.13	5.95	1.14	13.5	3.5
Band III (150-250 MHz)	10.26	1.14^{-3}	5.72^{-9}	1.29^{-8}	1.90	3.27	3.67	14.5	4.0
Bands IV & V (450-1000 MHz)	10.28	1.25^{-3}	6.57^{-16}	1.49^{-9}	1.72	5.96	3.84	12.0	4.0
4. Maritime Subtropical Overland	III.25	7.24^{-3}	4.26^{-15}	1.12^{-6}	1.35	5.41	2.56	12.7	8.4
5. Maritime Subtropical Oversea	(deleted)								
6. Desert (Sahara)	III.27	3.19^{-2}	5.66^{-8}	7.39^{-11}	1.14	2.76	4.40	11.4	3.3
7. Equatorial	III.28	6.51^{-3}	2.53^{-4}	2.61^{-16}	1.36	1.36	6.55	8.4	2.7
8. Continental Subtropical	III.29	3.49^{-3}	1.08^{-9}	9.15^{-11}	1.55	3.49	4.48	10.1	3.5

Note - These constants will yield positive values, i.e., $-Y(0.9, d_e)$. Corresponding curves of $Y(0.9, d_e)$ are drawn on the figures listed above.

When a prediction is required for a period of time not shown on the figures or listed in the tables, it may sometimes be obtained by mixing the known distributions. For example, the distributions for time blocks 5 and 6 would be mixed if one wished to predict a cumulative distribution of transmission loss for summer afternoon and evening hours. In mixing distributions, it is important to average fractions of time rather than levels of transmission loss. Distributions of data for time blocks may also be mixed to provide distributions for other periods of time. For example, data distributions for time blocks 1, 2, 3, and 8 were mixed to provide distributions of data for "winter". When averages are properly weighted, such mixed distributions are practically identical to direct cumulative distributions of the total amount of data available for the longer period.

The cumulative distribution of N observed hourly median values is obtained as follows: (1) the values are arranged in order from smallest to largest, L_1, L_2, L_3, ---, L_n, ---, L_N, (2) the fraction q of hourly median values less than L_n is computed:

$$q(n) = \frac{n}{N} - \frac{1}{2N};$$

(3) a plot of L_n versus $q(n)$ for values of q from $1/(2N)$ to $1 - 1/(2N)$ is the observed cumulative distribution.

To mix two distributions, the following procedure is used: (1) choose ten to fifteen levels of transmission loss L_1, ---, L_n, covering the entire range of $L(q)$ for both distributions, (2) at each of these levels, read the value q for each distribution and average these values, (3) plot each selected level of transmission loss at the corresponding average fraction of time to obtain the "mixed" distribution. In this way, any number of distributions may be combined, if each of them represents the same number of hours. If the number of hours is not the same, a weighted average value q should be computed, using as weights the number of hours represented by each distribution.

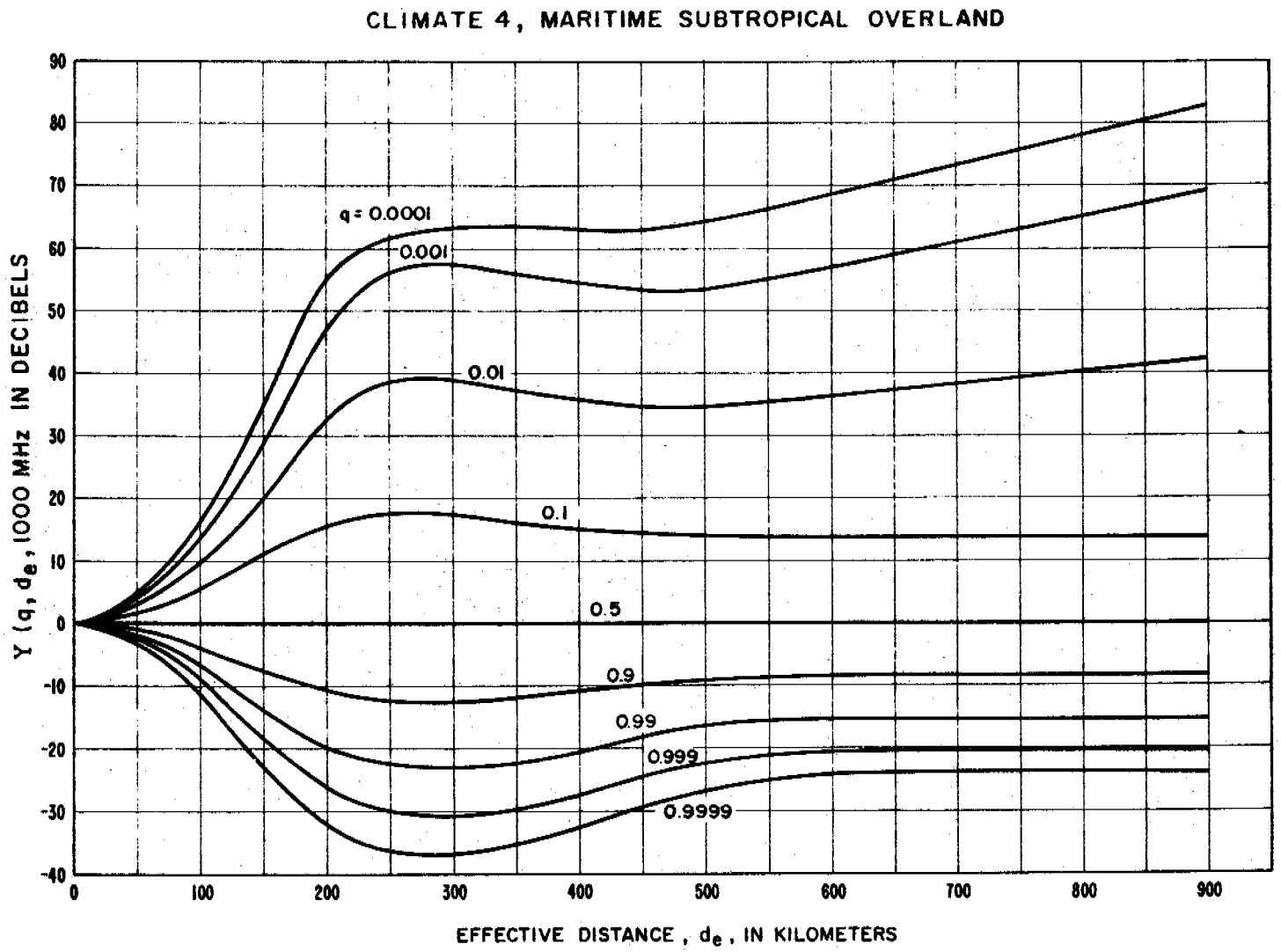

Figure III.25

The curves for climate 5, Maritime Subtropical Oversea, have been deleted. These were based on a very small amount of data. Data obtained since the preparation of these curves indicate that the following give good estimates:

Climate 4, Maritime Subtropical Overland, for hot moist tropical areas or climate 3, Maritime Temperate Oversea, for coastal areas where the prevailing winds are from the ocean.

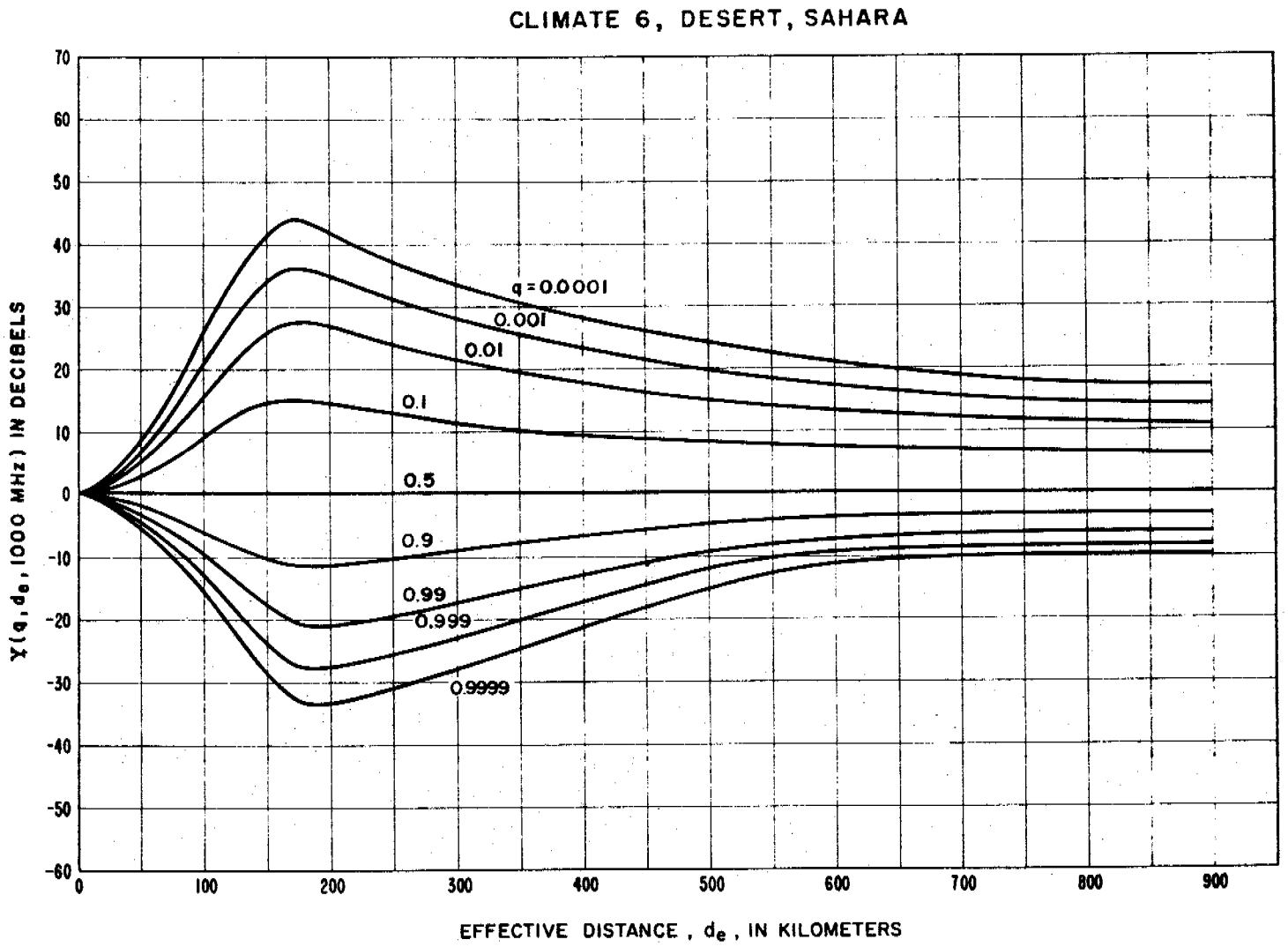

Figure III.27

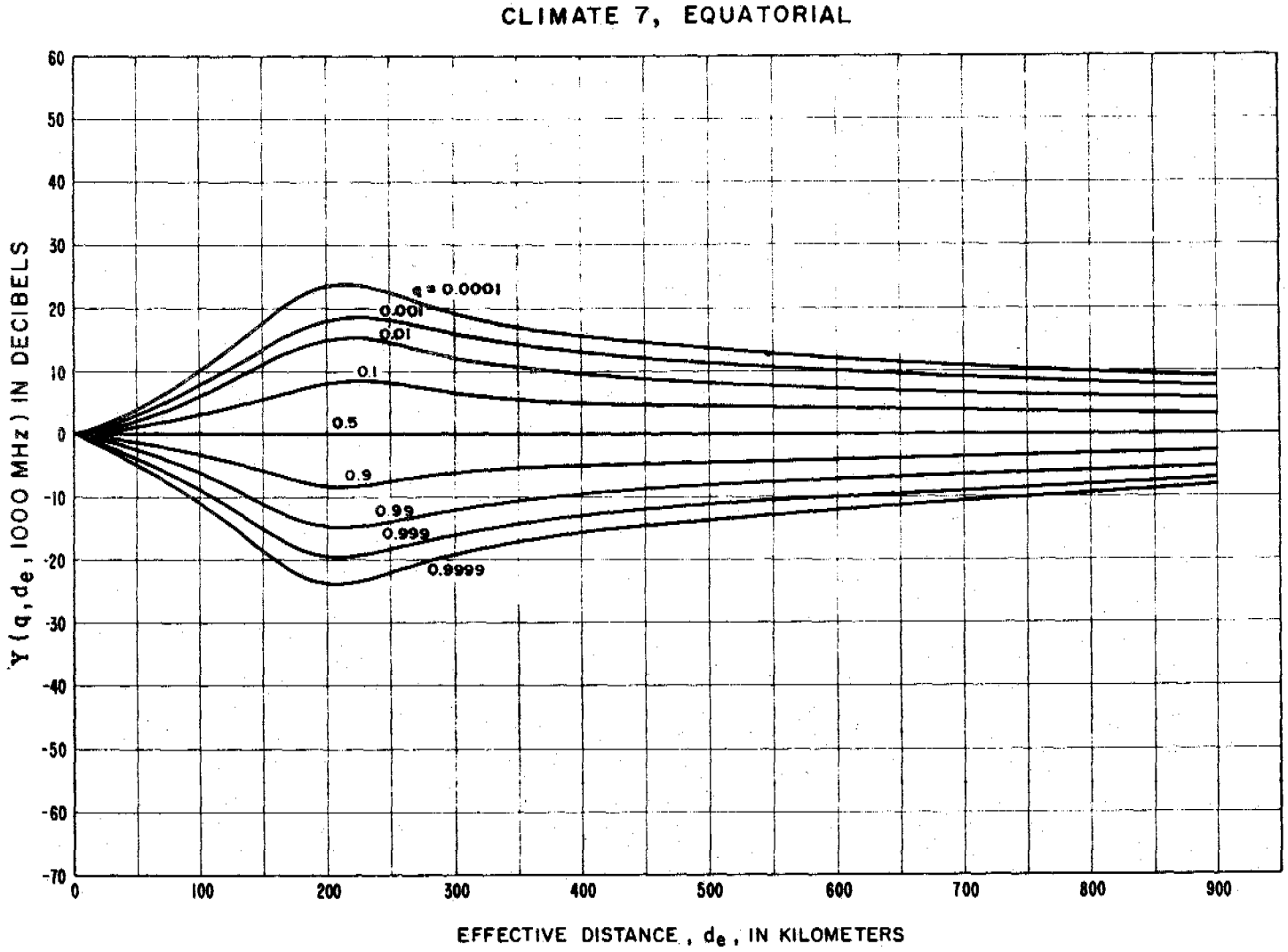

Figure III.28

CLIMATE 8, CONTINENTAL SUBTROPICAL

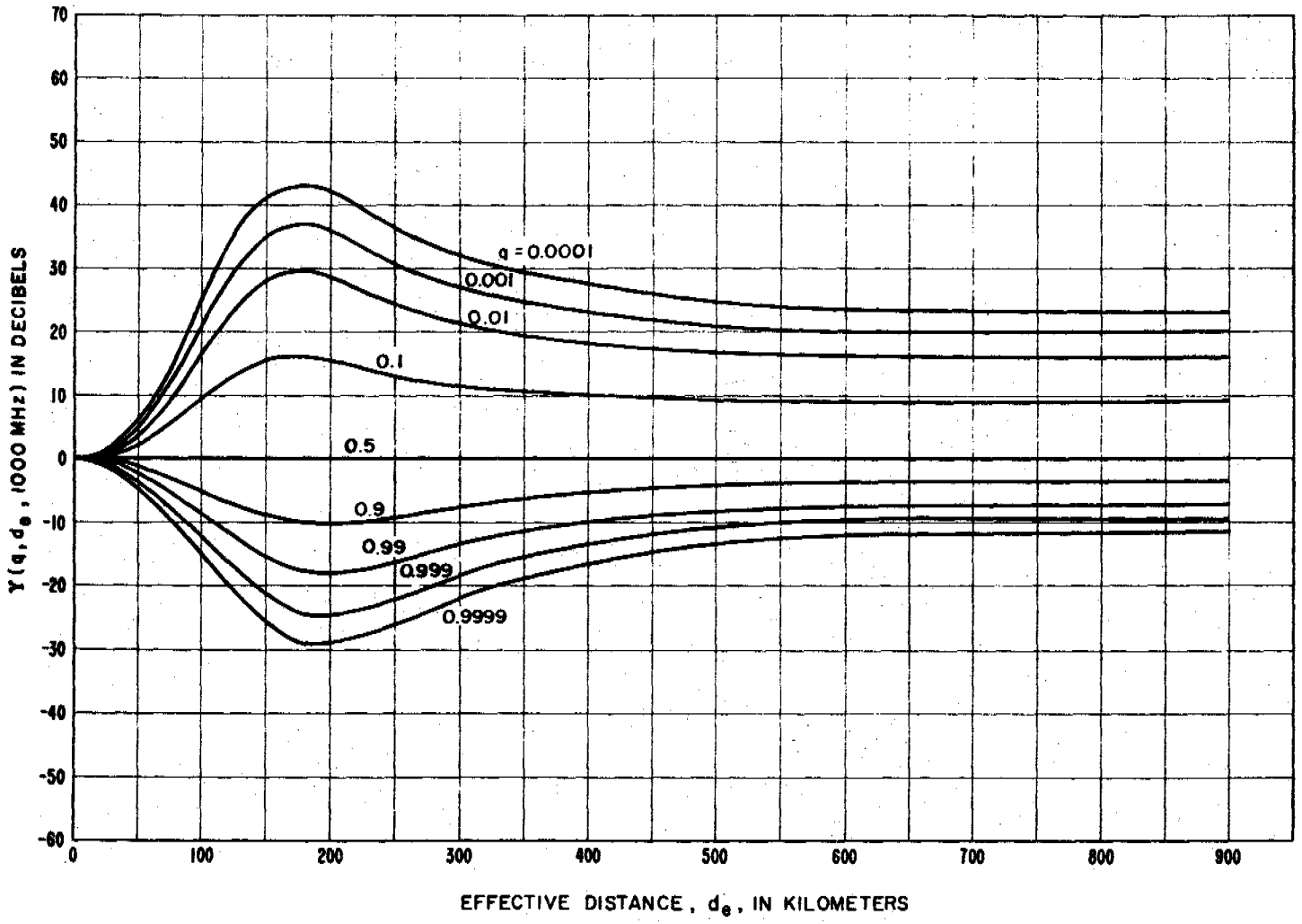

Figure III.29

THE FACTOR g(f)

g(f) = 1 FOR CLIMATES 4, 5, AND 7.

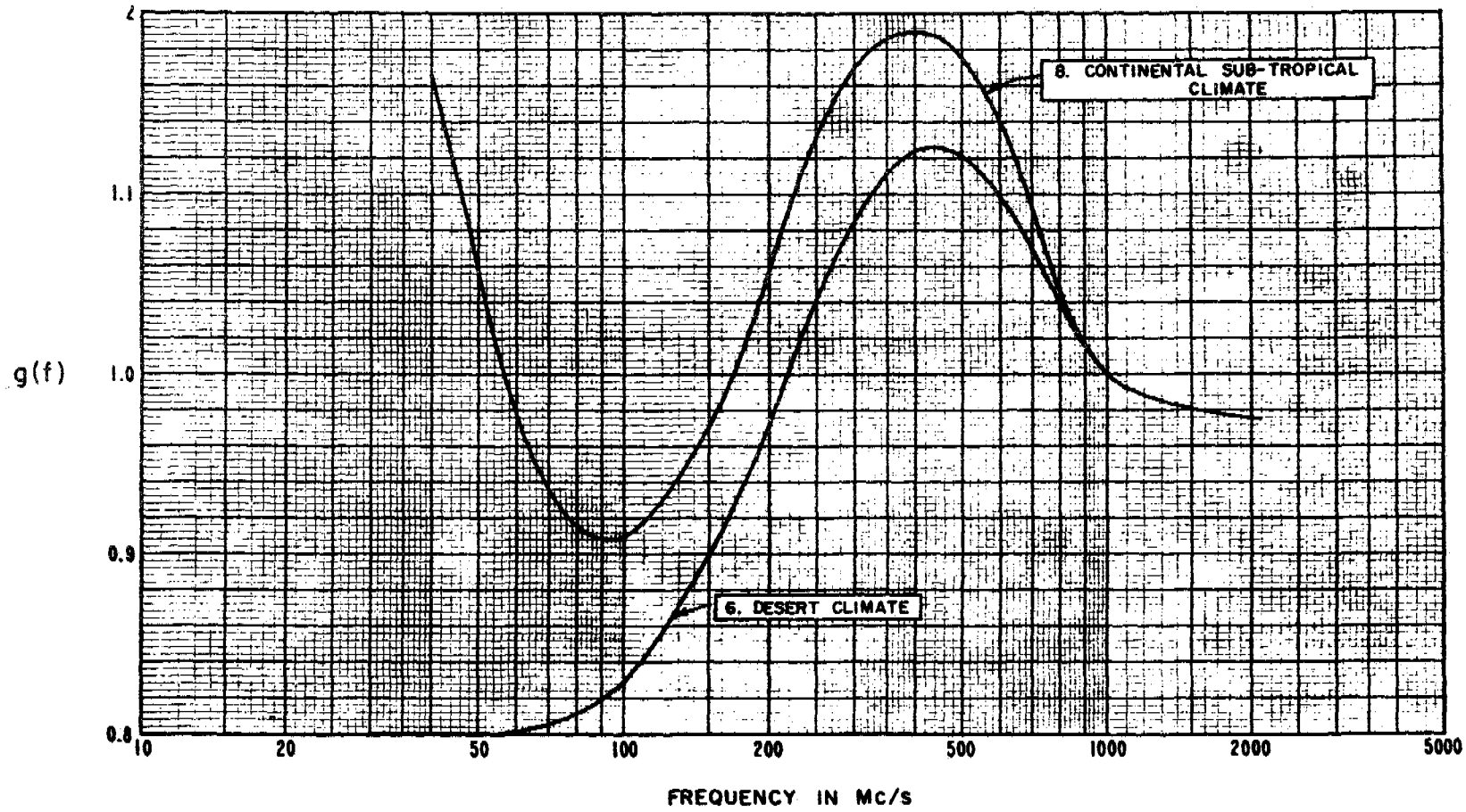

Figure III.30

ANNUAL RANGE OF MONTHLY MEAN N_s

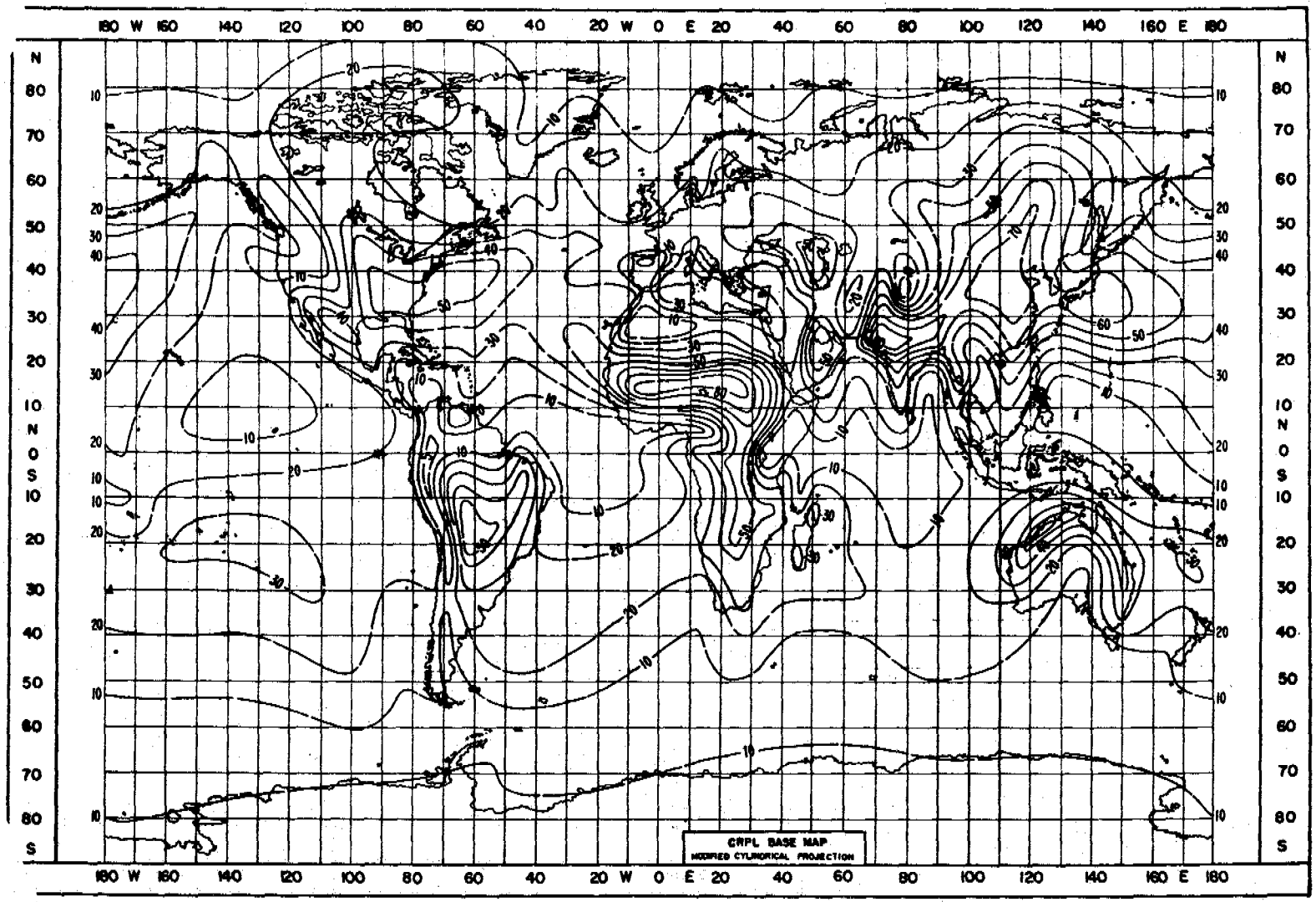

Figure III.31

THE FUNCTION $V(0.5, d_e)$ FOR VARIOUS PERIODS OF TIME IN THE U.S.A.

$L(0.5) = L_{cr} - V(0.5, d_e)$ db

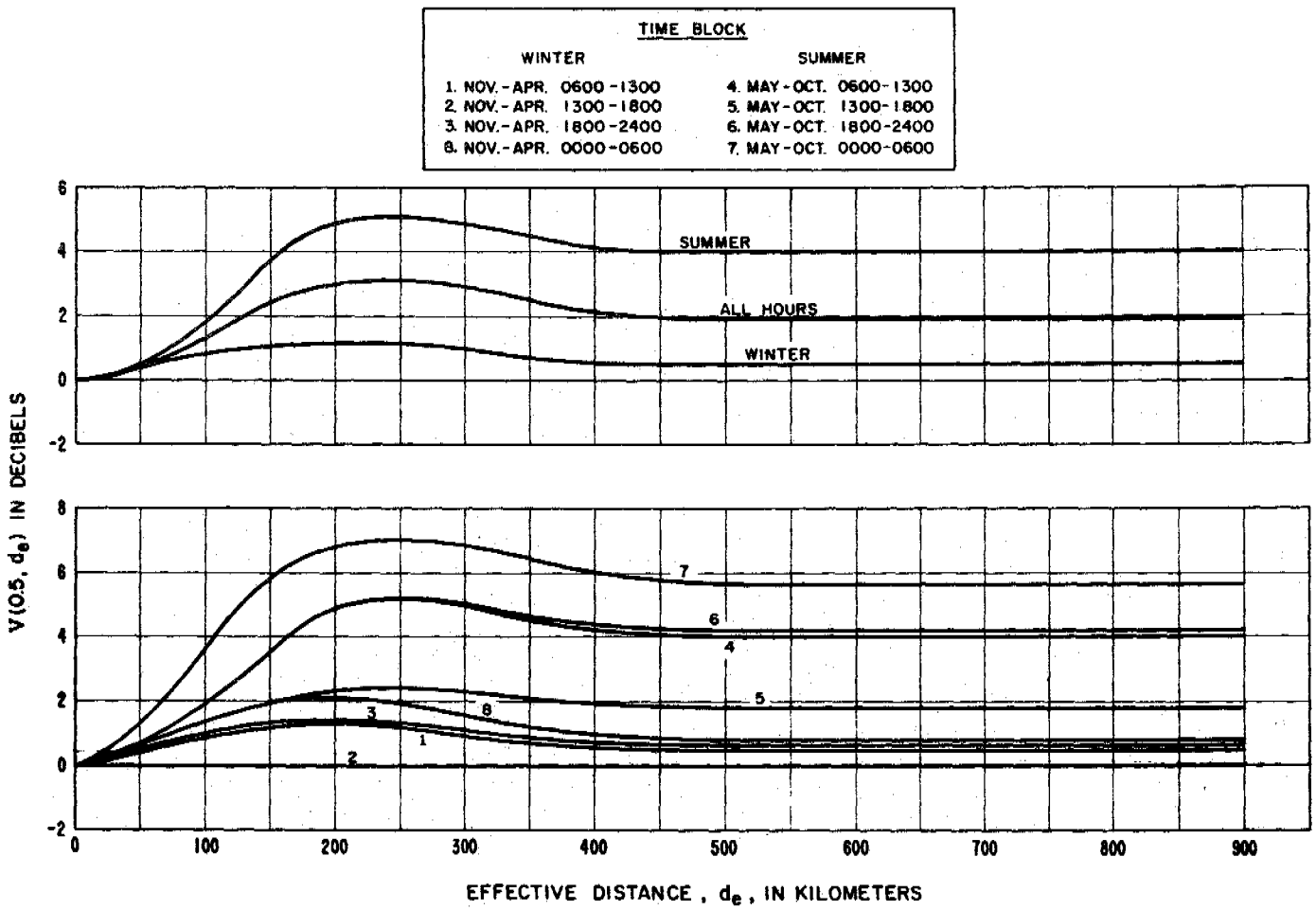

Figure III.32

WINTER TIME BLOCKS, NOV. - APRIL, U. S. A.
CURVES FOR 88-108 MHz

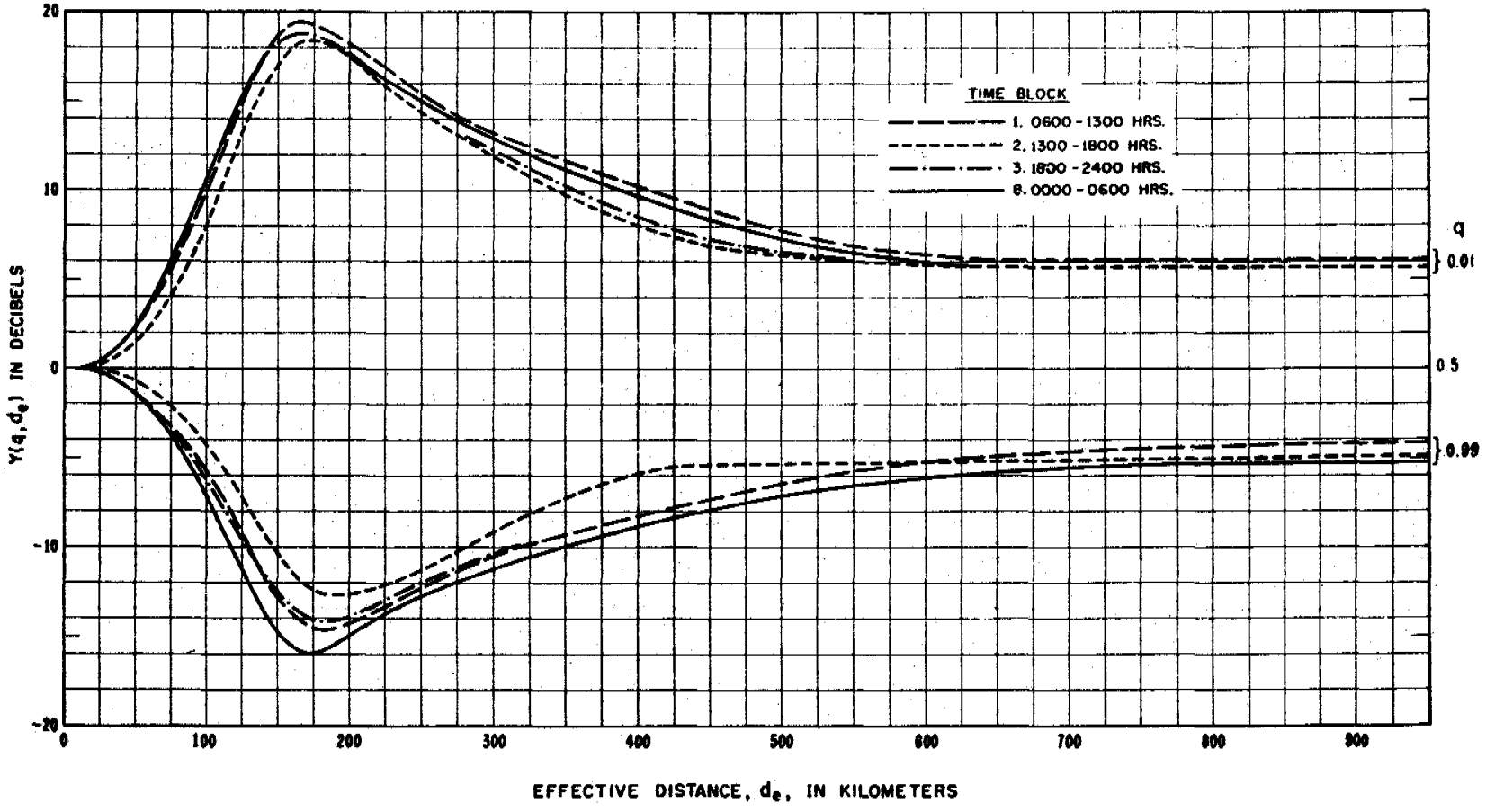

Figure III.33

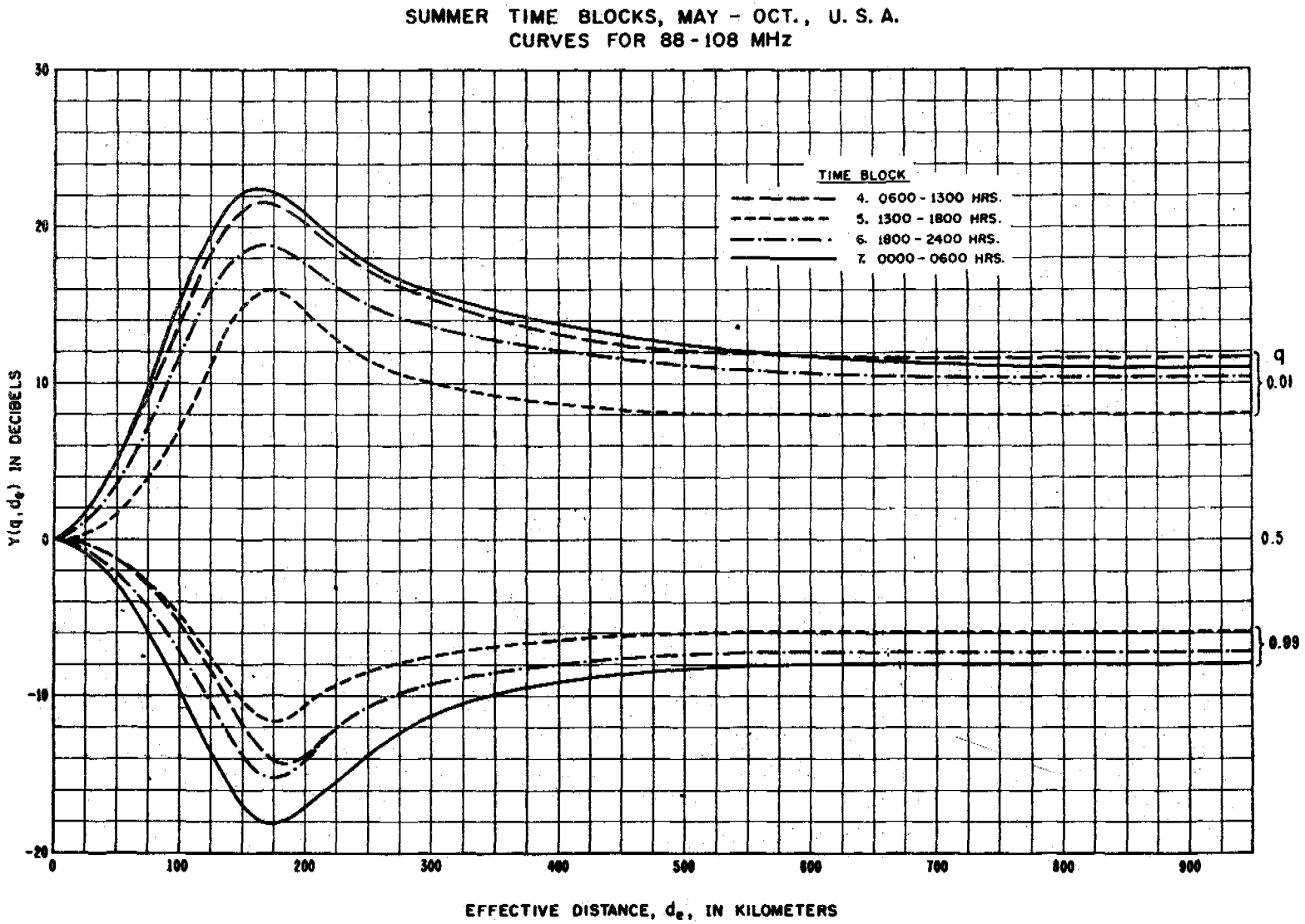

Figure III.34

TIME BLOCK 1, NOV. - APRIL, 0600 - 1300 HRS., U. S. A.
CURVES SHOW Y(q, d_e) FOR THE FREQUENCY RANGE 88 - 108 MHz

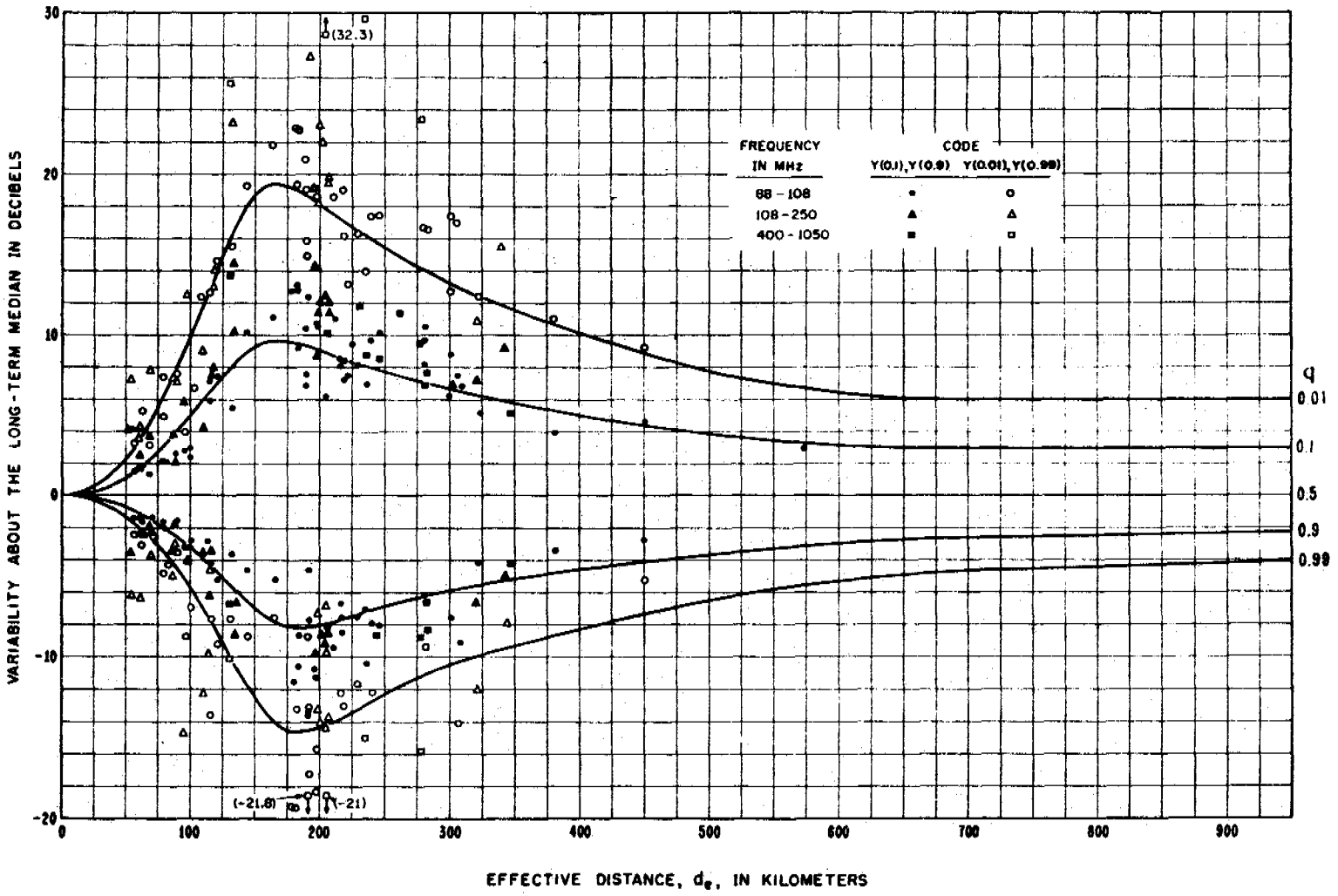

Figure III.35

TIME BLOCK 2, NOV. - APRIL, 1300 - 1800 HRS., U. S. A.
CURVES SHOW Y(q, d_e) FOR THE FREQUENCY RANGE 88 - 108 MHz

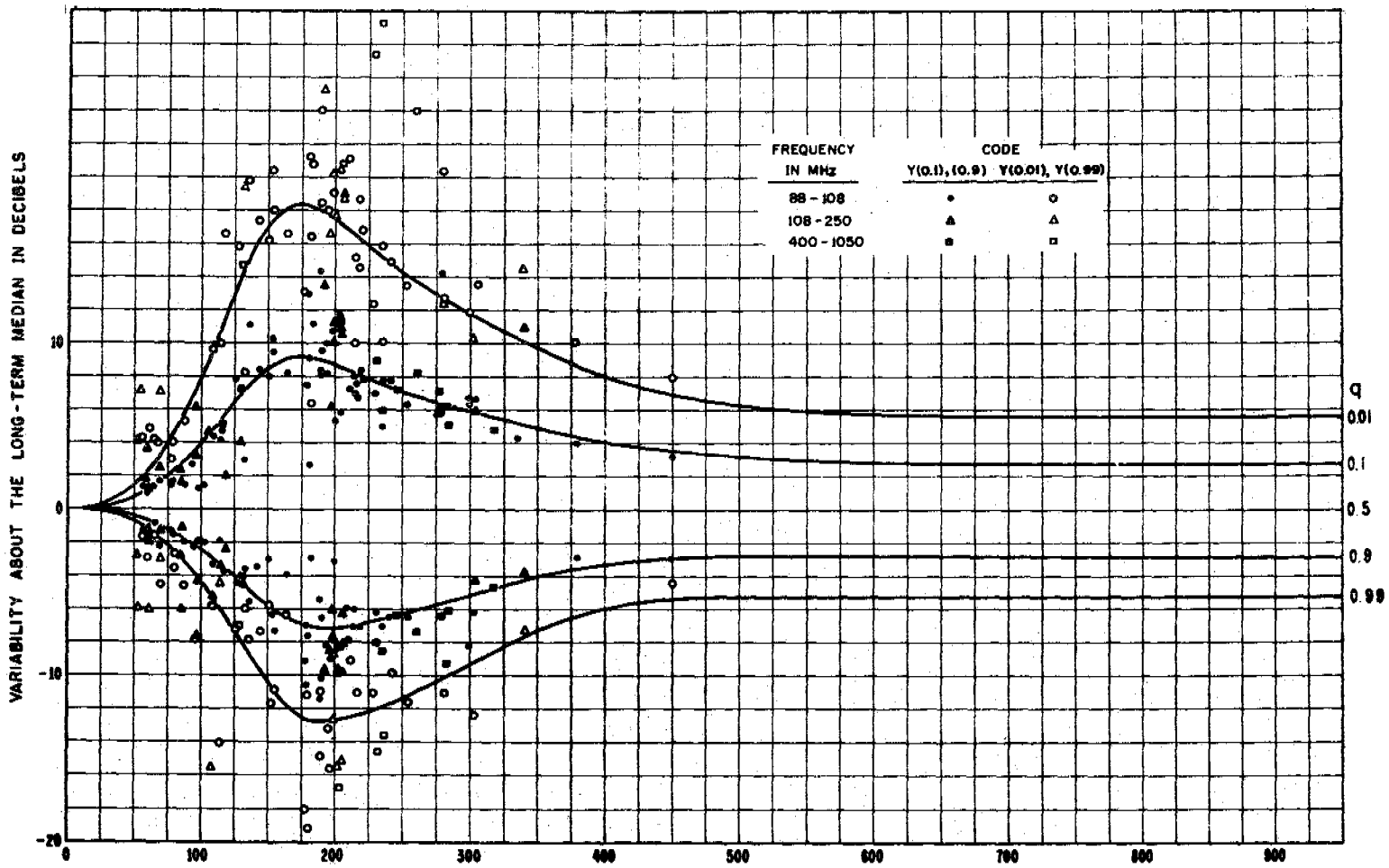

Figure III.36

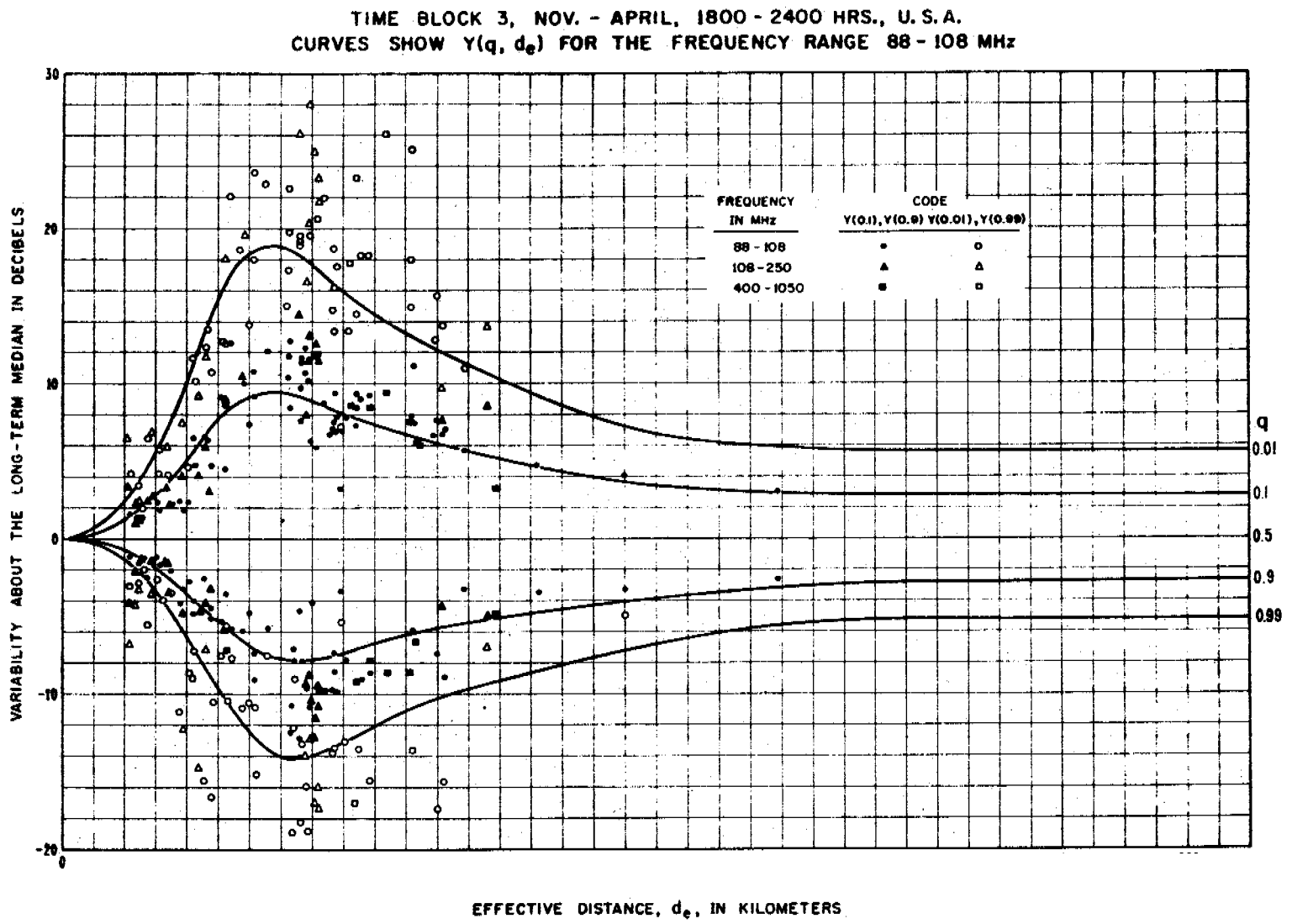

Figure III.37

TIME BLOCK 8, NOV. - APRIL, 0000-0600 HRS., U.S.A.
CURVES SHOW $Y(q, d_e)$ FOR THE FREQUENCY RANGE 88 - 108 MHz

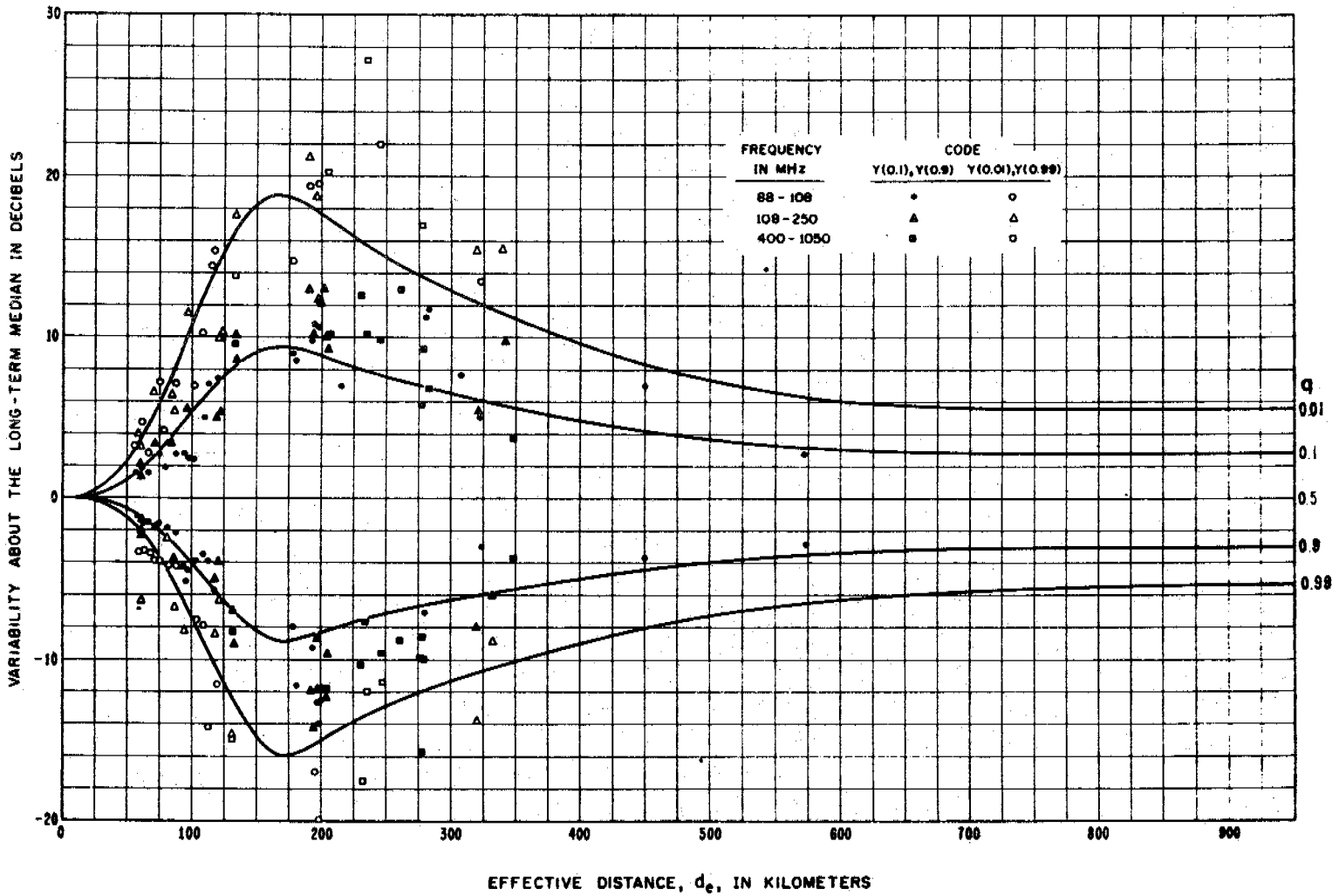

Figure III.38

TIME BLOCK 4, MAY - OCT., 0600-1300 HRS., U.S.A.
CURVES SHOW $Y(q, d_e)$ FOR THE FREQUENCY RANGE 88 - 108 MHz

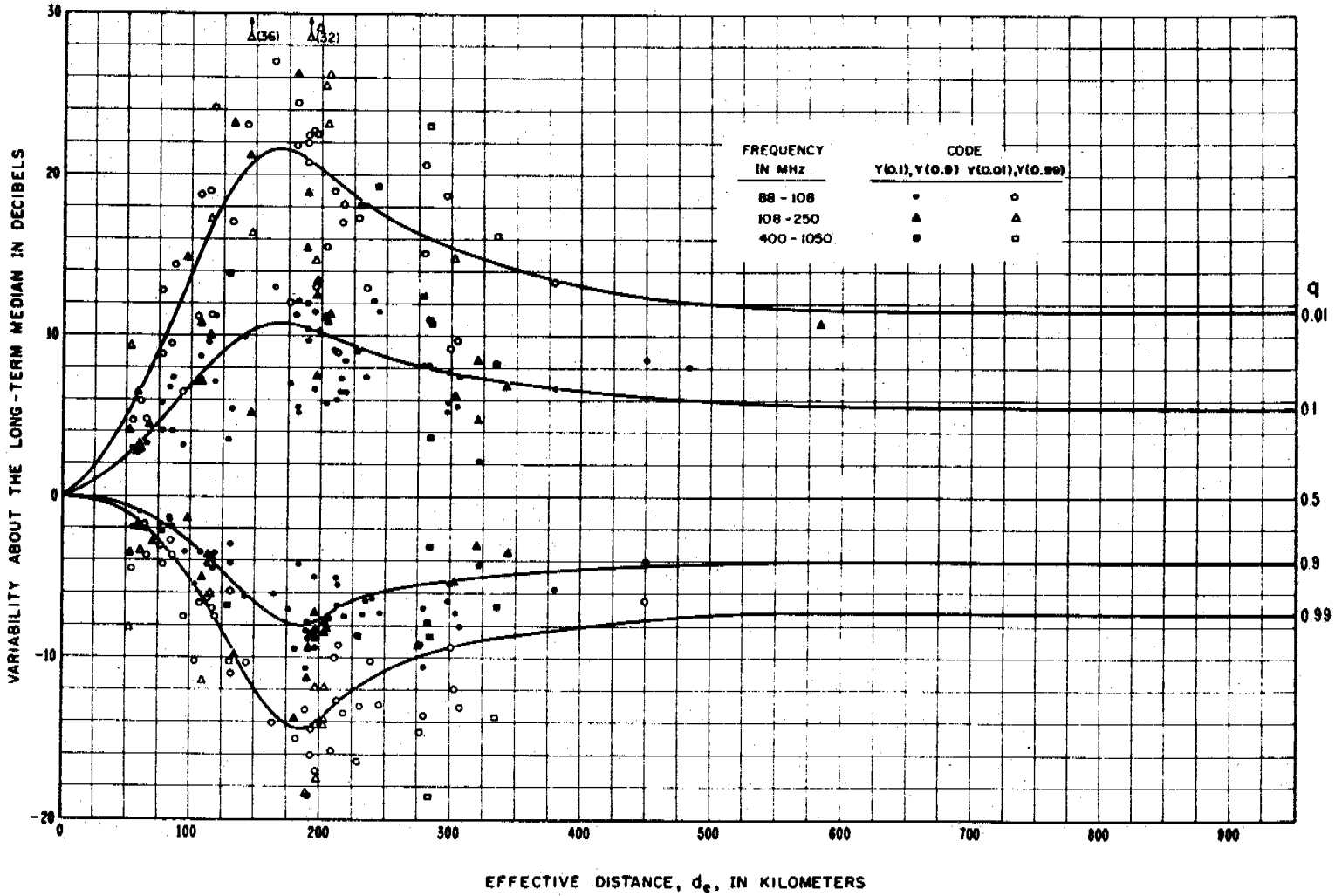

Figure III.39

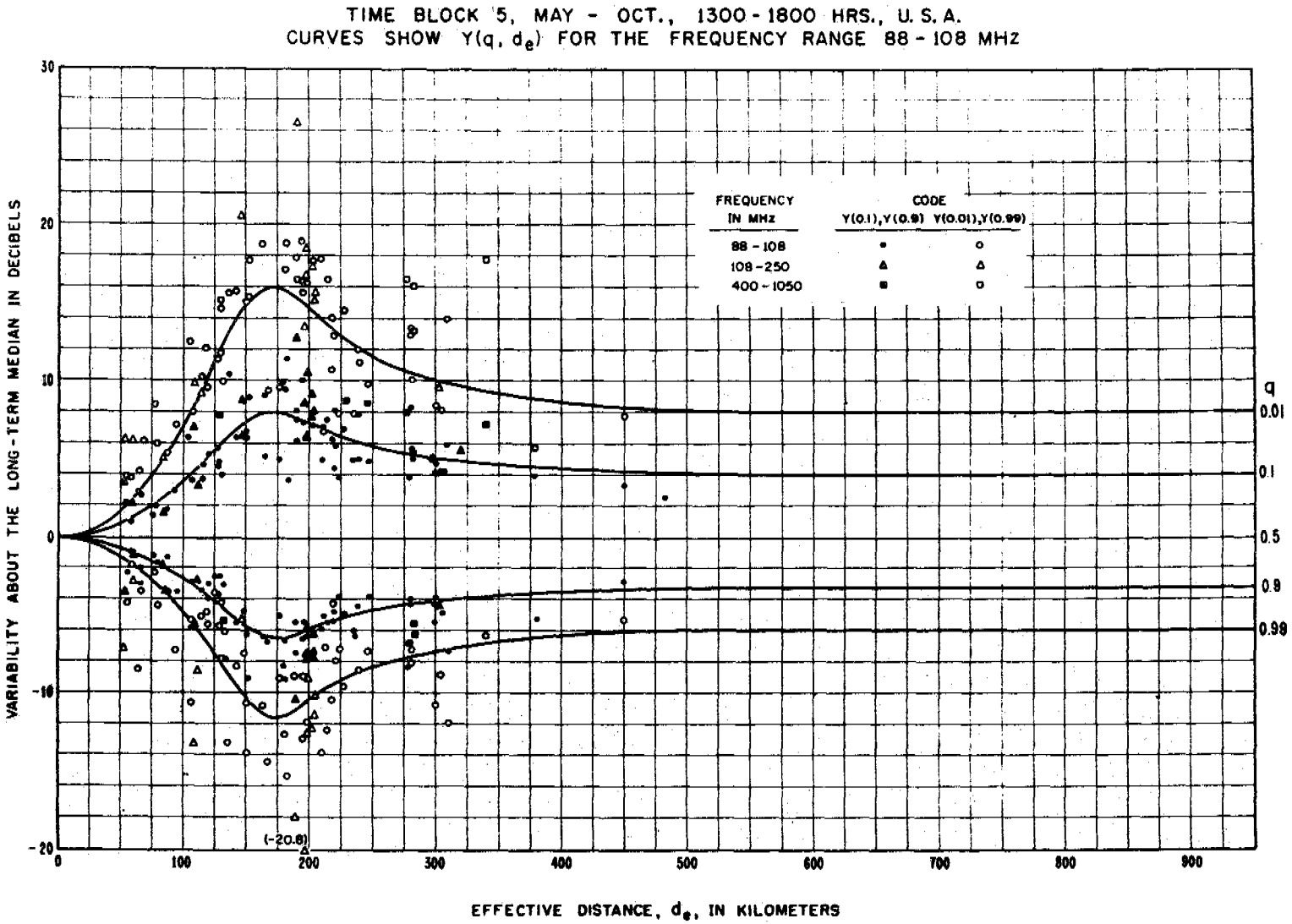

Figure III.40

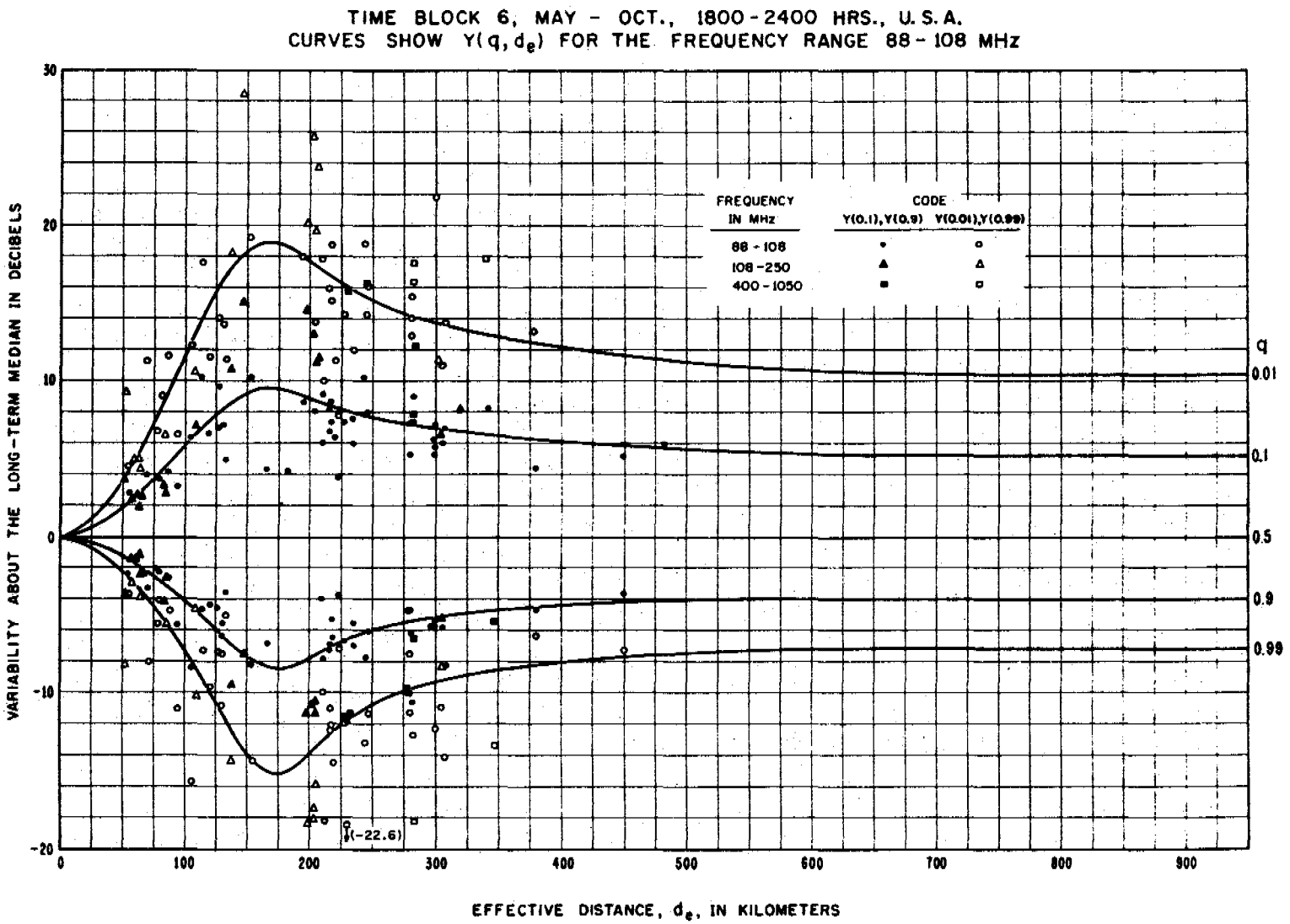

Figure III.41

TIME BLOCK 7, MAY - OCT., 0000 - 0600 HRS., U. S. A.
CURVES SHOW $Y(q, d_e)$ FOR THE FREQUENCY RANGE 88 - 108 MHz

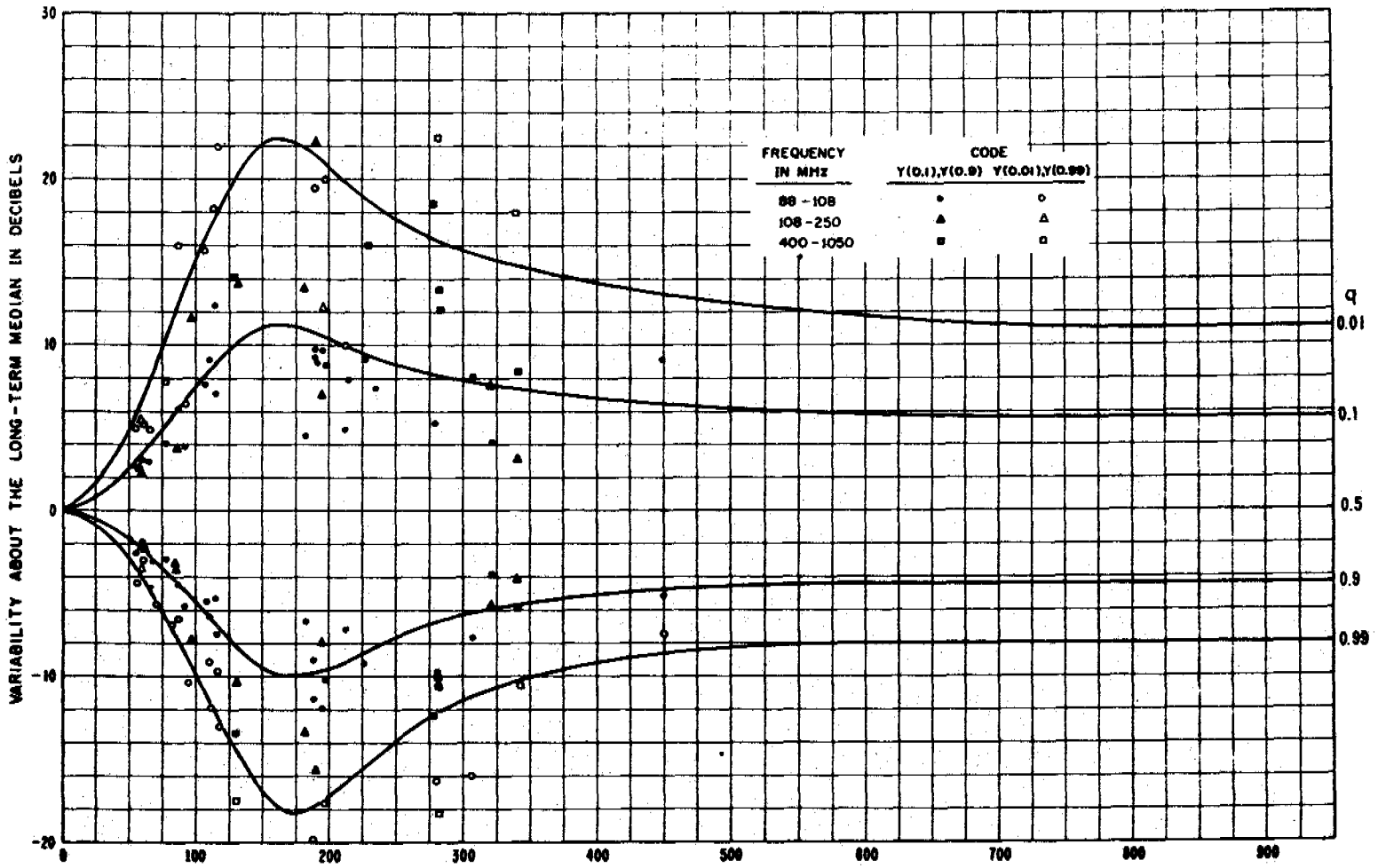

Figure III.42

III.8 List of Special Symbols Used in Annex III

$A(v_j)$ Attenuation relative to free space for each of several rays as a function of the parameter v_j, where $j = 1, 2, 3, 4$, (III.34).

b The parameter b, a function of ground constants, carrier frequency, and polarization, expressed in degrees, figure 8.2, and equations (III.40) and (III.41).

b_h The parameter b for horizontal polarization defined by (III.40).

b_v The parameter b for vertical polarization, (III.41).

c A parameter showing the phase change associated with the complex plane wave reflection coefficient $R \exp[-i(\pi - c)]$ corresponding to reflection from an infinite smooth plane surface, (5.4) figures III.1 through III.8.

c_h, c_v Values of c for horizontal and vertical polarization, respectively, (III.13) and (III.14) figures III.1 through III.8.

C_j Fresnel integral, (III.33), where $j = 1, 2, 3, 4$.

$Ci(r)$, $Ci(r_1)$, $Ci(r_2)$ Cosine integral as a function of r, (III.51), r_1 and r_2 (III.50).

d_r Distance used in calculating ground reflections in knife edge diffraction; d_r is defined by (III.29).

d_{11}, d_{12}, d_{21}, d_{22} Distances used in computing diffraction attenuation with ground reflections, (III.31) figure III.9.

f_j Diffraction loss for each of several distinct rays over an isolated obstacle, where $j = 1, 2, 3, 4$, (III.32-III.35).

f_1, f_2, f_3, f_4 Diffraction loss for each of four distinct rays over an isolated obstacle, (III.32).

$f(r_1)$, $f(r_2)$ Functions of the normalized antenna heights r_1 and r_2, (III.50).

$f(v_j)$ A function identically equal to f_j for $v = v_j$, (III.33) figure III.10.

$f(\theta_h)$ A factor used to reduce estimates of variability for antenna beams elevated above the horizon plane, (III.65) figure III.22. See θ_h and θ_b.

F_{oi} Scattering efficiency correction term for the i^{th} lobe of an antenna pattern, (III.63).

$F(\theta_{ei}d)$ This function is the same as $F(\theta d)$ with the effective angular distance θ_{ei} substituted for the angular distance, θ, annex III, (III.57).

g_b, g_{bt} A high gain antenna radiates g_b watts per unit area in every direction not accounted for by the main beam or by one of the side lobes of an antenna. The gain g_b for a transmitting antenna is g_{bt}, section III.6.

$g(f)$ A frequency correction factor shown in figure III.30, (III.66).

G_b, G_{bt} Decibel equivalent of g_b, $G_b = 10 \log g_b$, and of g_{bt}, annex III section III.6.

G_{ri}, G_{ti} Gains of the i^{th} lobe of receiving and transmitting antennas, respectively, (III.57).

h_e A height, using elevated beams, that is equivalent to h_o for horizon rays, (III.63).

h_{rm}, h_{tm} Height of a knife edge above a reflecting plane on the receiver or transmitter side of the knife edge, (III.37).

$h(r)$ A function of r shown in figures III.20 and III.21.

$h(r_1)$, $h(r_2)$ A function of r_1 or r_2 defined by (III.50) and shown on figures III.20 and III.21.

H_{oi} The frequency gain function for the i^{th} beam intersection in a scattering plane (III.57).

j Represents a series of subscripts 1, 2, 3, 4, as used in equations (III.27) to (III.35).

K_h The diffraction parameter K for horizontal polarization, section III.4.

K_v The diffraction parameter K for vertical polarization, section III.4.

L_{gi} Loss in antenna gain for the i^{th} scattering subvolume, (III.57).

L_i Transmission loss associated with the i^{th} power contribution, (III.55) and (III.57).

$L_1, L_2 \ldots L_n \ldots L_N$ A series of hourly median values of transmission loss arranged in order from the smallest to the largest value, section III.7.

$L(q)$ Transmission loss exceeded a fraction q of the time, (III.68).

m_h, m_v Parameters used in computing the magnitudes R_h and R_v of the smooth plane earth reflection coefficient R, (III.10).

mho. A unit of conductance, the reciprocal of resistance which is measured in ohms, figures III.1 to III.8.

p A function of the dielectric constant and grazing angle used in computing the plane wave reflection coefficient, (III.8).

q A parameter used in calculating a plane wave reflection coefficient, (III.7) to (III.14).

$r_{11}, r_{12}, r_{21}, r_{22}$ Distances to and from the bounce point of reflected rays, (III.28) figure III.9.

R_h Plane earth reflection coefficient R for horizontal polarization, (III.12) and figures III.1 to III.8.

R_v Plane earth reflection coefficient R for vertical polarization, (III.12) figures III.1 to III.8.

s_e Path asymmetry factor for beams elevated above the horizon. $s_e = \alpha_e / \beta_e$, (III.64).

$Si(r)$ Sine integral as a function of r, (III.51).

S_j Fresnel integral, (III.33).

v_j The parameter v for each of j paths over an isolated obstacle, (III.27).

w_{ai} Contribution to the total available power from the i^{th} scattering subvolume, (III.55) and (IV.11).

x_a, x_b Points at which a first Fresnel ellipse cuts the great circle plane, III.18 to III.23.

α_e, β_e The angles between the "bottoms" of transmitting or receiving antenna beams or side lobes and a line joining the antennas, (III.61).

α_{ei}, β_{ei} Angles α_e and β_e for the i^{th} lobe of an antenna pattern.

α_{eo}, β_{eo} When beams are elevated sufficiently that there is no bending of the ray due to atmospheric refraction $\alpha_e = \alpha_{eo}$, $\beta_e = \beta_{eo}$, (III. 60); when ray bending must be considered α_e and β_e are computed using (III. 61).

α_{oj}, β_{oj} The angles α_o, β_o made by each of j rays, over an isolated obstacle, (III. 36).

α_{o1}, α_{o2}, β_{o1}, β_{o2} The angles α_o and β_o for each of four rays over an isolated obstacle, (III. 36).

δ A parameter used in computing the first Fresnel zone in a reflecting plane, (III. 18).

δ The effective half-power semi-beamwidth of an antenna, section III. 6.

δ_e The effective half-power semi-beamwidth of an antenna that is elevated or directed out of the great circle plane, section III. 6.

δ_o The semi-beamwidth of an equivalent beam pattern with a square cross-section $\delta_o = \delta\sqrt{\pi/4}$, section III. 6.

δ_{rwo}, δ_{two} Azimuthal equivalent semi-beamwidths with square cross-section, (III. 58) figure III. 23.

δ_{rzo}, δ_{tzo} Vertical angle equivalent semi-beamwidths with square cross-section, (III. 58) figure III. 23.

δ_{wo} Azimuthal equivalent semi-beamwidth with square cross-section, section III. 6.

δ_{zo} Vertical angle equivalent semi-beamwidth, section III. 6.

Δ_j The j^{th} value of Δr, where $\Delta r = r_1 + r_2 - r_o$, (III. 27) and (III. 29).

Δ_1, Δ_2, Δ_3, Δ_4 Ray path differences between a direct ray and a ray path over a single isolated obstacle with ground reflections, (III. 28) figure (III. 9).

Δ_{1r}, Δ_{2r}, Δ_{3r}, Δ_{4r} Ray path difference between straight and ground reflected rays on either side of an isolated obstacle, (III. 31), (III. 37).

ϵ Ratio of the dielectric constant of the earth's surface to the dielectric constant of air, figures 8.1 and 8.2, annex III. 4.

ϵ_{r1}, ϵ_{t1} Angle between the axis of the main beam and the axis of the first side lobe of an antenna pattern, figure III. 22 .

ϵ_{tw1}, ϵ_{tw2} Azimuth angles of the first and second lobes of a transmitting antenna relative to the main beam axis, figure III. 23.

ϵ_{tz1}, ϵ_{tz2} Elevation angles of the first and second lobes of a transmitting antenna relative to the main beam axis, figure III. 23.

ζ The angle that a scattering plane makes with the great circle plane, (III. 60), (III. 61), and figure III. 22.

η_{se} A function of h_e and N_s used in computing F_{oi} and H_{oi} for scattering from antenna beams directed above the horizon or away from the great circle plane, (III. 64).

θ_b Angle of elevation of the lower half power point of an antenna beam above the horizontal, (III. 62). See θ_h and $f(\theta_h)$.

θ_{br}, θ_{bt} Values of θ_b for the receiving and transmitting antennas, respectively, (III. 61).

θ_{bri}, θ_{bti} Values of θ_b for the i^{th} beam intersection, (III. 59).

θ_e The angle between radio rays elevated above the horizon and/or away from the great circle plane, (III. 64).

θ_{ei} The angle θ_e at the i^{th} intersection of radio rays elevated above the horizon and/or away from the great circle plane, (III. 57).

θ_{e1}, θ_{e2}, ... θ_{en} The angle θ_e for the first, second, ... n^{th} intersection of radio rays, figure III. 22.

θ_{hr}, θ_{ht} Angle of elevation of a knife edge relative to the horizontal at the receiving or transmitting antenna, (III. 38).

θ_j Angle between direct and/or reflected ray over a knife-edge, where $j = 1, 2, 3, 4$ as shown in figure III. 9.

θ_{jr} Angles defined in (III. 29), where $j = 1, 2, 3, 4$, which are added to θ to determine $\theta_j = \theta + \theta_{jr}$.

θ_{1r}, θ_{2r}, θ_{3r}, θ_{4r} Values of θ_{jr} for $j = 1, 2, 3, 4$, (III. 29).

θ_1, θ_2, θ_3, θ_4 The angle between rays from the transmitting and receiving antennas over an isolated obstacle with ground reflections, figure III. 9.

σ Surface conductivity in mhos per meter, figures 8. 1 and 8. 2, section III. 4.

τ The amount a radio ray bends in the atmosphere, (III. 62).

$\tau(\theta_b, d, N_s)$ Bending of a radio ray that takes off at an initial angle θ_b and travels d kilometers through an atmosphere characterized by a surface refractivity N_s, (III. 61).

$\phi(v, 0)$ Component of phase lag due to diffraction over an idealized knife edge, (7. 13) figure 7. 1, and (III. 30).

$\phi(v\rho)$ Component of phase lag due to diffraction over an isolated perfectly-conducting rounded obstacle, (7. 13) figure 7. 5 and (III. 30).

$\phi(0, \rho)$ The component of the phase lag of the diffracted field over an isolated perfectly-conducting rounded obstacle for $v = 0$, (7. 13) figure 7. 4 and (III. 30).

Φ_j The phase lag of the diffracted field for the j^{th} ray over an isolated perfectly-conducting rounded obstacle (III. 30a), where $j = 1, 2, 3, 4$.

$\Phi_j(v, \rho)$ The phase lag of the diffracted ray over an isolated rounded obstacle for the j^{th} ray, $\Phi_j(v, \rho) \equiv \Phi_j$, (III. 30).

$\Phi_j(v, 0)$ The phase lag over an ideal knife edge for the j^{th} ray, (III. 30).

Φ_1, Φ_2, Φ_3, Φ_4 The phase lag $\Phi_j(v, \rho)$ for values of $j = 1, 2, 3, 4$, (III. 32).

ψ_r, ψ_t The angle between the plane of the lower half-power point of an antenna beam and the receiver or transmitter horizon plane, (III. 60).

ψ_{ri}, ψ_{ti} The angle ψ_r or ψ_t for the i^{th} lobe of an antenna pattern, (III. 59).

ψ_1, ψ_2 Angle of reflection at the ground of a reflected ray that passes over a knife-edge, (III. 36) figure III. 9.

Ω The half-power beamwidth, $\Omega = 2\delta$, (9.10) and figure III.22.

$\Omega_{ro}, \Omega_{r1}, \Omega_{to}, \Omega_{t1}$ Half-power beamwidths corresponding to $2\delta_o$, $2\delta_1$ for the receiving and transmitting antenna patterns, respectively, figure III.22.